ENERGY HARVESTING SYSTEMS FOR THE INTERNET OF THINGS WITH APPLICATIONS TO SMART AGRICULTURE

A Dissertation

by

ALFREDO COSTILLA-REYES

Submitted to the Office of Graduate and Professional Studies of
Texas A&M University
in partial fulfillment of the requirements for the degree of

DOCTOR OF PHILOSOPHY

Chair of Committee,	Edgar Sánchez-Sinencio
Committee Members,	Kamran Entesari
	Arum Han
	Duncan Henry M. Walker
Head of Department,	Miroslav M. Begovic

May 2020

Major Subject: Electrical Engineering

ABSTRACT

The Internet of Things is the interconnection of everyday objects to the web, with the purpose of exchanging information to enable smarter actions and potentially make a process more efficient. However, how power is provided and stored in remote sensing applications is still one of the main modern electronics challenges of such technology and can become one of the main constraints to prevent its mass adoption.

Energy Harvesting is an emerging technology that can transform energy in the environment into usable energy, among such environmental energy are electromagnetic waves, thermal, solar, kinesthetic transducers, fuel cells, to name a few. Because this technology makes use of the available ambient energy, it has the potential to increase the power readiness for battery-operated electronics and more importantly, it can become the technology that fully powers the next generation of internet-enabled agricultural solutions.

This dissertation centers around the design and development of high-efficient power management systems for AC and DC energy harvesting sources. The proposed architectures not only consider circuits, systems and algorithms that make a more efficient power extraction but also focuses on providing inherent sensing functionalities at no extra system complexity, which in turn not only achieves the goal of extending the battery life of proposed smart sensor applications but also proposes new charge extraction methods to permanently power an electronic device.

The work presented in this dissertation demonstrates that energy harvesting, and internet of things devices can be implemented in multiple smart agriculture scenarios by proposing algorithms, circuits and systems capable of performing energy harvesting operations while providing reliable data to the end user. The analysis of the design of such proof-of-concept prototypes are provided in this dissertation along with its implementation and testing. The first part of this dissertation proposes novel algorithms for maximum power extraction and new power measurement techniques. The second part focuses on front-end circuits for AC energy harvesting sources and circuits that can provide sensing capabilities along with energy harvesting operations.

DEDICATION

A Dios, a mi madre hermosa y a mi padre que tanto extraño.

ACKNOWLEDGMENTS

I thank God, for all the opportunities He has poured during my lifetime and for giving me the strength to follow the path He has planned for me.

I would thank my advisor, Dr. Edgar Sánchez-Sinencio, for taking the chance and believing in me, for his advice, and most importantly, his friendship throughout my studies here at Texas A&M University.

I would like to thank my committee members, Dr. Kamran Entesari, Dr. Arum Han, and Dr. Duncan Henry M. Walker, for their support throughout the course of this dissertation.

I would like to say that my work and all I am will always be devoted to my amazing family. My parents who are my world and without them I would not be half the man I am. And my brothers, who are my closest friends and who have given me my most cherished memories growing up together. Thank for all your support dear Diana Zapata, you are an extraordinary human being.

I would like to give a big thank you to Johan Estrada and Amr Abuellil for our numerous technical discussions and their friendship, I certainly have seen an exponential growth as an engineer, scientist, but most importantly, as a human being working as part of such talented team.

Thanks also to my close friends, Salvador Carreon, Celal Erbay and Jorge Zarate for their guidance since my early days in graduate school, Sergio Soto and Erika Garcia for being the first friends I made when I first came to Texas A&M and to my friends Fernando Lavalle, Hatem Osman, Efrain Gaxiola, Miguel Rojas, Xiaosen Liu, Judy Amanor-Boadu, Carlos Briseño, Congyin Shi, Mohamed Abouzied, Joseph Riad, Adriana Zanabria, Guillermo Garayar, Sung Yoon, Samuel Annor Fordjour, Sanghoon Lee, Zizhen Zeng, Shashank Naphade, Anish Joshi, Ashtrid, Sylvia Odio, Bud Kirchner, Blair, Steve Dauphin, Kate Thorton, Adrian García, Karla Rascon, Tere, Ame, Zuemy, Segio, Roberto and Gabriel.

I would also like to thank Ms. Ella Gallagher for her unconditional help, I certainly going to miss chatting with her, and also special thanks to Katie Bryan and Melissa Sheldon.

Finally, I would like to extend my thanks to the National Council of Science and Technol-

ogy of Mexico (CONACYT), the Mexiquense Council of Science and Technology (COMECYT), Mexican Secretary for Public Education (SEP), Mexican and Mexiquense Secretary for Social Development, Autonomous University of the State of Mexico, Silicon Labs, Texas Instruments, Startup Aggieland, Mays Business School, College of Engineering and College of Agriculture and Life Sciences at Texas A&M University, McFerrin Center for Entrepreneurship, Texas A&M Engineering Entrepreneurship, Thought For Food and Kirchner Group for their economic support during my doctoral studies.

CONTRIBUTORS AND FUNDING SOURCES

Contributors

This work was supported by a dissertation committee consisting of Professors Edgar Sánchez-Sinencio, Kamran Entesari and Arum Han of the Department of Electrical and Computer Engineering and Professor Duncan Henry M. Walker of the Department of Computer Science and Engineering.

The MFC devices, equipment, laboratory space and materials used in Chapter 4 were provided by Celal Erbay. Salvador Carreon-Bautista contributed with industry insight in the area of power management systems for the development of the system developed in Chapter 4. Design and layout of the rectifier and activity detection circuits for the harvesting system presented in Chapter 5 were conducted in part by Amr Abuellil, Johan Estrada-López and Salvador Carreon-Bautista.

All other work conducted for the dissertation was completed by the student independently.

Funding Sources

Graduate study was supported by the following fellowships: Texas Instruments Fellowship, Silicon Labs Fellowship, Kirchner Food Fellowship, McFerrin Fellowship for Entrepreneurship, as well as a scholarship by the National Council of Science and Technology of Mexico (CONACYT), the Mexiquense Council of Science and Technology (COMECYT) and the Mexican Secretary for Public Education (SEP).

NOMENCLATURE

AC	Alternating Current
AI	Artificial Intelligence
CMOS	Complementary Metal Oxide Semiconductor
DC	Direct Current
EH	Energy Harvesting
EM	Electromagnetic
FET	Field Effect Transistor
GND	Ground
IC	Integrated Circuit
IEEE	Institute of Electrical and Electronic Engineers
IoT	Internet of Things
LED	Light Emitting Diode
LUT	Lookup Table
MFC	Microbial Fuel Cell
ML	Machine Learning
MPP	Maximum Power Point
MPPT	Maximum Power Point Tracking
NVC	Negative Voltage Converter
PA	Precision Agriculture
PCB	Printed Circuit Board
PEM	Proton Exchange Membrane
PMOS	Positive Channel Metal Oxide Semiconductor

PMS	Power Management System
PMU	Power Management Unit
PV	Photovoltaic
PZ	Piezoelectric
VLSI	Very Large Scale Integration
WSN	Wireless Sensor Network

TABLE OF CONTENTS

Page

LIST OF FIGURES

FIGURE Page

LIST OF TABLES

TABLE Page

1. INTRODUCTION

1.1 Motivation

The increasing demand of agricultural goods such as crops and animal-derived products to feed the growing global population has forced farmers and agricultural companies in general to implement technological solutions to their fields to maximize their production. Internet of things (IoT) for agriculture are devices that can collect data from crops and animals not only to improve crop and animal development, but also to prevent the spread of pest or any other disease.

On the other hand, for the introduction of IoT technology to the fields, it is paramount to have access to reliable sources of power, which is very limited for most farms. Therefore, energy storage along with power management systems (PMS) become two critical components for the proper adoption of technology in agriculture.

Energy harvesting (EH) can be found from different sources, on one hand piezoelectric and electromagnetic transducers transform movement into electrical energy and they can be ideal to extract power from the natural movement of animals. On the other hand, solar cells, wind technology and microbial fuel cells, are better suited to be implemented from crop-tailored wireless sensor nodes, that are designed to measure different parameters of a plant and its environment in a confined geographical location. In both cases, the EH system will power an IoT technology that can perform sensor measurements to transmit such information to the internet for further data processing, one of the most important goals of such applications is to provide the farmer with meaningful information to maximize production.

Another important requirement for IoT-based agricultural solutions is not only the reliable data extraction from sensors in the field but also the processing of such data. Data processing can happen in the IoT device itself, the cloud or a combination of both. IoT devices are suited to process raw data from its sensors to only send data with less noise and avoid wasting both power and bandwidth on unusable data. Server infrastructure are appropriate to perform more

complex data analysis, such as the use of statistical methods, pattern recognition, machine learning and artificial intelligence. Such data processing tools are essential for an efficient production of agricultural products.

1.2 Research Impact

This dissertation focused on three main things: first, to provide the guidelines for the design of devices for agriculture considering not only the environmental conditions but also highlighting the intrinsic differences for animal and crop-based IoT applications. The second part focuses on EH techniques to power IoT smart nodes, specifically by transforming energy from the environment into usable energy to power the next generation of internet-enabled devices. Lastly, this dissertation considers the proper interconnection of IoT devices to the cloud, its remote data processing and interpretation to deliver meaningful data to farmers.

Wireless sensor networks, wearables and other IoT products for agriculture demand solutions to make possible and practical to generate power on-the-go to not only extend the battery life of such devices but to potentially fully power them. By having a source of power available through EH not only new, and more power-hungry systems can be implemented in farms, but since the limitation of power is removed, more data can be sampled from the field leading to greater granularity for different variables or the integration of more sensors that can help farmers detect and prevent problems at their farm. However, one of the most important points of this dissertation is the data processing that can theoretically be collected from multiple farms across the world that can help understand how crops and animals are affected by different variables, from unpredicted weather conditions to human-produced farm practices.

This dissertation can potentially benefit individuals and companies that are adopting internet-enabled technology to improve their agricultural outputs. Data scientists working on Artificial Intelligence for agriculture, for example, can benefit from the development of hardware and software presented in this dissertation to accurately extract agricultural-related data at a wide range of sampling rates, that paired with proper algorithms, can potentially find new ways to mitigate and even prevent the spread of pest and disease in agriculture.

1.3 Dissertation organization

This dissertation is organized as follows. Chapter 2 reviews IoT systems for industrial applications along with an introduction to different EH systems centered around smart agriculture. A brief review of IoT applications is discussed. Different EH sources are discussed in terms of their electrical models, electrical properties, output power available. A brief review of power management techniques and different energy storage devices currently used for IoT and EH applications are provided to understand its current limitations in smart agriculture.

Chapter 3 elaborates on the different power management systems for EH applications tailored for IoT. In this section an extensive analysis is given for power conditioning systems. The electrical structure of boost converters along with an operation analysis presented here.

Chapter 4 describes Microbial Fuel Cells (MFC) as an emerging EH source capable of powering wireless sensor networks (WSN) in agriculture. This technology is a novel EH source that can transform organic substrates in wastewater into electricity through a bioelectrochemical process. However, its output power available per liter is very limited, and insufficient to power an IoT smart node. Different state-of-the-art techniques to reach a usable power output from several MFCs are examined as well as their tradeoffs.

In this chapter, a custom PMS is proposed to allow maximum power harvesting from multiple MFCs while providing a regulated output voltage as seen in Figure 1.1. To enable a more efficient and reliable power-harvesting process from multiple MFCs that considers the biochemical limitations of the bacteria to extend its lifetime, a power ranking and MFC health-protection algorithm using an interleaved EH operation was implemented in a microcontroller. A power extraction sub-block of the system includes an ultra-low-power step-up DC-DC converter, which integrates MPPT capabilities. The energy harvesting technique presented in this chapter is tested to power an internet-enabled smart node.

Chapter 5 presents a power management system for technology that can be worn by animals and based on a custom made electromagnetic (EM) transducer as seen in Figure 1.2, a front-end circuit for EH and activity sensing. Due to the AC-output nature of the EM transducer, this

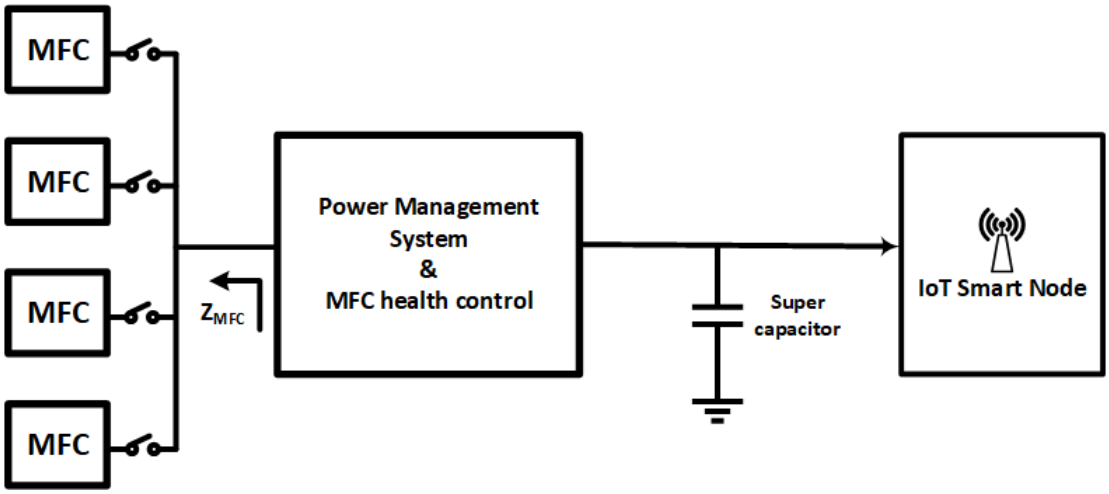

Figure 1.1: Proposed solution for power extraction from multiple MFCs.

chapter proposes a reconfigurable rectifier that can switch from passive operation to a more power-efficient active topology depending on the available power in the system. This work also introduces an activity detection circuit that enables the use of the inherent sensing capabilities of the EM transducer.

In this chapter it is demonstrated that the combination of both, a reconfigurable rectifier and an activity detection circuit, allows the system to gather information like that of an accelerometer regarding the activity of the user, but at net-zero power consumption and lower cost.

Chapter 6 summarizes this dissertation. Appendix A includes the schematic and algorithm for system described in chapter 4. Appendix B includes further test scenarios for the power conditioning system presented in chapter 5.

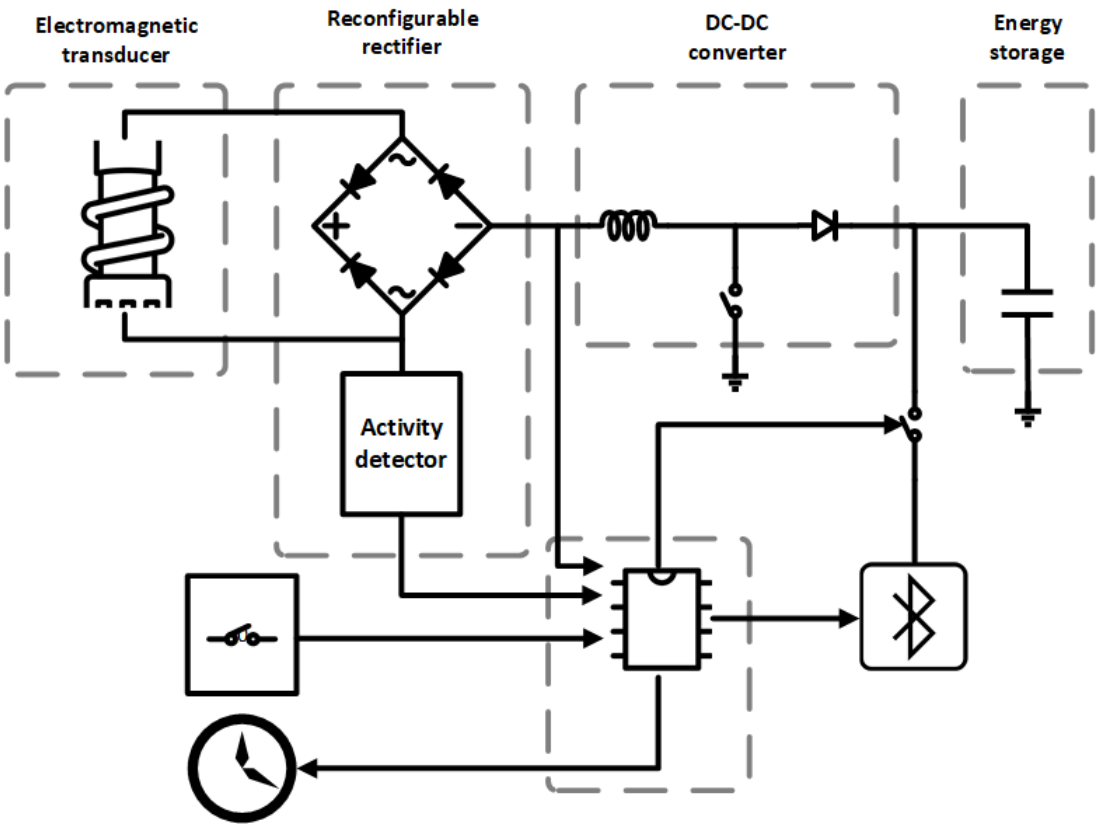

Figure 1.2: Proposed solution for energy harvesting and sensing.

2. ENERGY HARVESTING AND ITS USE IN AGRICULTURE

2.1 Introduction

Agriculture is the breeding of crops and animals, that is, the management of living things and its environments to produce services and goods for a population [1]. Agriculture includes farming; horticulture; animal husbandry; the production of fruits, vegetables, ornamental trees, flowers; the processing, storage and commercialization of agricultural products, to name a few.

The internet of things (IoT), on the other hand, is the interconnection of everyday objects to the cloud to make "things" capable of sending and retrieving information to and from the internet. One goal of this global interconnection of objects is to use such data to make a process more efficient even without human intervention. Therefore, there is potential for task-automatization that IoT can potentially bring for multiple applications in agriculture, transportation, education, healthcare, etc [2, 3, 4, 5, 6].

As IoT devices are set to reach 50 billion connected nodes by 2020 [7, 8] how these devices are powered is becoming an important area of research for multiple reasons, two of which are: first, a growing number of IoT applications are wireless, which sets a first constrain, battery limitation; second, as new and more complex processes are being executed by IoT systems, such as embedded machine learning, IoT devices incur in a higher power expenditure leading to faster battery depletion. Therefore, replacement, recharging or any other type of maintenance of batteries can be very costly, especially in remote areas where harsh conditions can make access to these devices a dangerous or even an impossible human task.

Outdoor applications of IoT can represent an important opportunity for a new wave of self-powered electronics, as it intersects two unique characteristics: on one hand, the advancement of low-power embedded systems and optimized software now allow the design and implementation of highly power-efficient electronics, and on the other hand, the available environmental energy that can be harnessed and recycled back to the device itself.

2.2 IoT and its applications in agriculture

Agriculture represents the backbone for numerous economies around the globe [2] and its modernization is of international interest. As new advances in IoT technology are available to the public, experts are finding new ways to bring it to the hands of farmers.

Farmers require quality data to track the health state of their animals and crops, by using this information farmers can improve their profits by producing high harvest yields. Precision agriculture (PA) is an approach to use precise internet-enabled tools and data about agricultural resources to improve the quality of crops and boost yields [9]. The recollection of data is usually done with sensors in the field, which can sample different variables, send it to the cloud to be processed and then it can look to historical data to predict a pest, for example, and help the farmer make the decision to implement a solution.

There is a big potential for new IoT applications and specially wireless sensor networks in agriculture. However, because of its rural nature, some devices may require to be powered with the energy available in the environment but still expect to have the maintenance cost of their electronic devices to be low. Therefore, energy scavenging can play an important role in the future of global agriculture.

2.3 Challenges in agriculture

Agriculture contributes immensely to the world economy as it is the source of employment, provides food to a growing population and provides vital products to other industries. Some of the most pressing problems in agriculture are presented in this section.

2.3.1 Weather

Agriculture and weather are intimately related as the effects of weather factors are directly reflected in the agricultural productivity being floods and drought two of the most damaging examples. Therefore, weather hazards that affect agriculture are one of the most pressing problems for traditional agriculture around the globe, as weather has proportional implications in the local and global economies.

In the same way, escalating interest in the topic of climate change have favored an extensive approach to the relationship of weather and agriculture and more importantly, to the importance of investing in meteorological advice and services focused solely in agriculture. Reliable weather data has placed meteorology as a paramount factor for national economy.

As explained by James A. Taylor in [10], he mentions that in broad terms, agro-meteorological studies may involve two main approaches. The first one, referred as a meteorological approach, estimates physical potentialities and then calibrates the environmental factors related to agriculture, such as water irrigation systems. And the second one, the agricultural approach, which determines agricultural adaptation by examining the pattern and trend of biological and agricultural systems and assesses them in terms of the physical environment. As James A. Taylor points out, there is a role of the meteorological factors on the incidence and spread of certain diseases in plants and animals.

It is safe to say that the success of a farmer depends on the correct management of a farm based on the reliability and promptness of the weather data available for their farm to make correct decisions on which equipment to use to make proper corrections depending on the weather variations but most importantly success in agriculture is also tied to the prompt responsiveness of the farmer's assets.

It is important to notice that weather challenges need the collaboration not only of farmers and meteorologist, but also economist, sociologists, geographer, statistician and engineers, as it becomes paramount to share different viewpoints in search of novel integrations of different techniques and methods.

2.3.2 Weed and pest

Plants that do not provide any value to the farmer's economic activity or weed represent an important challenge in agriculture since such plants waste nutrients and resources tailored for the crop that the producer wants to grow. Since the mechanical extraction of weed is very labor intensive and not cost effective, the use of pesticides is the most used approach in traditional agriculture. However, since pesticides are usually applied using sprayers to reach as much area as possible in

the minimum time, its use has its secondary adverse effects to humans and the environment.

Chemical methods, namely the application of herbicides, are used by most farmers to fight weeds. Of the considerable amounts of chemical herbicides applied, important quantities are lost because of evaporation or drift, as some of such chemicals reach the soil or the crop but only a very low percentage of the herbicide reaches the targeted undesired weeds. Beyond the potentially adverse ecological impact and the rising concerns of its negative effects on human health of pesticide residues in water and food, herbicides and their application represent an important problem faced in current agricultural practices. These concerns have led to governmental regulations in several countries and an increasing demand for organic food produced without herbicides. Therefore, an essential part of improving the efficiency of agriculture is through new weed control technology [11].

Another big problem in farming appear as insects and other animals are attracted to crops to spoil them. The current practices to fight insects use pesticides to control insects, which like the use of herbicides, very large quantities affect not only soil and drinking water but also other insects that are beneficial to the ecosystem around as it is the case of bees, for example.

Genetically modified crops have also been raised as an alternative to create more weather, pest and herbicide-resistant crops.

2.3.3 Resource depletion: water and soil

Water is essential for agriculture, and due to climate change and the rise of urbanization it also represents one of the most pressing challenges globally. Without proper water sources, food production cannot be viable. Therefore, water management emerges as necessary to ensure food production for a constant growing population. Even more importantlt, in the [12] report published in 2012, the Organization for Economic Co-operation and Development estimates that around 1.5 billion people live today in areas severely affected by water scarcity. According to the report, the number will increase to nearly 4 billion by 2050, which will trigger a global food crisis unless the current approach to water consumption changes.

Agriculture already consumes two thirds of the world's water and forecasts show that by 2050,

we will need as twice as much food as we produce today for the more than 9 billion people that will inhabit the world. It is important to highlight that agriculture is also a major source of water pollution in the form of livestock residues, pesticide and agricultural fertilizer run-off and all contribute to the pollution of groundwater and waterways. In the same way, a significant impact in the agricultural sector is due to intensive groundwater pumping for irrigation depletes aquifers [13].

A mayor contributor of water pollution in agriculture is the result of inefficient use of pesticides, herbicides, fertilizers and other organic and non-organic matter lost into water systems. As mentioned in [14] "Clean water is vital in securing economic benefits for agriculture and other sectors, meeting human health needs, maintaining viable ecosystems, and providing societal benefits, such as the recreational, visual amenity and cultural values society attaches to water systems."

Resource depletion and the costs of industrial agriculture are closely tied to water, and sophisticated irrigation systems are born as direct solution to this problem. More technologies are needed to reduce water consumption, as is the case of more efficient irrigation methods or agricultural systems such as hydroponic warehouses that have the potential to reduce more than 25% of water consumption as opposed to farms with such technologies.

2.3.4 Further problems and challenges

Agriculture face multiple challenges, such as resource depletion, associated to intensive water usage, monoculture that degrades farmland making the use of fertilizers mandatory, not to mention the risk and uncertainty that comes with changes in weather and the appearance of pest and weed. Additionally, while cultural shifts in the past few years have led to a large population concentration in urban areas , more recently, labor in agriculture is also becoming scarcer as immigration policies become stricter in the US .

Because of multiple challenges faced in traditional agriculture, and as a result of an urgent and substantial need for more climate resilience, indoor farming close to or inside urban areas has raised as a new form of agricultural cultivation to grow products closer to where they are consumed. However, small greenhouses and vertical farming facilities usually lack the management tools and equipment to be operated more efficiently and meet the demands of their local markets at a

competitive price .

Farming at any scale is a business, and horticulture, and more specifically flower growing is a clear example of a high value crop that can be commercialized by small urban farmers. However, technology for vertical farms or greenhouses for horticulture aimed for urban farmers, is very capital intensive or has very poor efficiency to be profitable, thus limiting its potential for a larger adoption. It is worth mentioning that the poor or nonexistent traceability technology for most horticultural products is a missed opportunity to improve the confidence of their buyers in cities.

2.4 Energy-harvesting-based IoT system

A simplistic three layer model of IoT [15] consist of objects layer that is mainly formed of sensors; a network layer that integrates transceivers that communicate the device with the cloud; and the application layer which is the user interface that provides with meaningful information to the customer.

The introduction of EH to IoT application involves the use of an energy harvester, which transforms the energy in the environment to electricity; a power management unit that transform raw energy into usable energy for the embedded system; and an energy storage element that is in charge of providing power to the application when there is a need to transmit or receive data when ambient energy is intermittent or nonexistent at all.

2.5 Energy harvesting sources

Different transducers can be used for EH while also using the outdoor characteristics of agricultural applications. Some of the most prolific EH technologies and its electronic models [16] are presented in this subsection.

2.5.1 Photovoltaic

Solar cells are among the most popular EH sources [17]. Photovoltaic (PV) cells transform light into electricity by using the photovoltaic principle where light absorption generates in the solar cell an electron-hole pair generation, thus carrier separate and build up the open circuit voltage V_{oc} across the p-n junction Fig. 2.1.

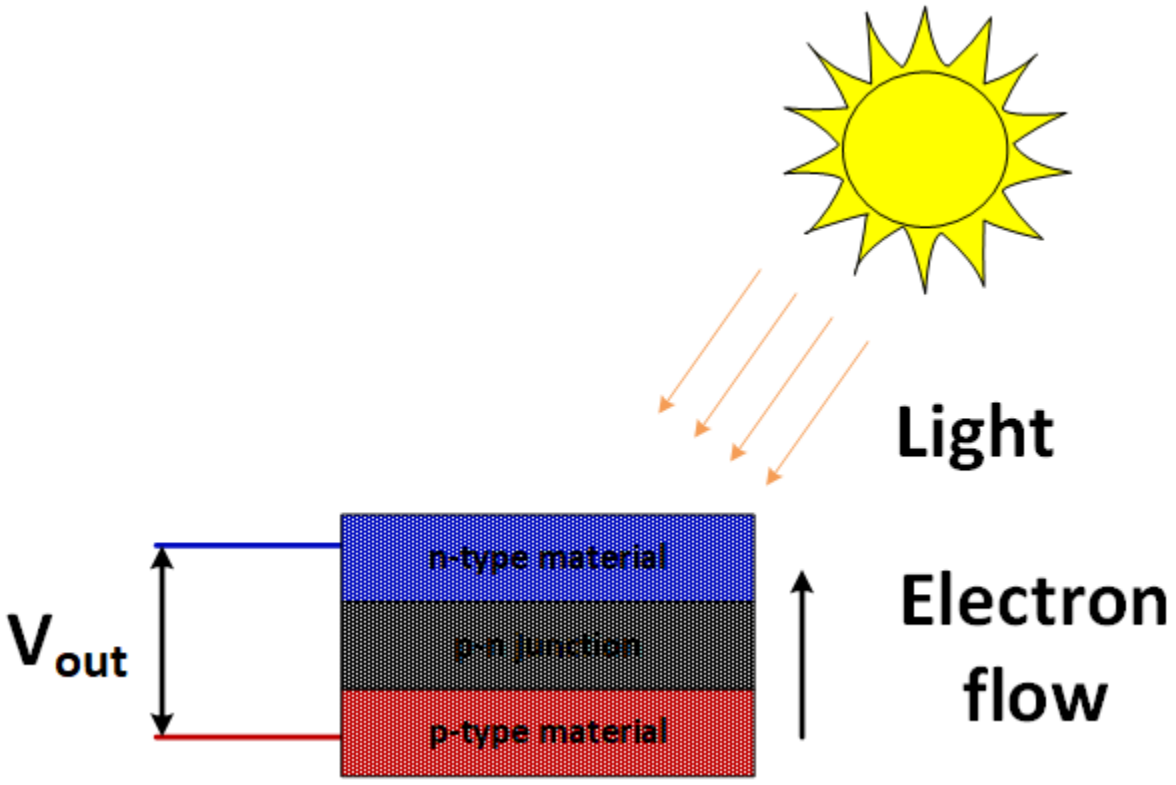

Figure 2.1: Simplified photovoltaic panel.

Because of its construction, a solar cell exhibits a rectifying behavior and its current can be determined by 2.1.

$$I = I_{ph} - I_d \tag{2.1}$$

Where:

$$I_d = I_0 \left(exp^{qV/KT} - 1 \right) \tag{2.2}$$

The open circuit voltage of the solar cell can be determined as:

$$V_{oc} = \frac{KT}{q} \log \left(1 + \frac{I_{ph}}{I_0} \right) \tag{2.3}$$

Figure 2.2 presents an electrical model of the solar cell where R_s is a series resistance, R_{sh} a

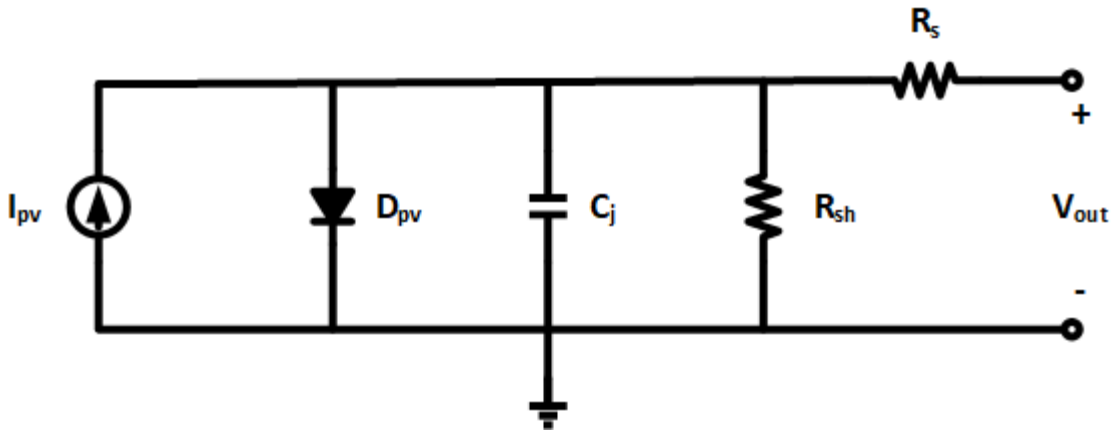

Figure 2.2: Electrical model of a photovoltaic panel.

shunt resistance, a rectifying diode is presented as D_{pv} in parallel with the current produced by the solar cell shown as I_{pv}.

2.5.2 Thermoelectric generators

Thermoelectric generators (TEGs) can transform gradients of temperature into electricity mainly throught the Seebeck effect [18] and the Peltier effect. As seen in Fig. 2.3, TEGs are formed by several alternate pairs of n- and p-type pieces serially connected. When a hot surface is applied to one side of the TEG and cold surface to the opposite side a temperature gradient is formed and power is generated. This type of transducer finds some of its use in applications of high heat loss, for example in internal combustion motors.

The relationship of a temperature gradient, existing between hot and cold surfaces, and output voltage follows the Seebeck effect and this is expressed in Eq. 2.4, where α_{H-C} is the Seebeck coefficient and ΔT is the temperature difference between surfaces.

$$V_{out} = \alpha_{H-C}\Delta T \tag{2.4}$$

The electrical representation of a TEG is presented in Fig. 2.4, where V_{TEG} is the voltage generated by this transducer when a temperature gradient is applied between both surfaces, and R_{TEG} is its equivalent series resistance.

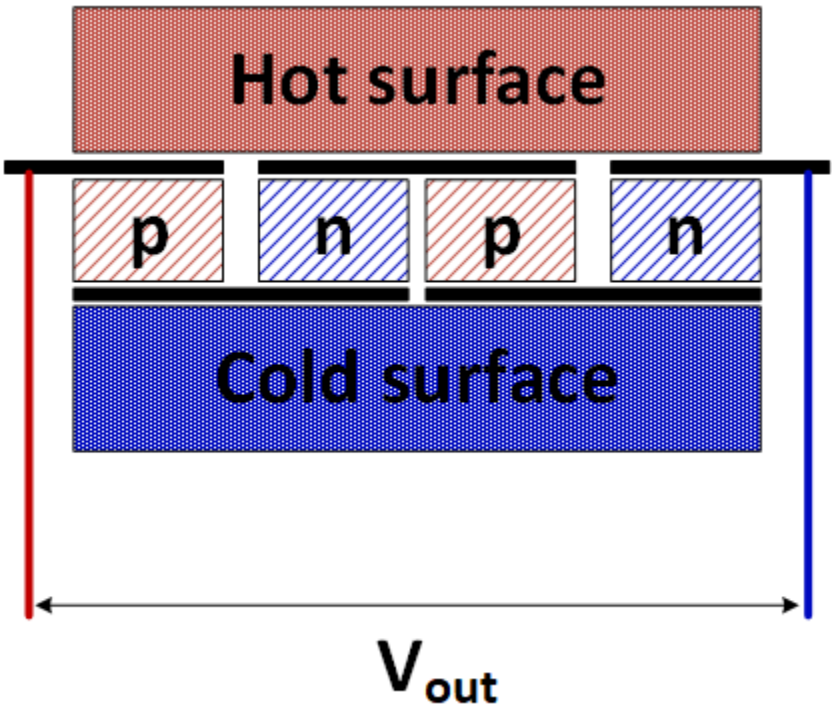

Figure 2.3: Thermoelectric generator transducer.

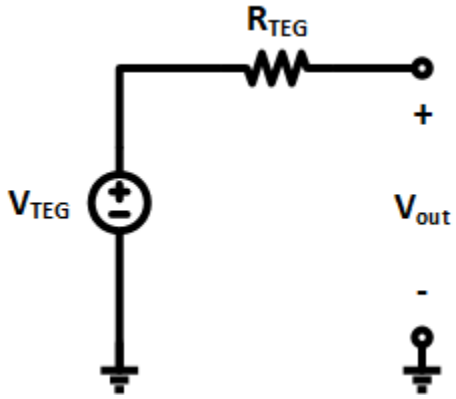

Figure 2.4: Thermoelectric generator electrical model.

2.5.3 Wind energy harvesting

Wind energy harvesting utilizes the ideas of large scale wind power generators, as the one shown in Fig. 2.5, for small scale applications, in a way that mini generators can provide energy

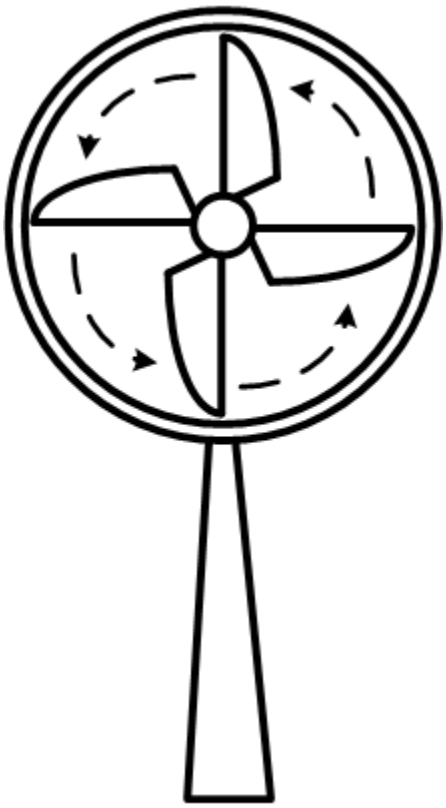

Figure 2.5: Wind powered generator

to a smart sensor, for example.

The electrical power delivered by a flow-driven generator can be expressed as Eq. 2.5 according to [19].

$$P_{out} = \eta C_p \frac{1}{2} \rho A V^3 \tag{2.5}$$

A simplified electromechanical circuit is shown in Fig. 2.6. Where I_{drive} is the wind flow power, M represents the mass of the rotational parts inside the generator, Cm is the coefficient of frictional torque, L_{in} and R_{in} refer to the intrinsic inductance and resistance of the internal generator, respectively [16].

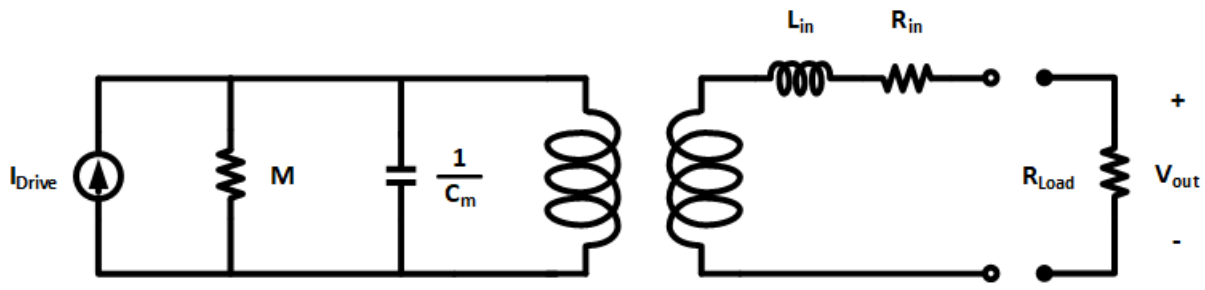

Figure 2.6: Wind powered generator electrical model

2.5.4 Kinetic energy harvesting

Due to its ubiquitousness, an attractive source of ambient energy is found in motion. Multiple ways to convert vibration to electrical energy exist and have been explored for kinetic-based EH [20] with output power ranging from a few microwatts to several miliwatts.

In agriculture specifically, WSN and IoT applications tailored to animals are a perfect candidate for motion-based transducers as this type of energy source is less dependent in the weather and relies more on the activity of an animal.

In this section, two of the most well-known transducers that uses vibration to generate electricity, namely piezoelectric [21] and electromagnetic harvesters [22], are presented.

2.5.4.1 Piezoelectric

A piezoelectric transducer is presented in Fig. 2.7. An important property of these devices is their high electromechanical coupling [23] which makes it suited to convert energy in the form of vibration to electricity. Vibrational energy can be found in numerous automotive and industrial settings, from the movement in motors to bridge repetitive displacements.

Piezoelectric generators can bend to become electrically polarized. The resonance at which these transducers vibrate determines its output power. Therefore its maximum power happens at its natural frequency ω_n, and it is given by:

$$P_{max} = \frac{mY^2\omega_n^3}{4\zeta_T} \tag{2.6}$$

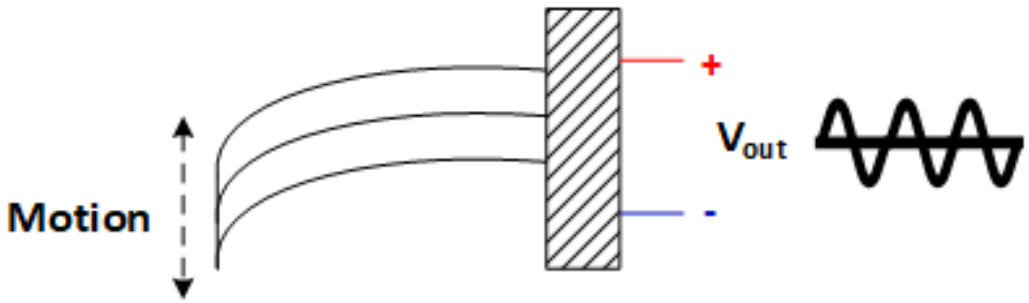

Figure 2.7: Piezoelectric transducer.

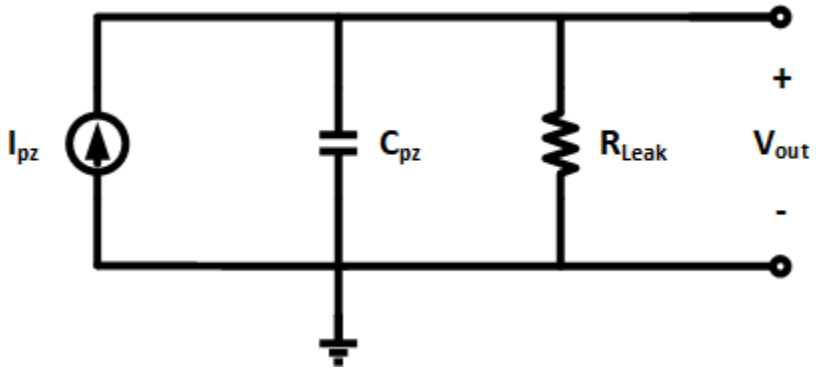

Figure 2.8: Piezoelectric transducer electrical model.

Where ζ_T is the damping factor; Y is the amplitude displacement; and m is the seismic mass that drives the shaking movement of the piezoelectric transducer.

An electrical model of this transducer is presented in Fig. 2.8 and it shows the relationship of the ac nature current source of this energy harvesting, denoted as I_{pz}, a piezoelectric internal capacitance C_{pz} and a leakage current R_{Leak}.

2.5.4.2 Electromagnetic

Electromagnetic transducers, Fig. 2.9, produce energy by the interaction of a magnet and a coil, that produces a magnetic domain that is translated into an electrical domain as shown in Fig. 2.10.

Further analysis of electromagnetic transducers is presented in chapter 5.

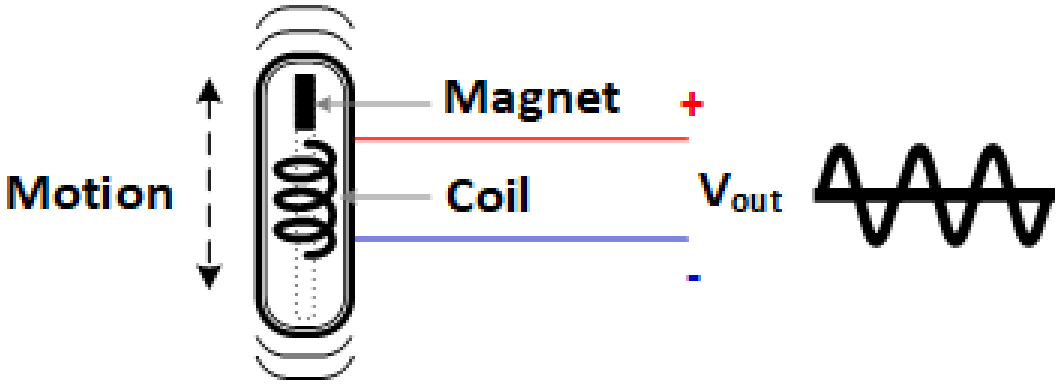

Figure 2.9: Electromagnetic transducer.

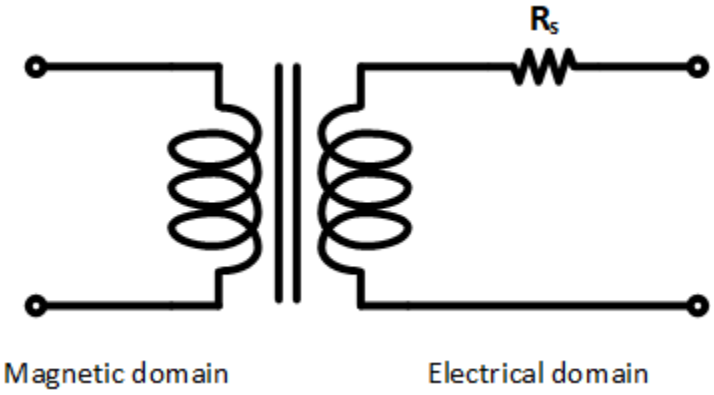

Figure 2.10: Electromagnetic transducer electrical model.

2.5.5 Radiofrequency harvester

Our world is transforming into a series of wireless connected devices. Frequency waves transmitted from Wi-Fi hotpots, AM and FM stations, cellular towers and so on, have the potential to be harvested as resembled in in Fig. 2.11.

Although RF power can be ubiquitous in urban areas, its power is still very limited. Its incident power density S directly depends on the incident electric field strength E, the free space characteristic impedance [16] and the source antenna such as how well aligned antennas are and the distance between emitter and receiver.

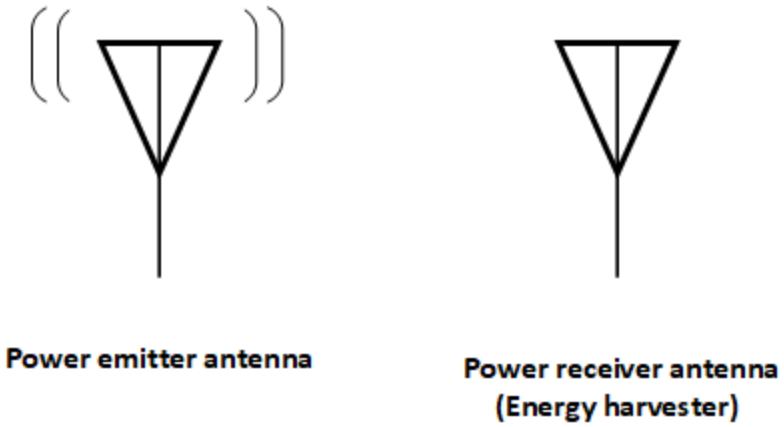

Figure 2.11: Radiofrequency harvester.

$$S = \frac{E^2}{Z_0} \tag{2.7}$$

2.5.6 Emerging energy harvesting sources

Different technological breakthroughs have made possible the design and construction of previous EH sources. As new technologies evolve numerous new discoveries are made scientist open the door to new ways to harvesting energy.

One of the most interesting areas of research for energy harvesting sources is the intersection of electrochemical processes [24] and highly-efficient embedded systems. Such devices have the potential of converting chemical substances into electricity.

2.5.6.1 Microbial fuel cells

Microbial fuel cells (MFC) are a promising technology that can transform organic substrates in wastewater into electricity and clean water [25]. In the anode chamber of an MFC, see Fig. 2.12, living bacteria oxidizes organic materials in wastewater and releases electrons that builds up to generate an output voltage while protons travel from the anode chamber to the cathode chamber through a proton-exchange membrane (PEM). Hydrogen protons interact with oxygen in the cathode chamber to generate water.

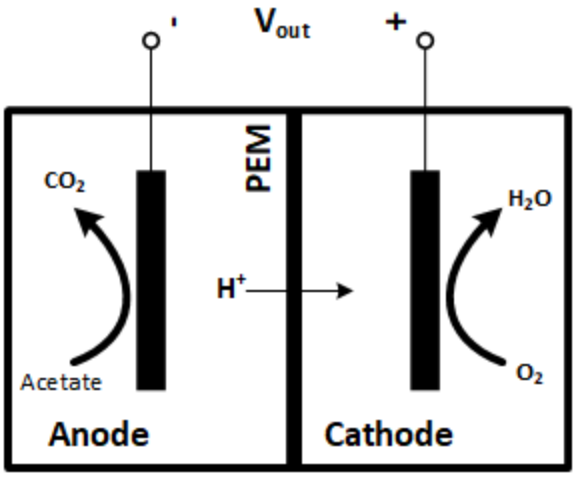

Figure 2.12: Microbial Fuel Cell schematic.

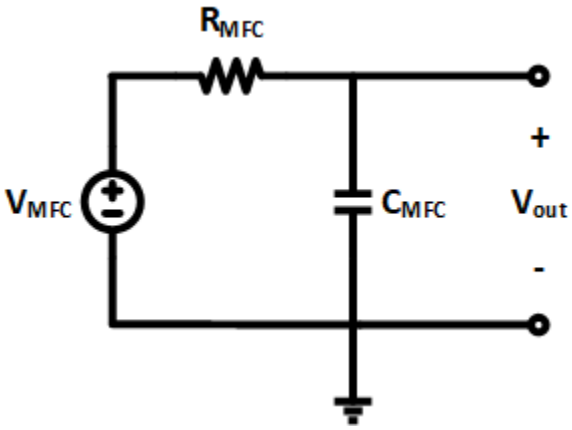

Figure 2.13: Microbial Fuel Cell electrical model.

A simplified electrical model of an MFC in Fig. 2.13 is composed by an MFC voltage source V_{MFC}, in series with the cell's characteristic resistance denoted as R_{MFC} and an output capacitor labeled as C_{MFC}. Further analysis of MFC are discussed in chapter 4.

2.6 Power Management Unit

For an IoT to efficiently use the energy of a transducer needs a power conditioning stage which in the case of ac transducers as it is the case of piezoelectric, radiofrequency, ac power generators a rectification stage is mandatory.

When the input voltage is in dc form then a switching converter can convert this 'raw' input voltage into voltage levels that are useful for microcontrollers, transceivers, sensors and multiple other peripherals integrated an IoT device.

Finally, certain elements in an IoT device may be less tolerant to voltage variation due to ripple from a switching converter. Therefore, a linear regulator may be required to provide source voltages and voltage references in such embedded systems.

2.7 Energy storage elements

Due to the intermittency nature of EH, a place to store energy after it has been extracted from a transducer is critical to ensure the proper performance of an IoT device. Two of the most prolific technologies are batteries and capacitors, being super capacitors the center of study in this dissertation because of the high power needs of IoT modules at the time of writing this thesis.

2.7.1 Batteries

Batteries are build from electrochemical cells capable of storing charges and are mainly used to slowly deliver them to electronic devices. Among the different chemistry used in batteries, Lithium ion has become the most popular for consumer electronics as it offers high power density at a reasonable size and weight and it can be rechargeable.

The cost of integrating lithium ion cell in embedded systems have been constantly decreasing at a point where can be integrated in larger IoT applications in the automotive industry.

2.7.2 Super capacitor

A clear advantage of supercapacitors is that it possesses high power delivery density and it can be charged and discharged more times than a battery in its lifetime. However, super capacitors have two important drawbacks, static leakage and size, which makes them unfeasible for applications that require high power density and require a steady power delivery for prolonged periods of time.

2.8 Relevance of energy harvesting in agriculture

As data analysis is becoming more useful with the advent of machine learning and artificial intelligence, sensors are also becoming crucial for agriculture. Therefore, there is a great interest in finding ways to provide ways to power such wireless sensor networks efficiently.

The advent of EH can reduce cost of production and maintenance for IoT devices in agriculture are likely to go down, this can represent an important factor to ease the adoption of such technologies to small holder farmers in developing countries.

Also, it possible to use this as an educational tool and even to help enable industrial-grade farming in urban areas.

2.9 Proposed agricultural implementation

The proposed agricultural implementation is divided in two:

The first one aimed to crop agriculture in the orchids category, which includes lettuce. Specifically, WSN that can extract different environmental variables, select the best ambient conditions and a subsequent implementation that can recollect data regarding the nutrient provided to a specific crop and then communicate the collected information to multiple farmers around the world.

And the second work related to a device tailored for farm animals, being cattle a popular example. The purpose of this IoT device is to track an animal and learn more about their behavior and correlate such data to information valuable to the farmer such as their caloric expenditure through movement throughout the day that can be of importance when selecting the diet of the animal.

It is worth mentioning that the application designed for moving animals that can also have other application such as in the consumer electronics market tailored to humans.

3. FUNDAMENTALS OF ENERGY HARVESTING POWER-MANAGEMENT SYSTEMS

3.1 Introduction

Modern embedded systems require multiple voltage and current levels to power their different sub-blocks (such as microprocessors, sensors, peripherals, transceivers, to name a few) according to a set of specifications. It is very unlikely for a single power source to provide the different power levels required reliably; therefore, producing consistent voltage and current levels for the different components in the energy-harvesting-based embedded system requires a suitable power processing unit.

First and foremost, such devices need a power supply, namely a transducer and/or a battery. In the specific case of ac-based EH systems a proper AC-to-DC power transformation is mandatory, which can be achieved by using a rectifier as shown in Fig. 3.1.

In this work, the energy harvesting sources and applications explored are in the low power range, which make them a great candidate for rectifiers implemented in CMOS technology. CMOS rectifiers transform raw AC power signals from transducers and convert them into DC power signals ready for a subsequent stage in the power processing unit. Another advantage of CMOS rectification is that it can be very efficient mainly in terms of the threshold voltage needed for it to achieve rectification or voltage conversion efficiency and to reduce its on resistance to improve the rectification stage power conversion efficiency.

Due to the low power characteristics of the transducers using in EH a DC-DC step-up converter is required as seen in Fig. 3.2. The main goal of this converter is to step-up the output voltage of the DC source to levels that can be used for other blocks, such as sensors. The operation of this converter involves the storage of energy in magnetic or electric fields in inductors or capacitors, respectively, and then switching such components to deliver the stored in series with the source energy to the output load, by doing so an effective increase of the output voltage/current levels is seen at the output of this step-up converter. The ratio at which the input voltage is boosted and

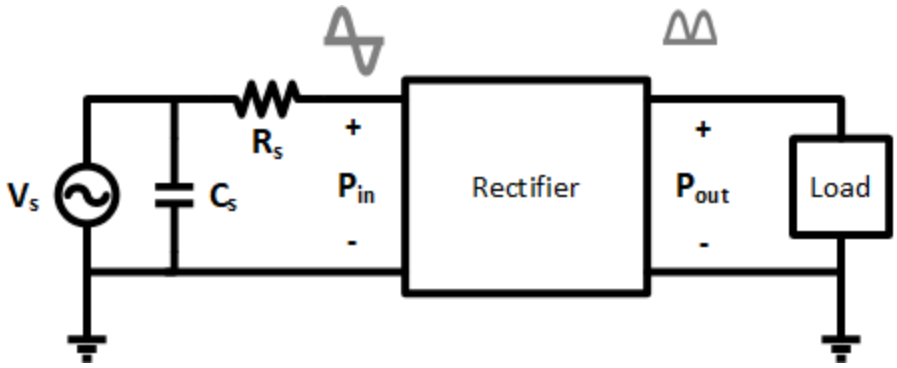

Figure 3.1: Rectifier for an EH source.

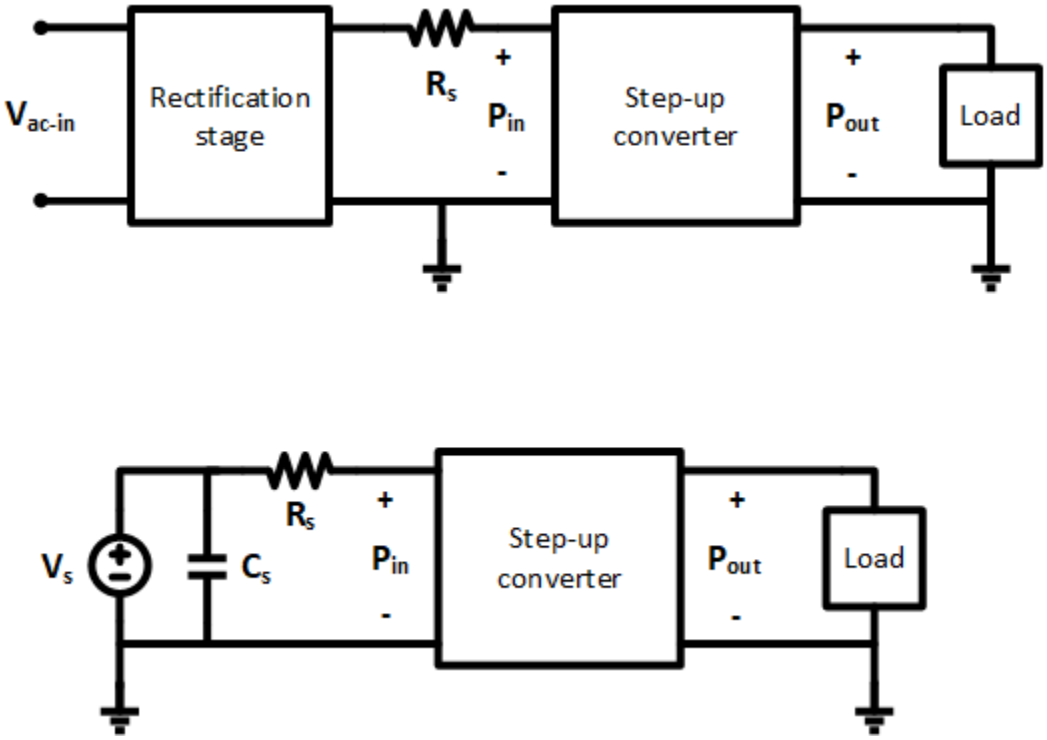

Figure 3.2: DC-DC converter with rectified input (top) DC-DC converter with EH source (bottom).

maintained at the output is determined by this extract-accumulate-deliver cycle.

Since the available power from an EH source is usually very intermittent a way to store energy to proper levels to allow a transceiver send and receive data packets is needed. Two of the most prolific ways to store charges for an EH application is by using rechargeable batteries or super capacitors.

Different transducers present a specific impedance at its output, and even more importantly, all of them generate their power depending on its characteristics, while some of them depend on heat, movement or sunlight, as is the case of thermoelectric generator, piezoelectric and photovoltaic, respectively, other EH sources depend on living bacteria to produce energy, as is the case of Microbial Fuel Cells. Algorithms, that can control switching converters according to the specifications of an EH source can provide a better power efficiency and increase the life of such power sources by considering how its internal components wear off. Algorithms and embedded systems are also required in an EH system to sample sensors and to transmit data.

This chapter elaborates on the fundamentals of rectifiers, switching converters, storage elements, embedded systems and embedded software.

3.2 Rectification

Passive energy harvesting from mechanical vibration is naturally presented in the form of an AC power supply, and even though the study of AC power supplies that eliminate the need of the AC-to-DC conversion in EH have been the main case of study for numerous works [26, 27], most embedded systems still require a regulated DC input voltage source. All of this, makes the study of high-efficient, low-power rectifiers for EH an unavoidable challenge [28].

3.3 Passive rectification

A rectification circuit is a crucial interface for EH and it is essentially the conversion of alternating current (AC) to direct current (DC). Such interface involves a circuit to ideally allow a unidirectional flow of charges by blocking the power path when the rectified voltage becomes dominant with respect to the input AC signal.

In this subsection we will review different passive rectification circuits for AC-to-DC power conditioning.

3.3.1 Diode rectifier

Diodes in its ideal form, rectify AC signals very efficiently, as they do not present current resistance and a zero threshold voltage. On the other hand, he main drawbacks of real diodes are

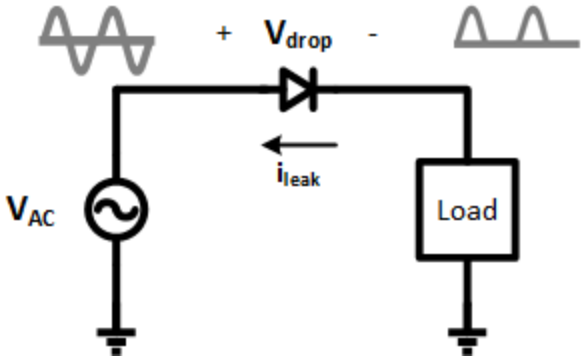

Figure 3.3: Half wave diode rectifier.

mainly presented first in leakage current when diodes are reverse biased, which can considerable hurt its rectification efficiency and second the voltage drop when diodes are forward biased [29] which makes them unsuitable for small-voltages application as in EH [30].

The simplest topology of a rectifier in its passive form is a circuit based on a single diode as presented in Fig. 3.3, this circuit is also known as a half-wave rectifier. Despite using the minimum number of components, this topology is also one of the less efficient rectification circuits because it only allows one half of an AC waveform to be presented to the load circuit; therefore, it only delivers half the available power from the source.

The full rectification of an AC waveform can be achieved by using a full-wave rectifier. The simplest and most prevalent circuit oriented to EH is a full-bridge diode rectifier [31, 32], presented in Fig. 3.4, this standard topology [33, 34] is composed by four rectification diodes and is often used as the benchmark to other works. Among the advantages of this basic topology, is that it can be used in self-startup systems as it does not require external circuits nor pre-stored energy to operate.

3.3.2 Diode-connected CMOS rectifier

Schottky diodes are available to implement in standard CMOS processes [35], but since they are not directly compatible to CMOS processes, the integration of schottky diodes result in higher production cost that makes them less attractive for most consumer electronic applications. For this

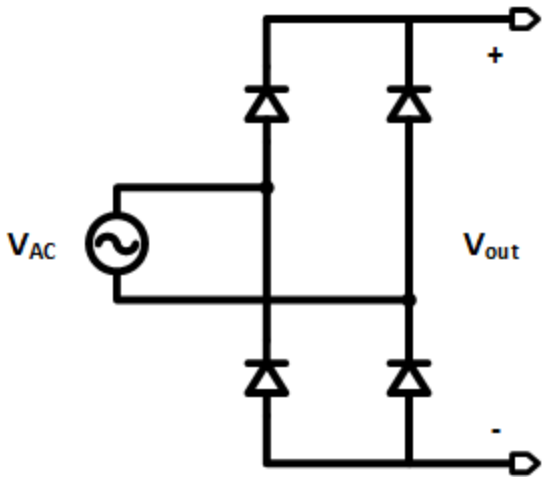

Figure 3.4: Full-bridge diode rectifier.

reason, the most used form of integration of diodes in standard CMOS processes are commonly done with diode-connected MOS transistors. As shown in Fig. 3.5, gates of MOS transistors are shortened to their source resembling a two terminal device that in general terms, behaves as a diode.

Even though this passive implementation of a rectifier has a higher power efficiency and small output ripples when compared to half-wave rectifiers [36], its efficiency is still affected by its threshold voltage V_{th}, Eq. 3.1. However, and even more importantly, in this configuration diode-tied MOS transistors are not completely OFF or ON in this configuration [37], this effect increases the voltage drop across two devices and allows current leakage in the remaining transistors which in turn deteriorates the overall efficiency of the rectifier and therefore, decreased battery life of the entire EH application.

$$V_{rect} = V_{in} - (|V_{thM1}| + |V_{thM2}|) \tag{3.1}$$

As noted in [38], due to minimization of transistor technologies sizes, which allow the integration of more sophisticated functionalities into a microchip, structures as the diode-connected CMOS rectifier become increasingly inefficient. This is because in the diode-connected CMOS rectifier, the threshold voltage determines the minimum voltage level needed before the input sig-

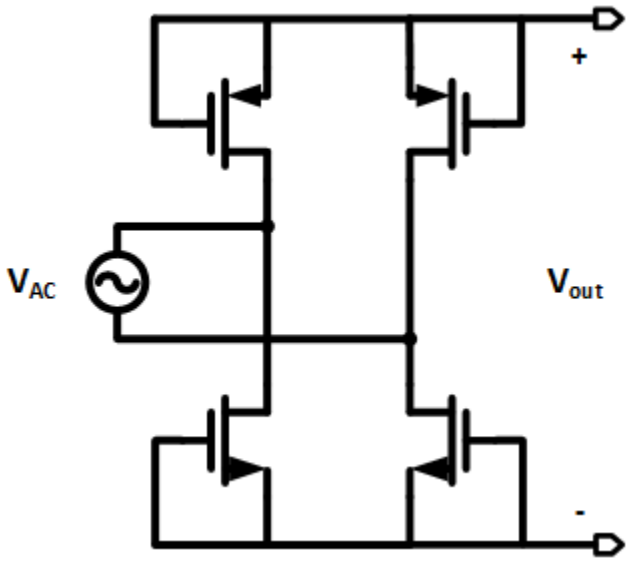

Figure 3.5: Diode-connected CMOS rectifier.

nal can be rectified. Therefore, one main constraint that leads to poor efficiency in low-voltage processes, is the ratio between power supply and threshold voltage of transistors.

3.3.3 Gate cross-coupled NMOS rectifier

A gate cross-coupled NMOS rectifier is shown in Fig. 3.6. In this circuit, since the input signal is connected to the gate of each cross coupled transistor, it is driven with a higher voltage swing as which allows an improved switch conductivity when compared to a diode-tied topology. This is expressed in Eq. 3.2.

$$g_{ds} = \sqrt{\mu \cdot C_{OX} \cdot \frac{W}{L}(V_{SG} - |V_{TH}|)} \tag{3.2}$$

Where W and L are the width and length of the transistors, and μ is the charge-carrier effective mobility and C_{OX} is the capacitance of the oxide layer

In the gate cross-coupled NMOS rectifier, at every source AC cycle, the effective voltage drop of a crosscoupled MOS switch, formulated in Eq. 3.3, replaces the threshold voltage of a diode-connected MOS transistor. Also, as compared to diode-connected CMOS rectifiers, the voltage swing driving the CMOS transistors of a gate cross-coupled NMOS rectifier is higher. Both char-

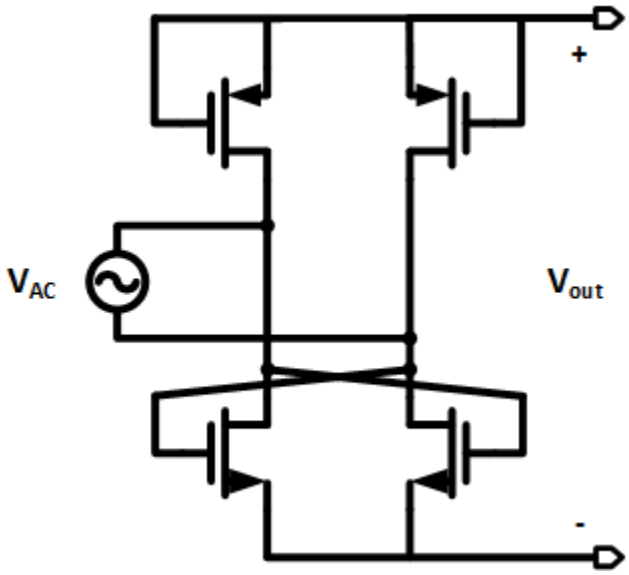

Figure 3.6: Gate cross-coupled NMOS rectifier.

acteristics allows a better MOS conduction and lower back leakage currents. As a result, the power conversion efficiency can be expected to improve for low input voltages [39].

$$V_{eff} = \sqrt{\frac{2i_d}{\mu \cdot C_{OX} \cdot \frac{W}{L}}} \tag{3.3}$$

The key advantage of an input-driven transistor-based passive rectifier is that the forward voltage drop is considerably reduced, especially when a combination of parallel transistor switches is used [40].

However, a threshold voltage drop from a diode-tied MOS transistor is always present in the power path, which considerable diminishes its power efficiency.

3.3.4 Cross-coupled rectifier

In a cross-coupled rectifier presented in [41] and shown in Fig. 3.7, the MOS transistors that are at the two main power paths are cross-coupled.

The main benefit of this power conditioning topology is that its low threshold voltage is around 70% [42]. On the other hand, this topology also shows a poor power efficiency due to parasitics

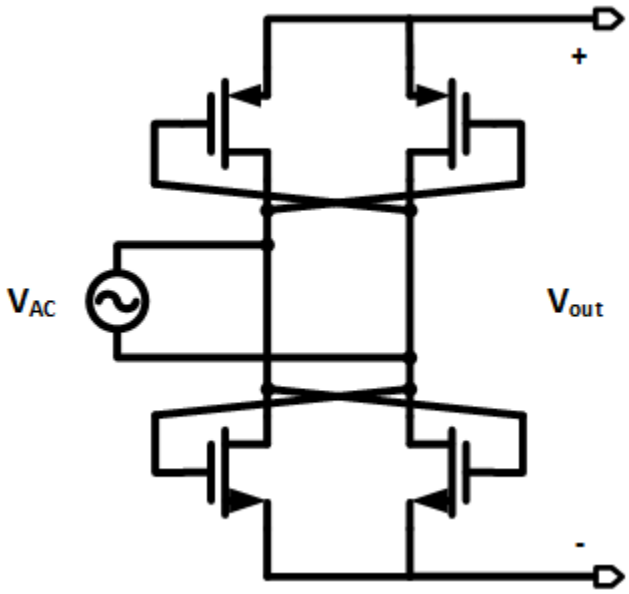

Figure 3.7: Cross-coupled rectifier.

[43].

3.4 Active rectification

Multiple works have shown that active rectifiers can be more efficient [44, 45, 46]. The circuit diagram shown in Fig. 3.8 displays a basic structure of an active half-wave rectifier, where a MOS transistor and a comparator replaces the diode in Fig. 3.3. Active rectifiers are driven by an active control circuit based on a comparator that provides the proper signal depending on the input (V_{AC}) and output (V_{out}) levels at the rectifier.

The advantage of using a control circuit as resembled in Fig. 3.9 is that, each MOSFET can not only switch ON and OFF faster but to provide higher gate-drive voltages, boosting its power efficiency and its switch conductivity.

3.4.1 Active rectifier with cross-coupled PMOS switches

The circuit shown in Fig. 3.10 resembles an active rectifier with cross-coupled PMOS switches which is a power conditioning circuit that has been integrated in previous works [47, 48].

This topology uses two cross-coupled devices that are driven by two comparators that also turn

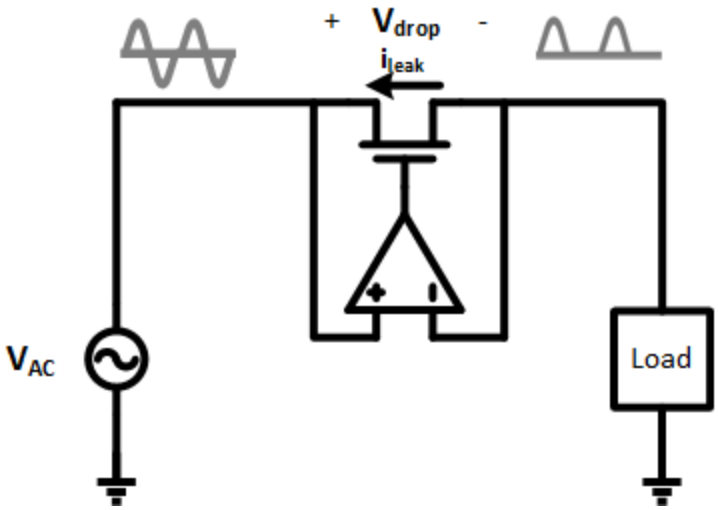

Figure 3.8: Active diode used as a half-wave rectifier.

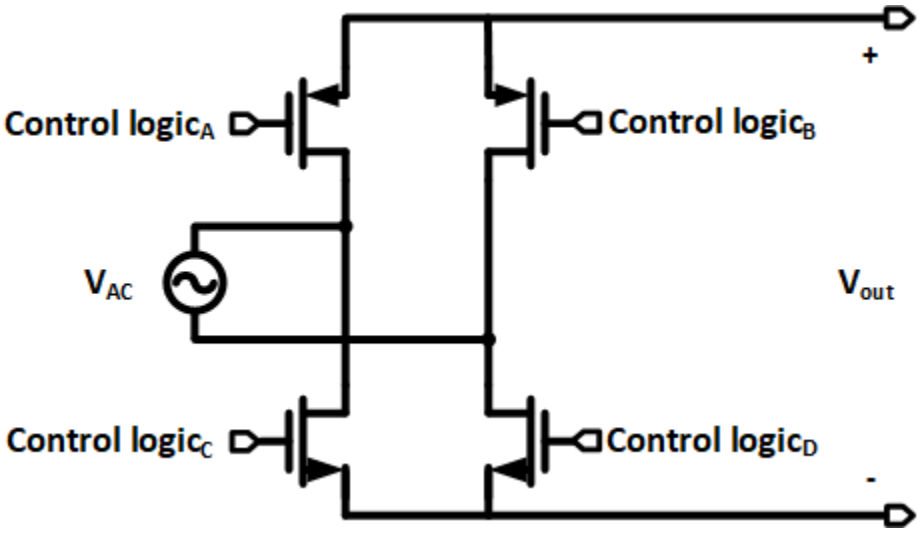

Figure 3.9: Active rectifier.

ON and OFF the gates, and consecutively, the power path branch of the rectifier according to its input signal.

3.5 Design implementation considerations

Passive and active rectifiers offer different advantages, while active rectifiers offer higher power conversion efficiencies, passive rectifiers do not require additional extra static power to operate.

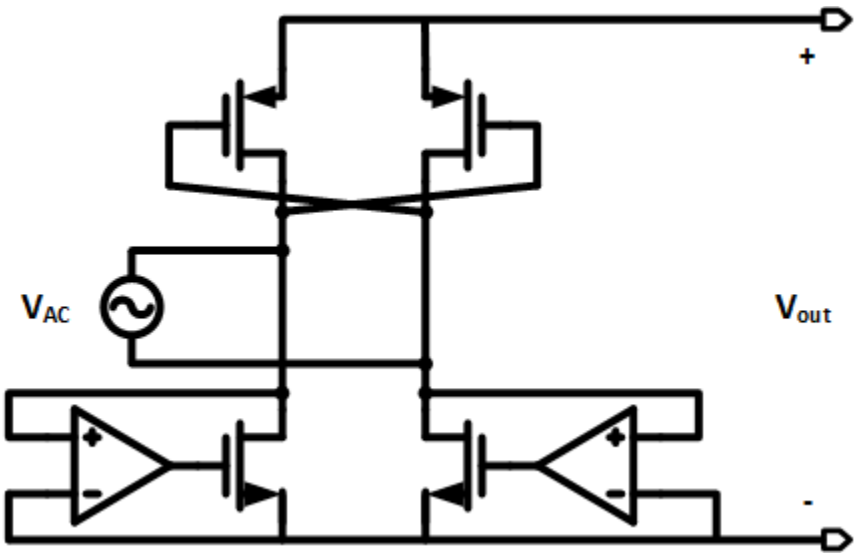

Figure 3.10: Active rectifier with cross-coupled PMOS switches.

One important implementation consideration center on the availability of power for the EH system to operate, but more importantly, if the system can rely in such source of power at the beginning of its operation. As stated before, passive power conditioning circuits do not require additional power to operate, which can make them very attractive for self-startup systems. On the other hand, active circuits can utilize alternatives such as having an auxiliary power source or even using a combination of a low efficient rectifier-mode for startup and a more efficient rectifier-mode after startup as presented in [49].

Another critical design consideration is power efficiency. This is mainly considering that while active topologies are usually more efficient in terms of better blocking reverse leakage and lower voltage drops across the MOS transistors, it should be noticed that active rectifiers consume static power to operate that may offset the benefits they offer.

3.5.1 Performance metrics

Despite each power conditioning topology offer their own benefits and disadvantages, the following are metrics that can be used to compare their performance.

3.5.1.1 Voltage conversion ratio

The voltage conversion ratio (VCR) is defined as the ratio of the average output voltage to the peak magnitude of the AC input voltage Eq. 3.4.

$$VCR = \frac{V_{out-av}}{|V_{in}|} \tag{3.4}$$

3.5.1.2 Power conversion efficiency

Power conversion efficiency (PCE) is defined as the ratio of the output power to the input power as shown in Eq. 3.5. The PCE takes into account all drops in the components in the power path, and therefore it provides with a figure that subtracts the power dissipated by the internal circuitry in series with the output load.

$$PCE = \frac{P_{out}}{P_{in}} \times 100 \tag{3.5}$$

$$PCE = \frac{V_{out}}{V_{in}} \times \frac{I_{out}}{I_{in}} \times 100 \tag{3.6}$$

$$PCE = \frac{V_{out}}{V_{out} + V_{drop}} \times \frac{I_{out}}{I_{out} + I_{leak}} \times 100 \tag{3.7}$$

3.6 Switching converter fundamentals

Modern embedded systems for agriculture, as well as mainstream consumer electronics, integrate numerous electronic elements such as analog operational amplifiers and digital logic gates [50]. Inside such electronic systems multiple power requirements are needed, for example analog circuits usually specify a minimum voltage supply to ensure an acceptable performance. In the same way, low power consumption is always desirable to offer the maximum efficiency, in the specific case of digital circuits Eq. 3.8, provides a look at how power consumption is affected by, f which is the output switching frequency, C the load capacitance and V the supply voltage. As it can

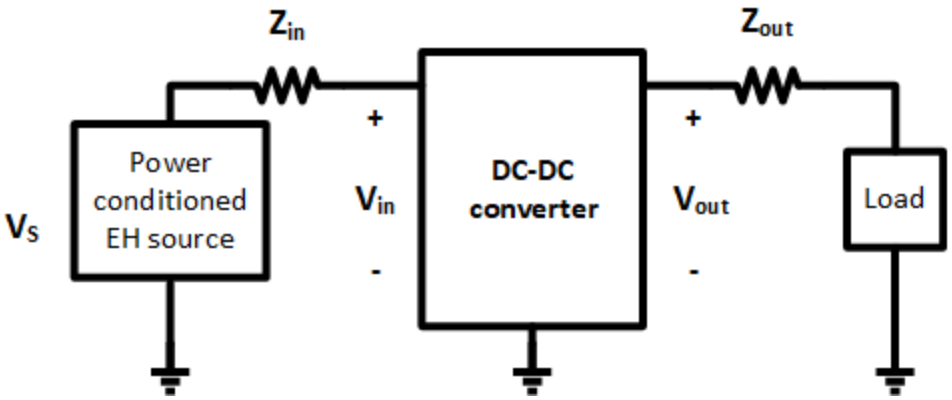

Figure 3.11: Switching DC-DC converter concept.

be noticed the supply voltage holds a quadratic and direct relationship to the power consumption. Therefore, lower voltage is desirable for digital circuits.

$$P = f \cdot C \cdot V^2 \tag{3.8}$$

For this, the different circuits integrated in an embedded system require multiple voltage levels. At the same time, it is usually a standard for an electronic system to have a single voltage source, namely a supercapacitor, a battery and even a transducer to power analog and digital circuits. Such requirements can be achieved with the implementation of a power conditioning circuit: a switching converter.

Among the different characteristics switching converters offer, Fig. 3.11, include to help isolate two circuits and as a impedance matching component, but particularly, the ability to efficiently convert a main supply voltage to multiple voltage levels for other circuits is the most important. All of this at a lower space and cost as opposed to having one voltage source, a battery for example, per integrated circuit inside an embedded system.

3.7 Boost converter

The structure of step-up or boost converter of Fig. 3.12 is based on an inductor L, that serves as an energy storage element, power switches S_1 and S_2 that charge and discharge the inductor

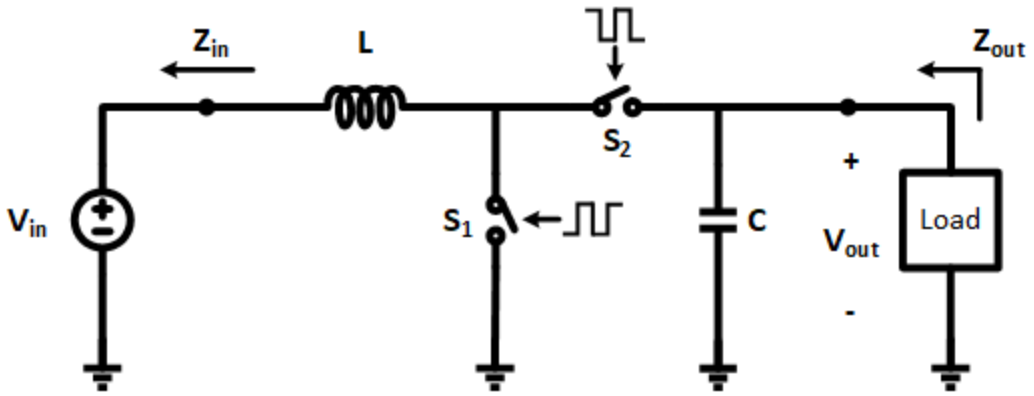

Figure 3.12: Boost converter circuit diagram.

cyclically, and an output capacitor C that acts as a charge-storage and output-voltage filtering component. Boost converters have the capability to produce output voltages V_{out} that are greater than the input voltage V_{in} of the converter, as it can be deduced from 3.9.

A basic understanding of the operation of a boost converter can be known from Fig. 3.12: during the first period defined in 3.10, with a duty cycle D of a pulsed width modulation signal (PWM) defined as T_{sw}, the inductor L is being charged by shorting S_1 and opening S_2. In the second phase of the cycle defined in 3.11 S_1 is opened and S_2 is shorted allowing the inductor L to transfer the stored charges to the load. This charging and discharging continue throughout the operation of the DC-DC converter.

$$V_{out} = \frac{1}{1-D} \cdot V_{in} \tag{3.9}$$

$$D_1 = D \cdot T_{sw} \tag{3.10}$$

$$D_2 = (1-D) \cdot T_{sw} \tag{3.11}$$

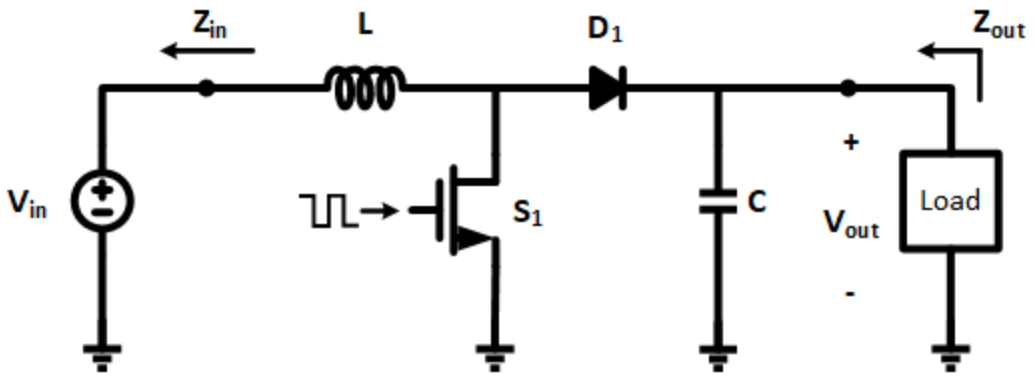

Figure 3.13: Asynchronous boost converter circuit diagram.

3.7.1 Power stage

Switches of the boost converter are implemented using active components, the key differences of both implementations, asynchronous and synchronous circuits, and their application considerations are described as follows.

3.7.1.1 Asynchronous

A typical asynchronous boost converter is shown in Fig. 3.13. The two switches in this circuit are S_1 that represents a MOS transistor and D_1 that represents a diode. When S_1, also know as the switching element, is on, L is connected in parallel to V_{in} to be charged by the effective input voltage. At this point D_1 is reverse biased as V_{out} presents a larger voltage than the $L - S_1 - D_1$ node. By switching off S_1, L is connected in series to V_{in}, which allows the circuit to forward bias D_1. This cycle repeats itself during the operation of the boost converter to regulate the output to a given voltage.

One of the advantages of the asynchronous circuit relies on its simplicity, this is mainly because only S_1 needs to be driven while there is no need for a control circuit for D_1. This is especially important as designers do not have to set circuit constrains for V_{out} short circuit issues. Therefore, circuit design for this topology tends to be less expensive and smaller.

A clear disadvantage of this circuit is the voltage drop associated to D_1, which can degrade the

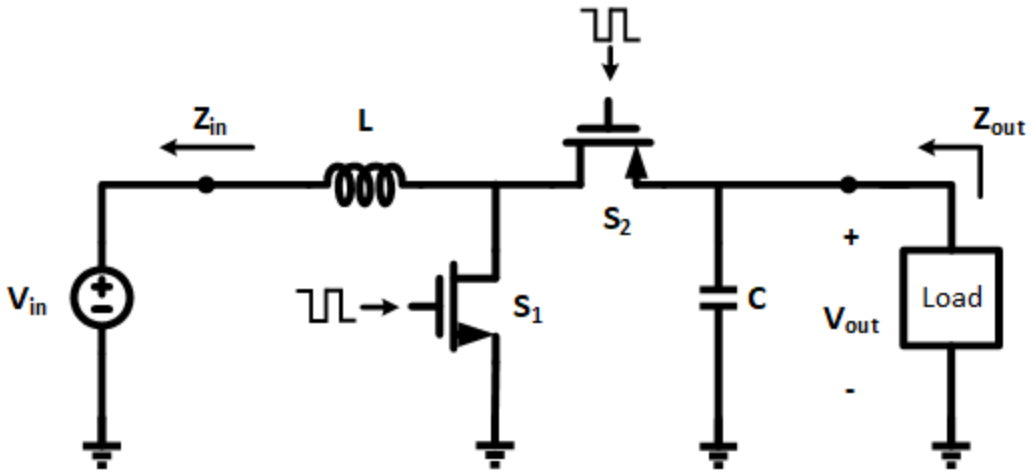

Figure 3.14: Synchronous boost converter circuit diagram.

power efficiency of the boost converter, especially for EH applications that usually provide a very limited voltage.

3.7.1.2 Synchronous

In this power stage type two switches are implemented with MOS transistors, as depicted in Fig. 3.14. In comparison to the asynchronous boost converter previously presented, the synchronous topology replaces diode D_1 for MOSFET S_2 that now charges the output capacitor C and supplies current to the Load.

The operation of this circuit is identical to its asynchronous counterpart, when charging and discharging L, with the difference that S_2 has to be driven with a control circuit of a complementary signal to the one controlling V_{gs} of S_1. That is, when S_1 is on, S_2 must be off and vice versa. The complementary switching of S_1 and S_2 regulates the output voltage.

Because voltage drop across S_2 is considerably reduced during the operation of this boost converter, synchronous circuits can achieve higher efficiency than nonsynchronous converters. Also, its back leakage can also be reduced as compared to diodes, optimizing this way the overall conversion efficiency.

On the other hand, the correct switching of S_1 and S_2 must be ensured to avoid grounding V_{out}, and deteriorating the DC-DC converter's power efficiency. This important main design constrain

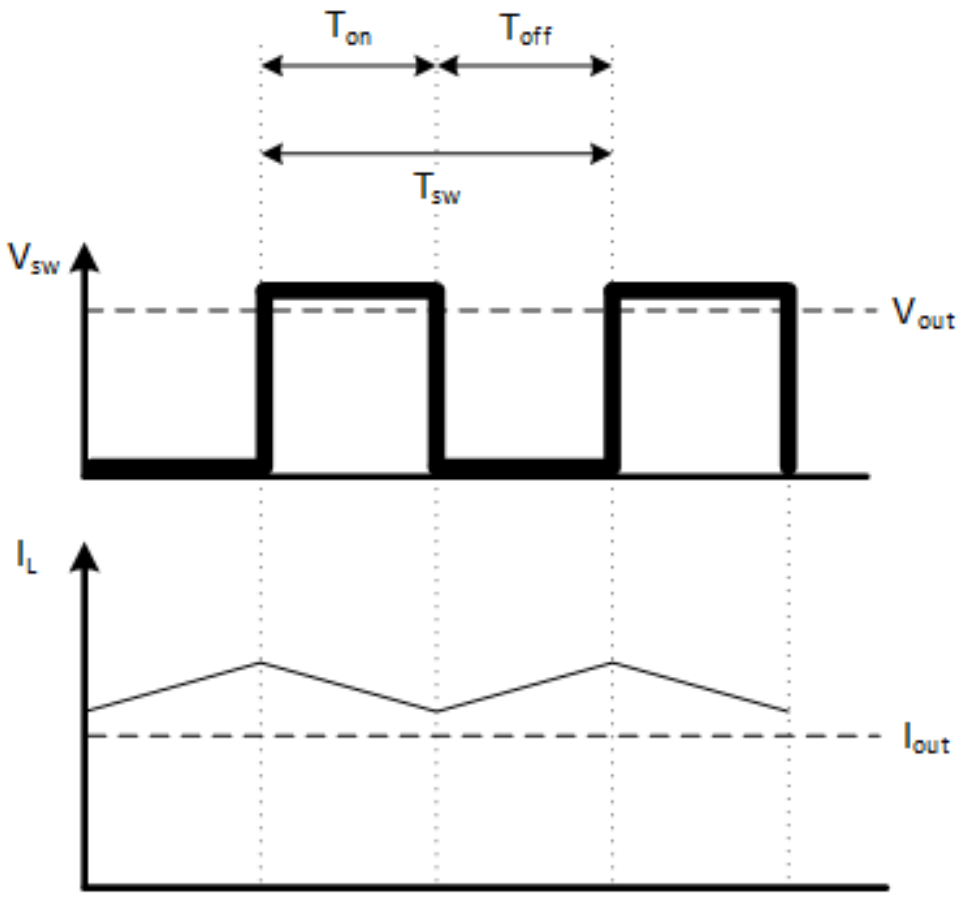

Figure 3.15: Boost converter continuous conduction mode power stage waveforms.

for this circuit comes at the expense of circuit complexity and overall system cost.

3.7.2 Operating modes

There are two different types of operation depending on the load of the DC-DC converter: Continuous Conduction Mode (CCM) and Discontinuous Conduction Mode (DCM). An steady-state analysis of each mode is presented below.

3.7.2.1 Continuous Conduction Mode

A characteristic of this mode is that the current at the inductor L is continuous. That is, it never reaches zero as displayed in Fig. 3.15.

For the analysis of this operating mode following are assumed too small to be negligible: volt-

age drop V_{ds} across MOSFETs and inductor L resistance.

During the inductor charging period, the constant input voltage V_{in} is directly applied to L. As a result of the applied voltage, the inductor current increases linearly. The increase in current can be calculated as follows:

$$V_L = L \times \frac{\Delta I_L}{\Delta t} \tag{3.12}$$

or

$$\Delta I_L = \frac{V_L}{L} \times \Delta t \tag{3.13}$$

Therefore, the increase in current for the on state is given by:

$$\Delta I_{L(+)} = \frac{V_{in}}{L} \times T_{on} \tag{3.14}$$

It is worth noticing that at this point the current supplied to the load comes from the output capacitor C.

During the second phase, switch S_1 is off and since the current through inductor L cannot change instantaneously, the current now passes through S_2. At this point, the inductor now sources current to the load, at the same time this current reduction in L changes the inductor's polarity. The voltage at the inductor is defined as $V_{out} - V_{in}$. Since the applied voltage does not change the inductor current decreases linearly with respect to time and it is defined as follows:

$$\Delta I_{L(-)} = \frac{V_{out} - V_{in}}{L} \times T_{off} \tag{3.15}$$

The conditions at steady state demand that the current increase and decrease at the inductor L remains the same. Thus:

$$\frac{V_{in}}{L} \times T_{on} = \frac{V_{out} - V_{in}}{L} \times T_{off} \tag{3.16}$$

By substituting the on and off states in terms of duty cycle D and switching period T_{sw} as follows $T_{off} = (1 - D) \times T_{sw}$ and $T_{on} = D \times T_{sw}$, an equation to calculated output voltage in terms of its input voltage can be calculated as follows:

$$V_{out} = \frac{V_{in}}{1 - D} \tag{3.17}$$

As it can be deduced from Eq. 3.17, The output voltage is controlled by setting the on-time of S_1. That is, by increasing the on-time more charges are stored to the inductor therefore more energy is delivered to the Load during the off-time.

The output current provided by the output capacitor should be zero for a full switching cycle, thus, the average current of the inductor can be equated to the output current as follows:

$$I_{L-average} = \frac{I_{out}}{1 - D} \tag{3.18}$$

Finally, most of the applications for the CCM are usually oriented to loads with high current demands.

3.7.2.2 Discontinuous Conduction Mode

A characteristic of this mode is that the current at the inductor L is not continuous. That is, it reaches zero amperes for some time of the switching period as presented in Fig. 3.16.

Three states can be clearly recognized in table 3.1.

State	Duration
On	$T_{on} = D_1 \times T_{sw}$
Off	$T_{on} = D_2 \times T_{sw}$
Idle	$T_{sw} - T_{on} - T_{off} = D_3 \times T_{sw}$

Table 3.1: Boost converter discontinuous conduction mode states.

The continuous and discontinuous modes are identical for states on and off, therefore its induc-

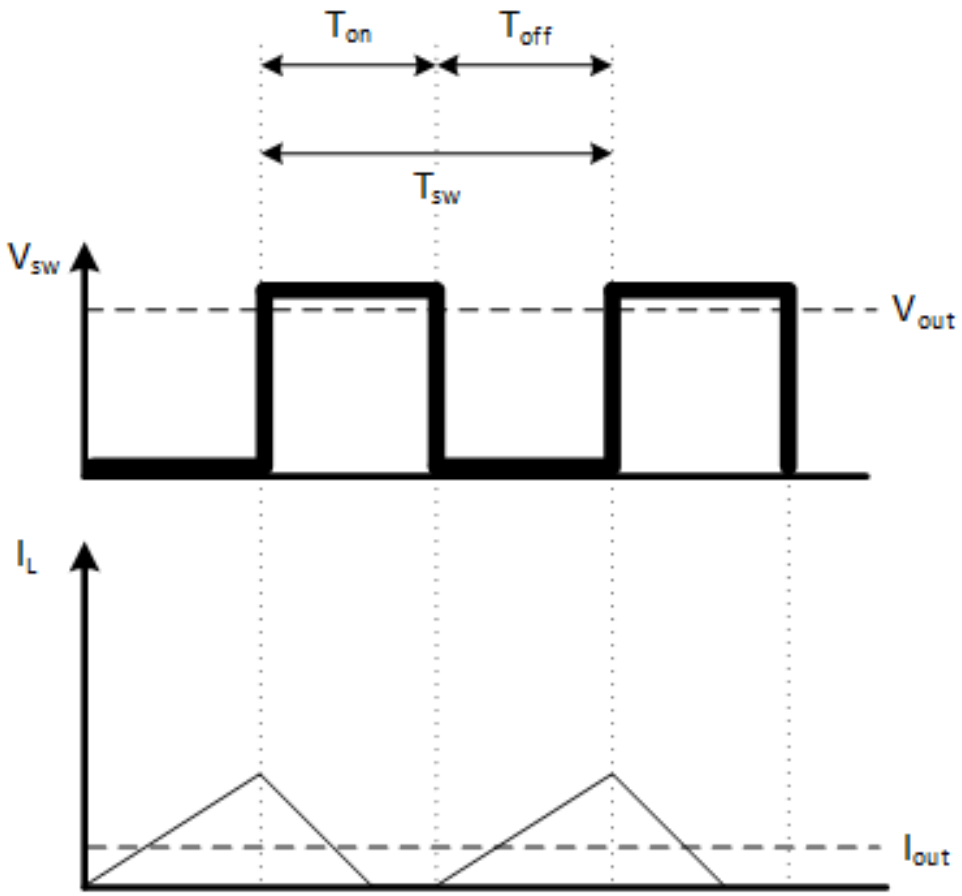

Figure 3.16: Boost converter discontinuous conduction mode power stage waveforms.

tor current can be calculated as follows:

$$\Delta I_{L(+)} = \frac{V_{in}}{L} \times T_{on} = I_{peak} \tag{3.19}$$

$$\Delta I_{L(-)} = \frac{V_{out} - V_{in}}{L} \times T_{off} \tag{3.20}$$

$$V_{out} = V_{in} \times \frac{D_1 + D_2}{D_2} \tag{3.21}$$

Similar to CCM, the output current is equal to the average of the peak current of L at the inductor-discharging period. That is:

$$I_{out} = \frac{1}{T_{sw}} \times 0.5 \times I_{peak} \times D_2 \times T_{sw} \tag{3.22}$$

Also we know that:

$$I_{out} = \frac{V_{out}}{R_{Load}} \tag{3.23}$$

By equating Eq. 3.22 and Eq. 3.23 and simplifying we get:

$$V_{out} = 0.5 \times \frac{V_{in} \times D_1 \times D_2 \times T_{sw}}{L} \times R_{Load} \tag{3.24}$$

Solving V_{out} using Eq. 3.21 and Eq. 3.24 we get:

$$V_{out} = V_{in} \times \frac{1 + \sqrt{1 + \frac{2 \times D_1^2 \cdot R_{Load} \cdot T_{sw}}{L}}}{2} \tag{3.25}$$

As it can be noticed, while V_{out} in CCM only depends on input voltage V_{in} and duty cycle D_1, V_{out} in DCM depends not only on input voltage V_{in} and duty cycle D_1, but also on the switching period T_{sw}, inductance L, and output load resistance R_{Load}.

3.7.3 Power efficiency

The main bottleneck of power efficiency of a boost converter centers in conduction losses present in the on-resistance of its switches expressed with the following equation.

$$P_{loss} = \frac{1}{2} \cdot f_{sw} \cdot C_{gate} \cdot V_{drive}^2 \tag{3.26}$$

Therefore the efficiency expression is defined as follows:

$$\eta_{loss} = \frac{P_{out}}{P_{out} + P_{S_1} + P_{S_2} + P_{inductor}} \tag{3.27}$$

where:

$$P_{S_1} = R_{S_1} \cdot D_1 \cdot \left(\frac{I_{out}}{D_2}\right)^2 \tag{3.28}$$

$$P_{S_2} = R_{S_2} \cdot D_2 \cdot \left(\frac{I_{out}}{D_1}\right)^2 \tag{3.29}$$

$$P_{inductor} = R_{inductor} \cdot \left(\frac{I_{out}}{D_2}\right)^2 \tag{3.30}$$

3.8 Multisource power extraction techniques

Power conditioning circuits have been presented in this section that have the potential to harvest energy from a single transducer. However, since energy harvesting circuits source its energy from low-levels of intermittent environmental power, this can set an important design challenge [51] that if neglected it can inevitable lead to system degraded effectiveness and even total device failure.

Low-power along with maximum transfer of power techniques have been developed for EH applications [52, 53]. However, using a single EH source, can still be too unpredictable or insufficient to meet the requirements for industrial applications that require long-term power supply [54].

Power extraction systems and techniques that can harvest energy from multiple sources, such as multiple microbial fuel cells, solar panels, thermoelectric generators, to name a few, can be a viable way to increase system reliability while implementing low-power techniques for higher power efficiency of well-know single-source EH circuits [55].

Time interleaved power extraction is a technique where multiple sources can be extracted by multiplexing them to a single DC-DC converter as seen in Fig. 3.17.

Priority assignment algorithms determine which input is harvested, while other sources are disconnected [56]. The authors in [57] propose an architecture that prioritizes the harvester with maximum available power and then efficiently channels its energy to the output load.

While a diode-based ORing structure can connect in parallel multiple harvesters [58, 59] it only

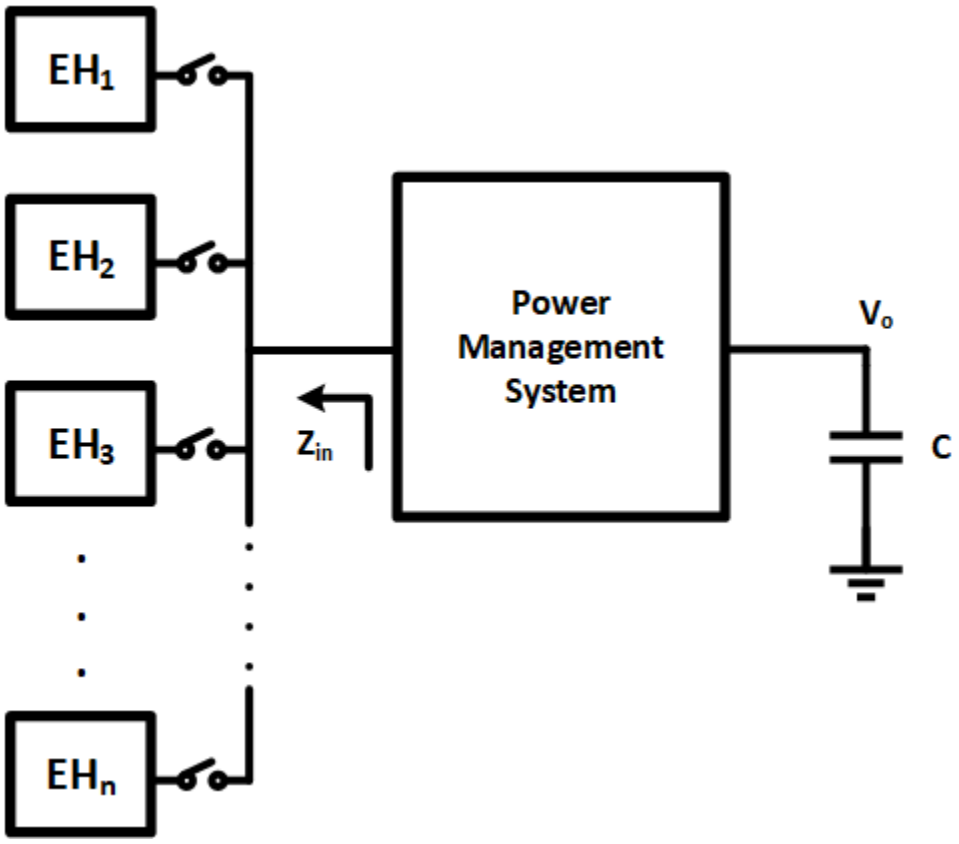

Figure 3.17: Power extraction from multiple EH sources.

hast the ability to harvest the energy from a single source at a time.

In [60], a reconfigurable multi-input, multi-output switch matrix is presented that is able to combine energy from photovoltaic, thermoelectric, and piezoelectric transducers. This technique is based in a time-interleaved shared inductor technique. Another work that used a shared-inductor is [61], the work introduced also explores energy aware technique implementations.

The ability to harvest multiple sources simultaneously have been explored in [62]. This switched-capacitor approach can combine energy from multiple EH transducers. The approach taken in this work combines the energy from multiple sources by using a voltage doubler core. One of the advantages of this approach is that it can be completely integrated.

As shown in [63] the combiner based in voltage-doubler has the ability to perform automatic MPPT. This work also introduces a power-based harvester ranking technique where from a four

input transducer interface the two sources that offer the highest energy are combined and delivered to the output. The work in [64] further elaborates in the voltage doubler approach to also offer improved MPPT for multiple sources.

As it can be seen from this section power conditioning are a crucial component for power management for EH. In this chapter, different rectifiers were reviewed pointing out their design trade offs.

This chapter also elaborated on how boost converters work along with presenting different techniques to improve power extraction efficiency from different and multiple EH sources.

4. A TIME-INTERLEAVE-BASED POWER MANAGEMENT SYSTEM WITH MAXIMUM POWER EXTRACTION AND HEALTH PROTECTION ALGORITHM FOR MULTIPLE MICROBIAL FUEL CELLS FOR INTERNET OF THINGS SMART NODES*

4.1 Introduction

It is projected that networked microsensor technology, in the form of Wireless Sensor Networks (WSNs), will keep playing an important role for the future of remote sensing [65]. Some of the applications for WSNs range from automation, human monitoring, equipment condition monitoring, defense, aerospace, building, structural health monitoring and agriculture [66, 67, 68, 69, 70].

As reported in [71], WSNs have been implemented in point-to-multipoint and local point-to-point communication networks achieving long-term field deployment but a limited sensing-data processing. However, WSNs are nowadays increasingly becoming part of a more pervasive concept, the Internet of Things (IoT), which allows devices to communicate with each other and collect information on a much larger scale through the internet [72]. This opens new possibilities to achieve more comprehensive data processing of the information being collected. IoT has the potential to foster a large amount of applications by enabling more devices to be connected to the web and make use of a wider range of pre-collected and pre-processed data.

A paramount challenge that can pose a limitation for a wider adoption in the use of IoT smart nodes in areas of difficult access, is inherently associated to its battery requirements for a considerable power specification needed to perform on-field sensor measurements and to send the collected information to the cloud. A desirable feature of WSN is to minimize not only the size and cost of the energy storage element itself, but also to reduce the maintenance needed to constantly replace the sensor's batteries. Harvesting enough energy from the environment where the WSN is physically located, can be a plausible solution to extend the battery life of a remote sensor and

*Reprinted with permission from " A Time-Interleave-Based Power Management System with Maximum Power Extraction and Health Protection Algorithm for Multiple Microbial Fuel Cells for Internet of Things Smart Nodes," by A. Costilla Reyes, C. Erbay, S. Carreon-Bautista, A. Han and E. Sánchez-Sinencio, 2018. Appl. Sci. 8, no. 12: 2404, Nov. 2018, Copyright 2018 by the authors

even fully power it for prolonged periods of time [73, 74]. The sources of energy that can be harvested from the ambient include solar, kinetic, thermal gradient, radiofrequency, electromagnetic and Microbial Fuel Cells (MFCs) [75, 76, 77, 78, 79, 80].

MFCs are a promising emerging source of energy harvesting that can transform organic and inorganic matter to generate electricity by using a bioelectrochemical conversion process [81, 82, 25, 83, 84]. MFCs can find a particular application in remote sensing [85] for places that are difficult to access routinely for maintenance but with abundant organic material available, such as sewage water and even oceans [86, 87, 88], where the use and replacement of batteries, can be costly or impractical [80, 86, 89, 90, 91, 92, 93]. A potential application that can combine IoT devices and MFC technologies is in the management and optimization of traditional public services, such as residual water treatment plants [94]. It is important to note that while MFCs can generate power from liquid and organic sediments found in wastewater and oceans, smart nodes can monitor and transmit conditions found in water being treated such as temperature, pH, conductivity, salinity, and organic sediment concentration, to name a few [86, 87, 88, 95].

Despite these opportunities, one of the main limitations of energy harvesting from MFC technologies is the low output power levels provided by each individual cell, typically in the order of microwatts to a few milliwatts per liter [96]. For this reason, a Power Management System (PMS) is required to maximize the power conversion efficiency and increase the voltage and current level to the nominal power levels required by wireless sensors. Some implementations of PMS have previously been reported to maximize the energy harvesting efficiencies of single MFCs [86, 91, 92, 93, 97, 98, 99]. To reach usable output voltage levels while at the same time increasing the output current density is by connecting several MFCs in series or in parallel to increase the overall power out level. However, differences in power production from individual MFCs, as well as voltage reversal issues when connecting multiple MFCs in series, present a challenge in the overall efficiency of the system, since these variations dramatically worsen the power production of MFCs arrays [96].

In this chapter a circuit topology for efficient energy harvesting from multiple MFCs to increase

the total available energy of the system to meet the voltage and current specifications of a power-demanding application is presented. A ranking algorithm was developed based not only on the voltage of the MFC, which does not contain information about MFCs internal resistance, but rather on the available power from each individual MFC to prioritize the charge extraction from the MFC that has the highest available power. At the same time, recovery time is a critical observed requirement for the MFC to recharge its internal capacitive elements as part of its power generation cycle, to avoid damaging the MFC, due to power over-depletion and extend its lifetime. The algorithm also includes an MFC-failure protection feature that isolates an MFC in the array when the algorithm notices a significant power drop during the energy harvesting process. The MFC output power is regulated by a step-up DC-DC converter that stores the extracted charges in an output supercapacitor. Finally, the energy harvesting technique presented in this work is tested and demonstrated through an internet-enabled smart node, capable of transmitting the collected data to the internet. A performance comparison to other power management works based on MFC is made in terms of charging time, topology features and efficiency.

The chapter is organized as follows: In subsection 2, a brief introduction to MFC is presented and its electrical model is described. subsection 3 discusses the choice of top level circuit architecture for multiple MFC power extraction and describes the MFC power ranking and power extraction algorithms. The experimental results are presented in subsection 4 and 5 summarizes this chapter.

4.2 MFC and Power Management System Specification

This section aims to provide accurate specifications of the construction of the MFCs used for this chapter, its electrical description to determine the proper PMS specifications and the proposed system specifications. All these components are described in the following.

4.2.1 MFC Construction and Characterization

Four MFCs were fabricated from an acrylic anode and cathode chambers. One 1,000 ml MFC and three 240 ml MFCs were constructed, the two different sizes were used to simulate MFCs

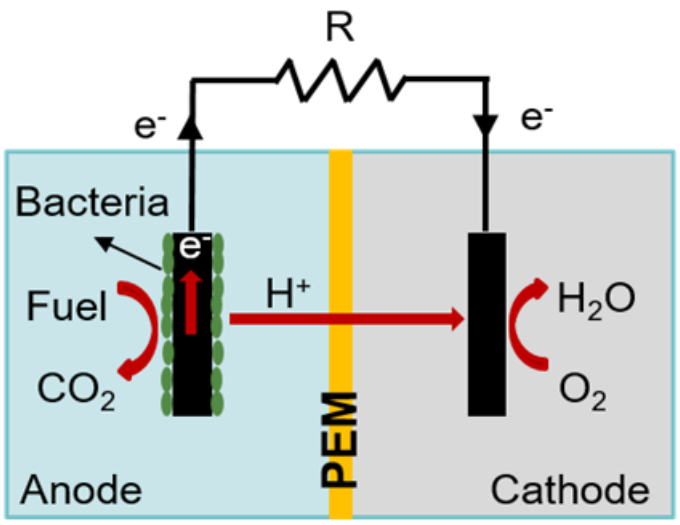

Figure 4.1: MFC device schematic description [100].

having different output power levels. A Proton Exchange Membrane (PEM) (Nafion 117^{TM}, Ion Power Inc.) was used to separate the anode and cathode chambers from each other, while selectively allowing proton generated by bacteria to cross over to the cathode chamber to complete the electrochemical reaction to produce power. The anode was a carbon felt (Morgan, UK) and the cathode was a carbon cloth containing $0.5mg/cm^2$ of Pt catalyst on one side (ElectroChem, Inc) for all MFCs. Both anode and cathode were connected through a titanium wire to a $1k\Omega$ load resistor that was placed between them to allow the electrons produced by bacteria to flow. The schematic diagram of the MFC is shown in Figure 4.1 [100]. The electrical model in Figure 4.2 is further discussed in the following subsection.

All MFCs were inoculated with anaerobic activated sludge collected from the Austin Wastewater Treatment Plant for the initial growth of the bacteria on anodes. Then growth medium containing acetate $(1.0g/L)$ in Nutrient/Mineral/Buffer (NMB) solution was used ($10mL/L$ mineral base 1,$10mL/L$ mineral base 2, and $1mL/L$ nutrient base). The solution was replaced with a fresh one when the voltage across the load resistor dropped below 50 mV [91, 101, 102, 103]. The constructed two-chamber MFCs are shown in Figure 4.3.

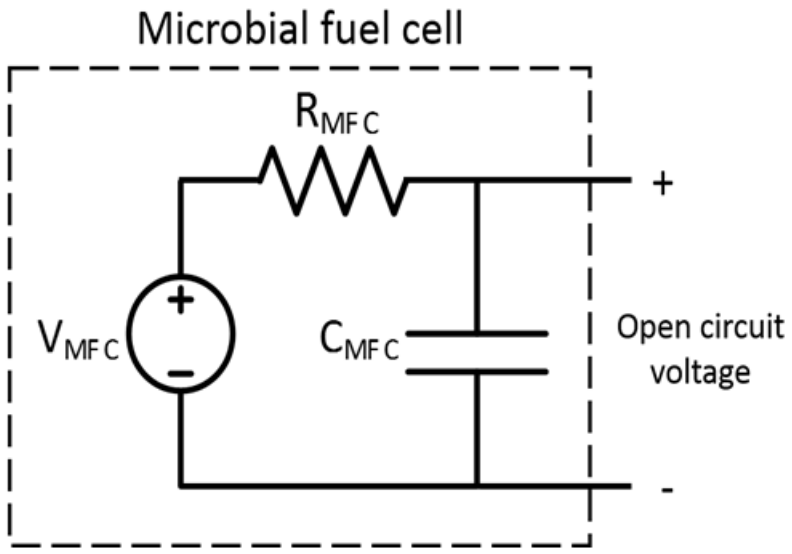

Figure 4.2: MFC electrical model [100].

The MFC voltages were monitored in real time in volts (V) against time in seconds (s) [104] by using a digital multimeter (Fluke 79 series II, Everett, WA, USA) through a multiplexer (Agilent 34970A, Santa Clara, CA, USA). Once the voltage production level was stable, power and voltage at maximum power point were obtained by varying a testing load resistor value between the electrodes in the range of $5k\Omega - 20\Omega$ [105]. Table 4.1 summarizes the specifications and typical power production of all MFCs.

Specification	MFC 1	MFC 2	MFC 3	MFC 4
Total volume (mL)	240	240	240	1,000
Catholyte	Air	Air	Ferricyanide	Ferricyanide
Anode area (cm^2)	12	12	12	50
Cathode area (cm^2)	12	12	12	50
Power at MPPT (μW)	595	484	435	6,400

Table 4.1: Specifications and performance of MFCs [100].

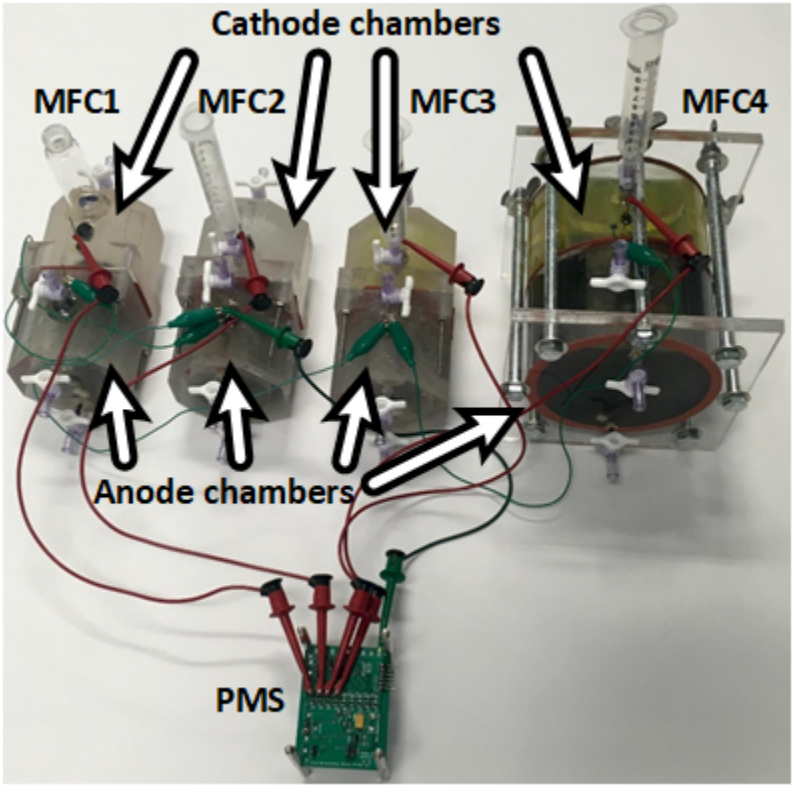

Figure 4.3: Two-chamber microbial fuel cell and power management unit set up [100].

4.2.2 MFC Electrical Equivalent Modeling

The MFC can be electrically modeled as a voltage source with an internal resistance R_{MFC}, open circuit voltage V_{MFC}, and internal capacitance C_{MFC} as shown in Figure 4.2. The value of R_{MFC} is composed of several different components (anode, cathode, membrane, and electrolyte resistances) [91, 92, 93]. The value of V_{MFC} is the MFC's thermodynamic voltage, which varies nonlinearly depending on the solution pH, temperature, and substrate concentration. Since MFCs produce a DC voltage, C_{MFC} is mostly ignored in similar works [80, 90]. However, due to the method of locating the maximum power point (MPP) through the open circuit voltage of the MFC in the proposed PMS, C_{MFC} is important for the proper design of a maximum power point tracking (MPPT) algorithm; thus, it is included in our model. The equivalent circuit model of the MFC was used for the design of the PMS and the dynamic MPPT in this chapter.

4.2.3 System Specifications

A voltage regulation stage is required to boost the low voltages (less than 1 volt) provided by each of the four MFCs to a nominal voltage that can provide proper power values for the wireless sensor to operate properly. The step-up converter integrated to the system provides dynamic impedance matching and low-power consumption for maximum-power extraction.

Since power extraction is performed to an array of four MFCs, MFC's health-state measurements, multiplexing control capabilities and the flexibility offered by a programmable device are key features required for the control block of the proposed system. Thus, an extremely-low power microcontroller is required to perform MFCs power ranking and multiplexing operations.

The energy-storage system specifications for the two wireless sensors, a short-range wireless transmission and an IoT smart node, required the integration of an output load supercapacitor of 0.1 F and 5 F, respectively, to meet the power specifications for each sensor and allow them to properly send a packet of data wirelessly of multiple temperature readings. The design specifications are presented in Table 4.2.

Specification	Value
Number of MFCs	4
Average Vin	350 mV
Vout	3.3 V
Output supercapacitor	5 F

Table 4.2: Specifications of the MFC-powered IoT system [100].

4.3 Circuit Architecture for Multi-MFC PMS

In this section, a summary of previous EH techniques for multiple MFC is presented along with a proposed architecture that considers a DC-DC converter with MPP capabilities that has been tailored for MFC technology. A PMS algorithm has been embedded in a programmable intelligent computer (PIC) microcontroller and explained here, its main purpose is to allow the

extraction of an array of MFCs while providing health protection features. Finally, a description of the final implementation of the proposed PMS is given.

4.3.1 Overview of Energy Harvesting for MFC

Due to the technology's nature, the MFC output voltage is very low and non-regulated [91], which represents a major challenge for efficient power extraction. A parallel configuration of MFCs can be used to increase the output current with the disadvantage that the output voltage will remain at low levels. Another drawback of the parallel connection of MFCs is that if their output voltage deviate from each other, this effect leads to a detrimental charge transfer among cells in the array, also known as voltage reversal, preventing the stack of MFCs to fully deliver its charges to a load [89]. This results in power losses that lead to a low overall power efficiency of the array.

On the other hand, a serial connection of MFCs provides higher output voltages based on the sum of individual V_{MFC}, with a common current that flows throughout the MFC array. In [96] a voltage balancer is used along with a DC-DC converter for an array of serially connected MFCs. By doing so, the output voltage, now higher than that of a single MFC, is efficiently harvested by providing an active switching capacitor method to balance the system. However, the system can also face multiple drawbacks including power extraction interruption and even system failure if a single MFC in the stack is damaged or physically disconnected due to a contact deterioration, for example. This can potentially disable the operation of the DC-DC converter block, leading to a loss of power available from the remaining properly-functioning MFCs.

Previous works in PMSs have mainly focused on power extraction from a single MFC [90, 106]. This approach is limited to the amount of power that a single MFC can generate, which can be depleted quickly, resulting in the interruption of the power supply at the load. In addition, if the system does not integrate an automatic MPPT algorithm, achieving maximum power harvesting can become cumbersome and time-consuming if conducted manually [86, 90, 96, 107, 108, 109]. Even more important, power extraction may not be efficient since the MPP can shift during the life-time of an MFC. For this reason, the integration of an MPPT is essential for the DC-DC converter to dynamically adjust to the electrical characteristics across multiple MFCs.

In this chapter, the system proposed is intended to harvest the energy from an array of MFCs in a time interleaved fashion, allowing the inactive MFCs to recharge its internal capacitances (C_{MFC}) when they are not being harvested. The system also integrates an MFC-failure protection mechanism, which automatically isolates one or multiple MFCs from the system if its available power is below a minimum threshold. The MFC-failure protection feature is intended to isolate an MFC when it has been depleted, damaged or it has been physically disconnected.

4.3.2 Overview of the Proposed PMS Circuit for Multi-MFC

The block diagram of the proposed system is shown in Figure 4.4. Each MFC in the array is individually connected to a low-R_{on} N-type CMOS switch DMN1019UVT (Diodes Incorporated®, Plano, TX, USA), controlled by an extremely low power microcontroller PIC24F16KA102 (Microchip Technology Inc.®, Chandler, AZ, USA) [110]. The PMS algorithm embedded in the microcontroller allows testing the total power available in each MFC in the array, by using a power measurement block, as shown in Figure 4.5. The microcontroller also regulates the power extracted from an individual MFC in the stack by defining the time interleaved EH sequence and the amount of time needed for each MFC before it is harvested again. The DC-DC converter block consists of an ultra-low power boost converter BQ25505 (Texas Instruments Incorporated®, Dallas, TX, USA) [111]. Finally, the extracted charges are stored in an output supercapacitor that powers the wireless sensor.

As the output voltage level of the MFC is not high enough for the proposed topology to allow for self-starting operation from the PMS, an external one-time pre-charging of an output secondary capacitor to 1.8 V is required to begin controller operation. Multiple different approaches may be taken to startup the system [112, 113].

Once the system begins extracting energy from the MFC, there is no longer need for an external power source to power the PMS.

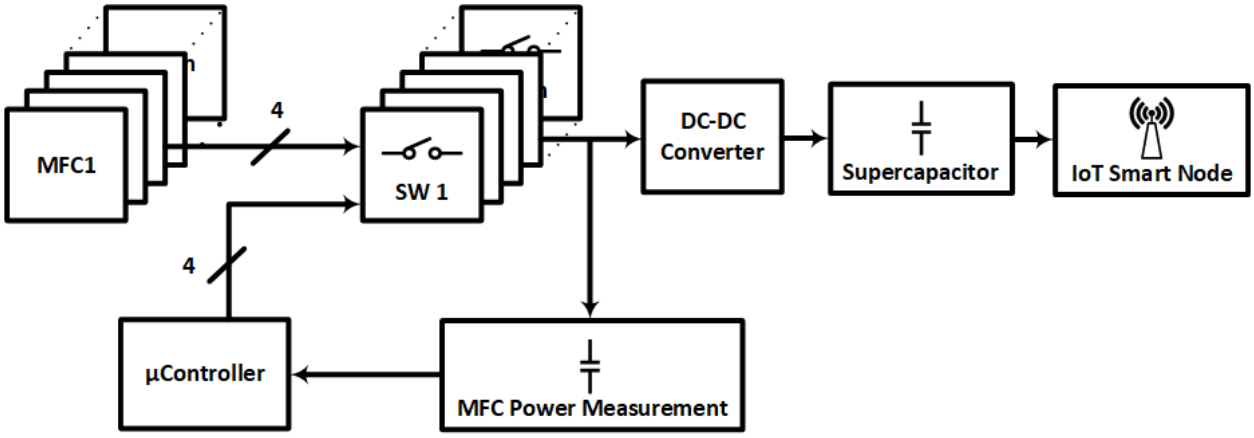

Figure 4.4: Block diagram of the proposed PMS [100].

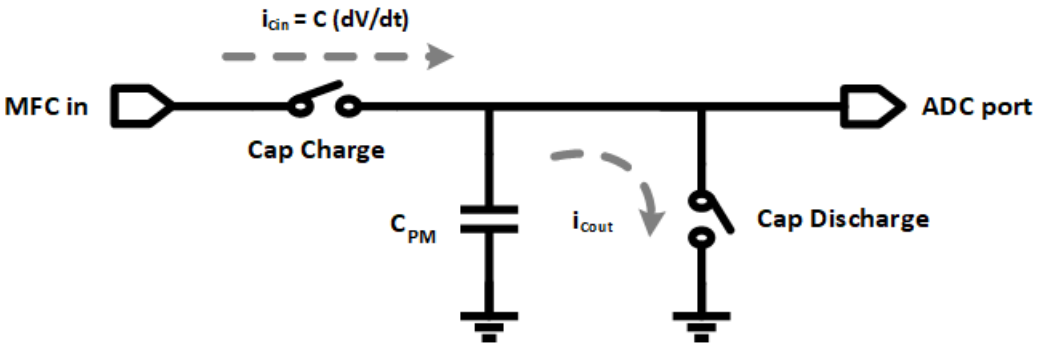

Figure 4.5: Diagram of the proposed power measurement circuit [100].

4.3.3 Maximum Power Point DC-DC Converter

Based on the electrical diagram presented in Figure 4.1, the DC-DC boost converter selected for this chapter was programmed to set its input resistance at 50% of the V_{MFC} open circuit voltage [92]. By using this reference, the input impedance of the boost converter is dynamically adjusted by regulating its input current and voltage to track the MPP of the MFC.

As shown in 4.1, since the maximum power point is reached when the input resistance of the PMS equals to the MFC's input resistance characteristic, it sets a minimum condition for the power losses that can be tolerated in by the internal resistance of switches, and sheet resistance for the printed circuit board (PCB).

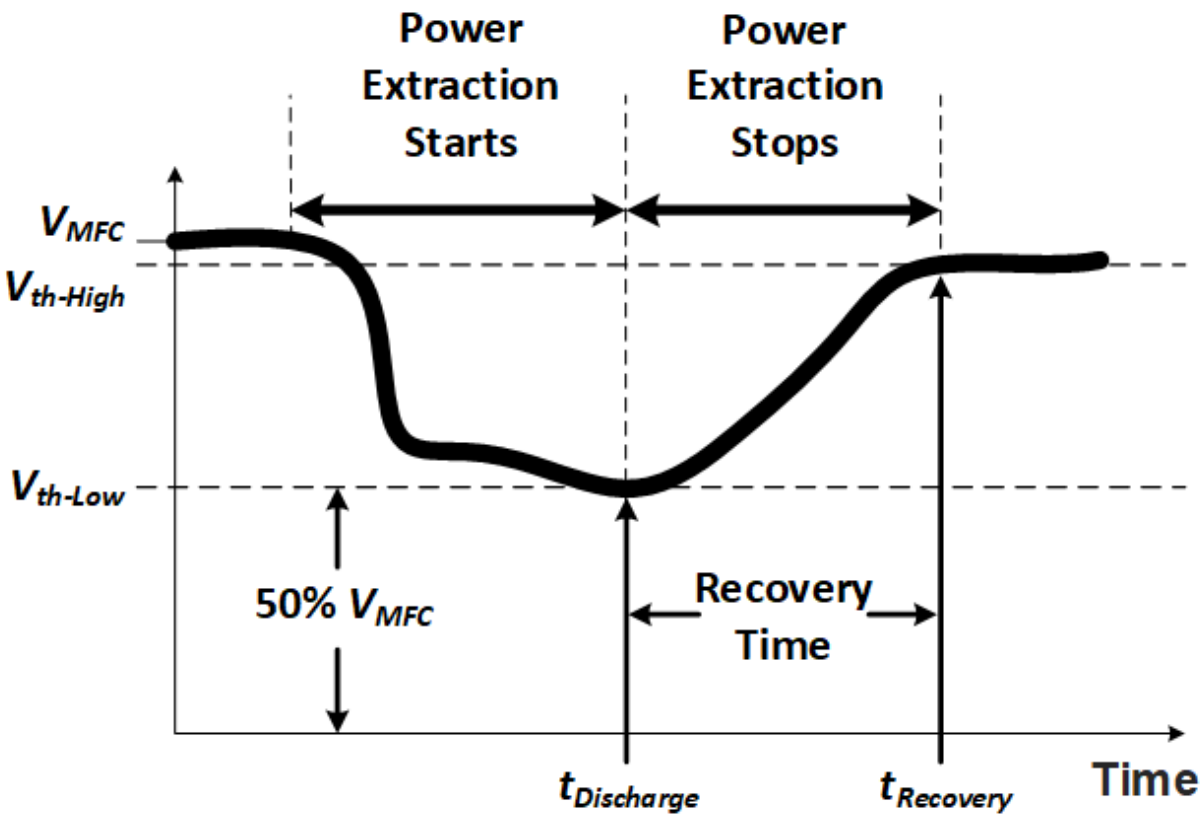

Figure 4.6: Key reference points for an energy harvesting algorithm for MFC power extraction [100].

$$P_{LOSS} = I^2 R_{LOSS}; R_{LOSS} = R_{MFC} \Rightarrow R_{PMU+PCB} \leq R_{MFC} \tag{4.1}$$

4.3.4 Multi-MFC PMS Algorithm

A microcontroller's 10-bit analog to digital converter (ADC) determines the interleaved power extraction time per MFC. As seen in Figure 4.6, the algorithm defines two thresholds for the power extraction $V_{th-High}$ and V_{th-Low} as follows:

V_{th-Low} determines when to stop the EH operation and is predefined at 50% of the initial measured V_{MFC}. When V_{th-Low} is reached, the MFC is removed from the PMS until the voltage threshold high, $V_{th-High}$, is reached. The recovery time is defined as the time it takes for the MFC to go from V_{th-Low} to $V_{th-High}$. V_{th-Low} and $V_{th-High}$ are determined after selecting the voltage

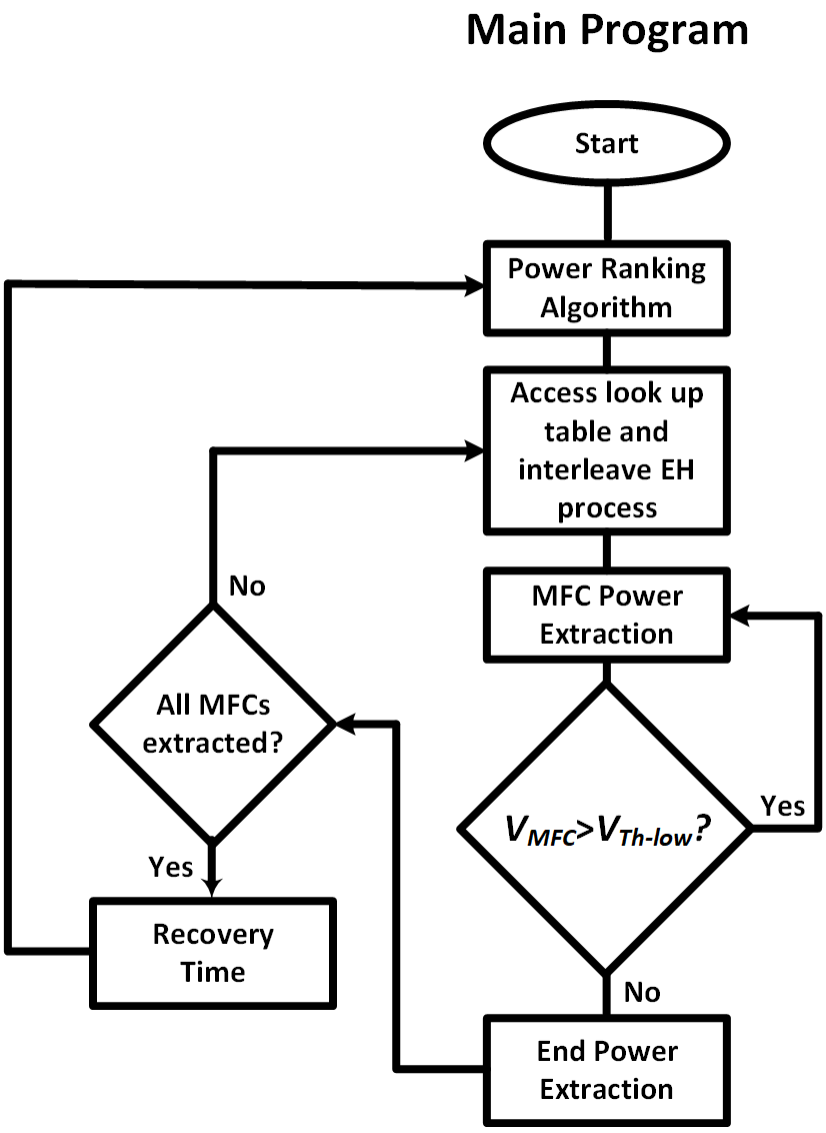

Figure 4.7: Flow diagram for MFC power extraction's main Program [100].

thresholds that yield the most optimum power extraction and recovery time for energy harvesting, without over-depleting the MFC from a series of threshold testing of an adaptive algorithm.

The power extraction algorithm presented in Fig. 4.7 (Main Program) is described below:

1. The Power Ranking Algorithm subroutine is executed. As a return variable, a look-up table is filled out with the individual MFCs' power rankings

2. The look-up table is accessed to interleave the MFC power extraction process

3. The DC-DC boost converter is enabled to start EH

4. V_{MFC} is compared to the low threshold voltage V_{th-Low}

5. When V_{th-Low} voltage is reached the DC-DC converter is disabled

6. If more MFCs in the array are waiting to be harvested, then the program jumps to instruction in numeral 2 (above). Otherwise, the system stops its EH mode and waits until the recovery time of the highest ranked MFC is reached

7. After the recovery time is completed, the algorithm restarts

The proposed interleaved energy extraction allows the step-up DC-DC converter to dynamically find the MPP of each individual MFC, ensuring a maximum power output per MFC while at the same time, the idle time for the remaining MFCs is used as a MFC's recovery time that directly affects the MFC's health status.

Another important feature of this approach is that if there is a failure at one or more MFCs, the system automatically adapts to it by assigning a rank of zero to that specific MFC, which allows the system to neglect the damaged cell.

4.3.5 Power Ranking from Multiple MFCs

Due to the bioelectrochemical nature of the MFC (parasitic reactive elements), its open circuit output voltage does not hold a direct relationship to the total amount of energy. Measuring the MFC open circuit output voltage it is not necessarily indicative of the amount of energy available from a specific device in the array because its internal resistance (R_{MFC}) is not considered. Therefore, the followed approach was chosen to properly estimate the power available per MFC:

The circuit shown in Figure 4.5 uses a $100\mu F$ power measurement capacitor (C_{PM}) and a charging switch (Cap Charge) in a series to an MFC under testing. A second switch (Cap Discharge) is in parallel with C_{PM} to reset its voltage conditions at the end of a power measurement by setting its initial voltage to zero. By neglecting parasitic elements, the power in circuit shown in Figure 4.5 can be calculated using 4.2 below:

$$P = VI = V(t) \cdot C_{PM} \cdot dV/dt \tag{4.2}$$

It can be noticed from 4.2 that the voltage change in time dV/dt of C_{PM} is directly proportional to the total available power of the MFC under test, and most importantly, such charging time, as estimated in 4.3, intrinsically considers resistances R_{MFC} and R_{Switch}, where the latter resistance is constant. Using this principle, the power ranking algorithm registers an accurate power measurement every 16.52 ms.

$$\tau_{Discharge} = C_{MFC} \cdot R_{out} = C_{MFC} \cdot (R_{MFC} + R_{Switch}) \tag{4.3}$$

Thus, the final value of C_{PM}, holds a direct relationship to the MFC's individual power. Both, the capacitor value and the constant charging time were selected to provide meaningful information regarding the electrical characteristics of all the MFCs connected to the system. The previously described process is repeated for each MFCs located in the MFC array. After all the MFCs are measured, the data is sorted in a look-up table that mandates the order in which each MFC is harvested.

The description of the power ranking sub-routine shown in Figure 4.8 is presented below:

1. The power ranking measurement capacitor is initialized to 0V by Cap Discharge switch
2. The MFC under testing is connected to the ranking circuit using Cap Charge switch
3. ADC values of MFC measured power are stored in the look-up table
4. The ADC values are sorted assigning the highest rank to the MFC with maximum voltage and lowest rank to the MFC with minimum voltage. MFCs that cannot provide significant power are ranked zero and neglected in the subsequent EH process

4.3.6 Implementation

The proposed PMS was developed on a two-layer PCB shown in Fig. 4.9. On the top side, a microcontroller was placed along with the low-R switches and the power measurement capacitor.

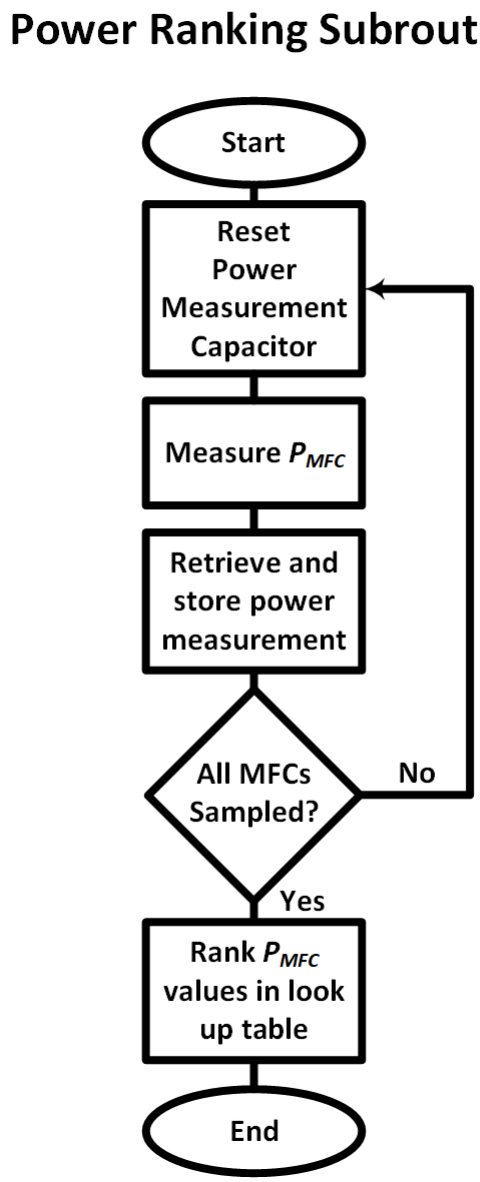

Figure 4.8: Flow diagram for MFC power extraction's ranking algorithm subroutine [100].

The DC-DC boost converter is found at the bottom side of the PCB.

The collected power is stored in an off-board output supercapacitors that powers the sensor nodes used to test the system.

The final algorithm was implemented using MPLAB X IDE and XC8 programmed in the PIC24F16KA102's non-volatile internal flash memory. It is important to mention that even though the information retrieved by the power ranking algorithm was stored in the volatile data memory,

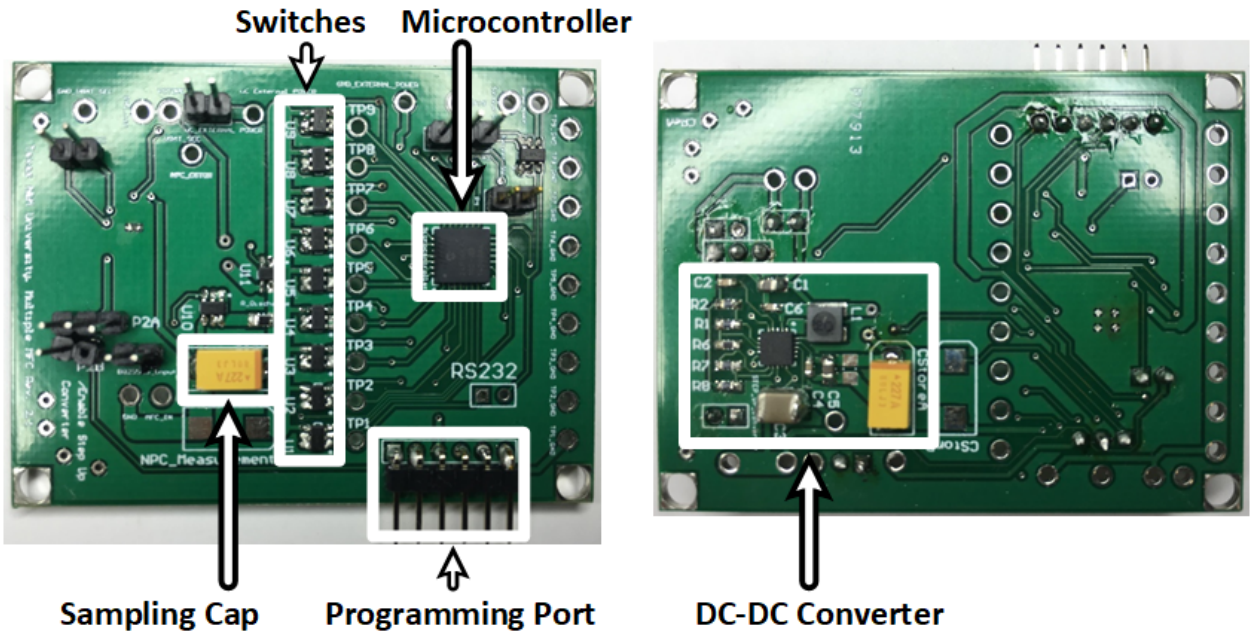

Figure 4.9: Printed Circuit Board of the PMS for multi-MFC power extraction, top view (left) and bottom view (right) [100].

the use of a non-volatile Electrically Erasable Programmable Read-Only Memory (EEPROM) to store such power ranking values is available in case further off-line data analysis is required. The sensor data collected in this chapter was acquired with the purpose to be transmitted and stored in a remote server in the cloud to enable further and more complex data analysis.

Even though the proposed system can natively support up to nine MFC devices without any further modification only four MFCs were tested in this chapter. It is also important to notice that if more MFCs are needed to increase the overall power available, the system can easily be adapted by adding more solid-state switches and digital multiplexers as needed.

4.4 Experimental Results and Discussion

4.4.1 PMS for Multiple MFCs

The operation of the power ranking subroutine operation is illustrated in Figure 4.10 which displays at the top, four channels represent the V_{MFC} waveforms of MFC1, MFC2, MFC3, and MFC4, respectively. The bottom plot represents the C_{PM} output voltage.

The label rank 1-4 at the bottom plot, indicate when the respective MFC 1-4 is power-measured by sampling its output power using C_{PM} such value is held to perform an analog-to-digital conversion. This sampling process is repeated for each MFC connected to the board periodically and its ranking values are grouped in phases. The ranking obtained at the phase is shown in Table 4.3, phase one. After the MFCs are sorted, then the power extraction can be performed. Phase two in Table 4.3, represents a second power-ranking measurement recalibration.

Device	Ranking (phase one)	Ranking (phase two)
MFC 1	1st	1st
MFC 2	4th	2nd
MFC 3	2nd	3rd
MFC 4	3rd	4th

Table 4.3: MFC power rank [100].

In Figure 4.11, the time interleaved power extraction operation of the proposed PMS is presented for different extraction phases. The four channels representing the MFC output voltages are labeled at the top of the graph. Initially, before power extraction, the voltage at the MFC represents its open circuit voltage; then, when the MFC is harvested its voltage drops to its MPP voltage. Finally, when V_{th-Low} is reached, the algorithm harvests the next MFC in the look-up table only if its output voltage is larger than $V_{th-High}$.

Figure 4.11 (left) shows the energy harvesting operation right after performing the MFC power ranking presented in Figure 4.10. Thus, the pattern for the power extraction, pointed out with gray arrows, follows the pattern described in Table 4.3 for phase one; however, after extracting power from the MFCs for 20 hours, the MFCs' power ranking look-up table recalibrates to the values shown in Table 3, phase two. Such power changes are illustrated in Figure 4.11 (right). It is important to highlight that, in phase two, not only are the power rankings changed for devices MFC2, MFC3, and MFC4, but at this point MFC1 now takes more time to reach $V_{th-High}$. This condition forces the algorithm to switch to the next available MFC that complies with the $V_{th-High}$

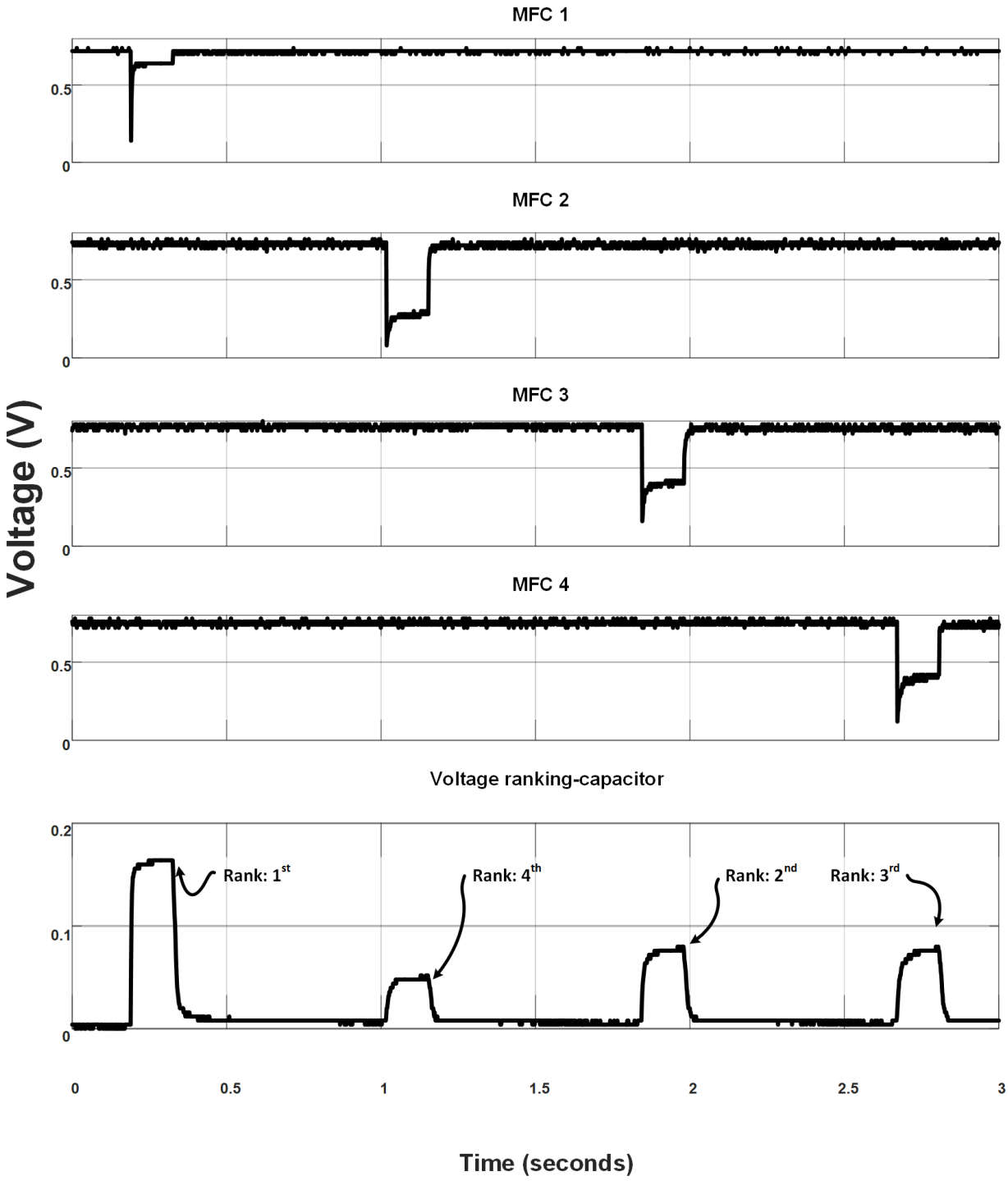

Figure 4.10: MFC power ranking waveform [100].

specifications, which in this case is MFC2. The algorithm continues its operation, and MFC1 is only harvested again when $V_{th-High}$ is reached as originally proposed.

Figure 4.12 shows the dynamic adaptability of the system. The highlighted section A shows the normal operation of the system if the pre-established threshold voltages are observed. On the other hand, section B demonstrates that when MFC4 does not reach the predefined voltage conditions, its port is neglected in an effort to optimize the power extraction time.

As demonstrated, an important characteristic of the power ranking feature previously demonstrated, is that if an MFC does not provide proper power conditions or has an internal failure, the system automatically isolates the damaged MFC and continues its operation without affecting the remaining MFCs or interrupting the energy harvesting process.

4.4.2 Wireless Smart Node Applications

A wireless temperature sensor (Monnit®) capable of transmitting data in a local network was fully powered by the PMS, four MFCs and a 0.1 F capacitor. Temperature measurements were transmitted and retrieved using a local PC as shown in Figure 4.13. Figure 4.14 (top) shows the 0.1 F output voltage capacitor charging curve. As can be seen, the 0.1 F supercapacitor was charged from 0 V to 2.5 V with an initial charging time (t_i) of 9.17 minutes; then, the temperature sensor was enabled and the data was transmitted wirelessly. After the packet was received by the PC, the sensor was disconnected from the supercapacitor. After performing the data transmission, the output voltage in the supercapacitor was 1.95 volts, from which it took an average recharging time (t_r) of 3.61 minutes to reach the 2.5 V level again. The process was repeated seven times in the span of 34 minutes. The temperature readings are shown in Figure 4.14 (bottom).

This first application replicates the load supercapacitor and the commercial WSN used in [90]. Moreover, as presented in Table 4.1, the MFC array used contains 3 MFCs comparable in size and electrical characteristics to the one used for the low-power MFC (LPMFC) example and 1 MFC similar to the one used for the high-power MFC (HPMFC) example. The results show a very substantial improvement in charging time: When comparing the results of this work to the measurements reported in [90] for the LPMFC, the initial charging time for the supercapacitor showed an improvement of 954% and an improved recharging time of 346%. When compared to the measurements reported for the HPMFC, the improvements in the initial charging time improvement

was 327% and the recharging time was 207%.

In a second experiment, an IoT application was implemented to test the capabilities of the proposed PMS for a power demanding extraction conditions. A Wi-Fi-enabled temperature smart node was designed and built for this purpose. This sensor node was based on the IoT platform Photon (Particle®, San Francisco, CA, USA)[114]. As seen in Figure 4.15, the IoT circuit board was wirelessly connected to a router to send the collected data over the internet, and the information gathered was retrieved using a handheld iPhone®device. Figure 4.16 (top) shows that the 5 F output supercapacitor was charged from 0 V to 3.3 V with an initial charging time (t_i) of 11.3 h; at 3.3 V the internet-enabled smart node was enabled, and the data was transmitted wirelessly to a remote server. After the data packet was received in the smartphone, the sensor was disconnected and the output capacitor voltage presented an output voltage of 2.8 V. It took an average recharging time (t_r) of three hours to fully recharge the supercapacitor from 2.8 V to 3.3 V. The process was repeated six times in the span of 24 h. The collected temperature readings are shown in Figure 4.16 (bottom).

By effectively powering the IoT application with the MFC array, the system robustness was confirmed after providing continuous power extraction in the span of 24 h, in such period the MFC did not show any abnormal stress or failure, validating in this way the potential use of MFC technology for power-hungry systems, such as IoT-applications.

4.4.3 Total Power Consumption and Efficiency

The PMS' power efficiency (η), as defined in 4.4, is presented in Figure 4.17. The peak end-to-end efficiency measured was $\sim$ 50.7% for a 3.3 output voltage. Table 4.4 summarizes and compares the presented chapter to previously reported systems.

$$\begin{aligned}\eta &= \frac{P_{out}}{P_{in}} \cdot 100 \\ &= \frac{P_{MFC} - \sum(P_{Losses})}{P_{MFC}} \cdot 100 \\ &= \frac{P_{MFC} - [I_{out} \cdot (R_{MFC} + R_{Switch}) + P_{loss-converter}]}{P_{MFC}} \cdot 100\end{aligned} \tag{4.4}$$

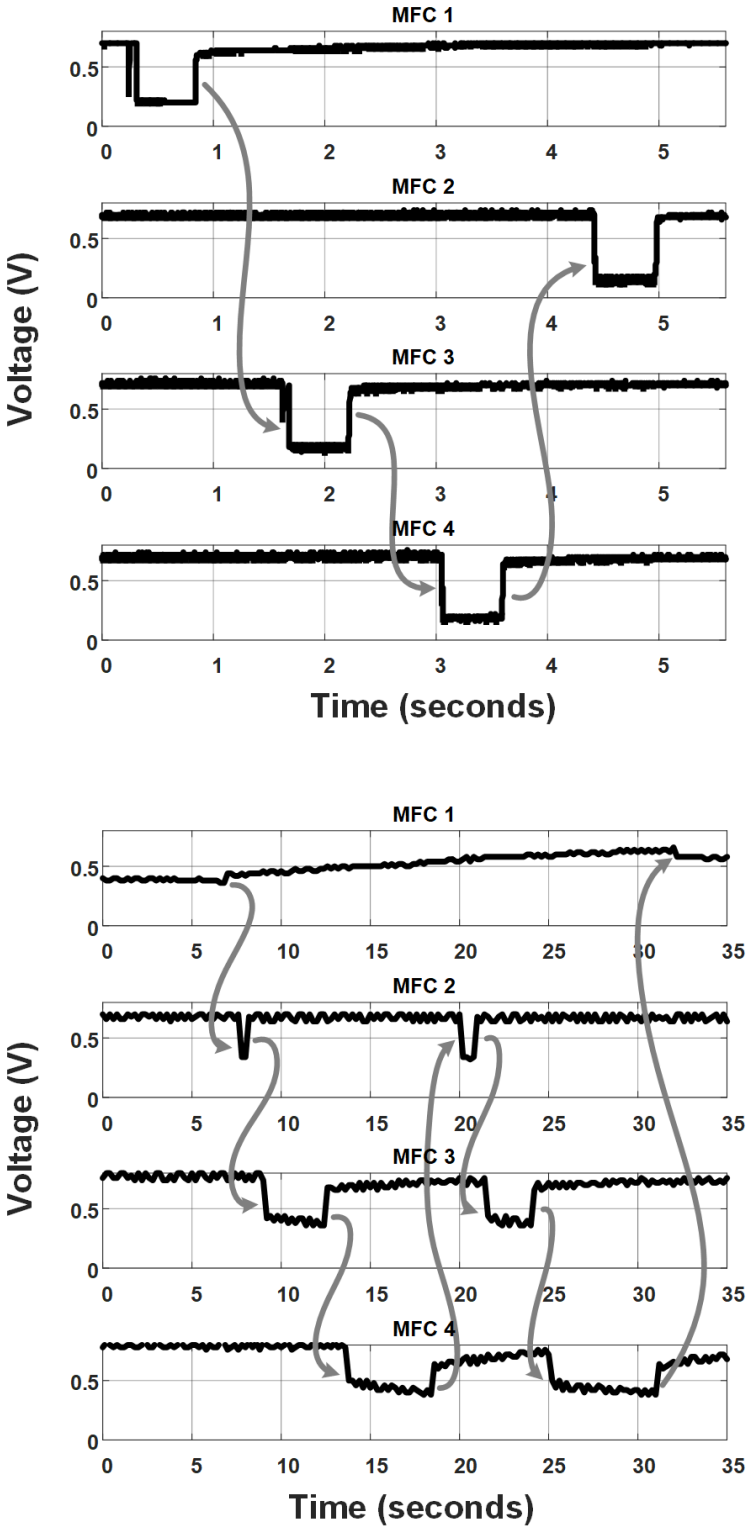

Figure 4.11: MFC interleaved power extraction measurements: phase one (top) and phase two (bottom) [100].

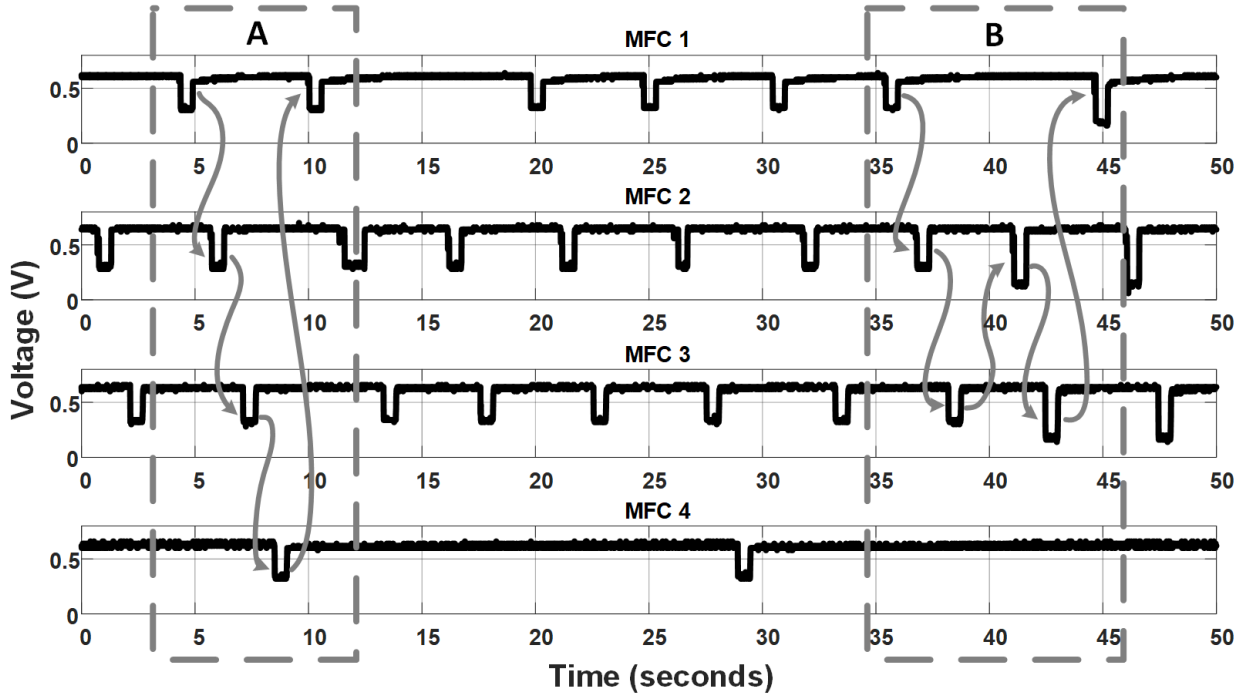

Figure 4.12: Dynamic adaptability of the system: normal operation (left) and change in MFC's power conditions (right).

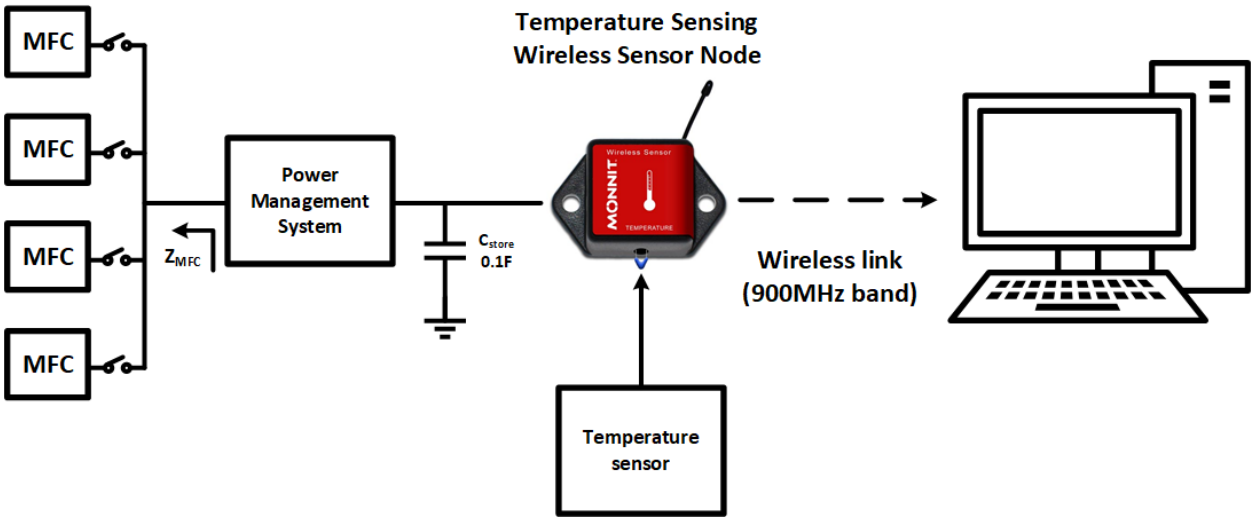

Figure 4.13: Local-network bluetooth sensor set up.

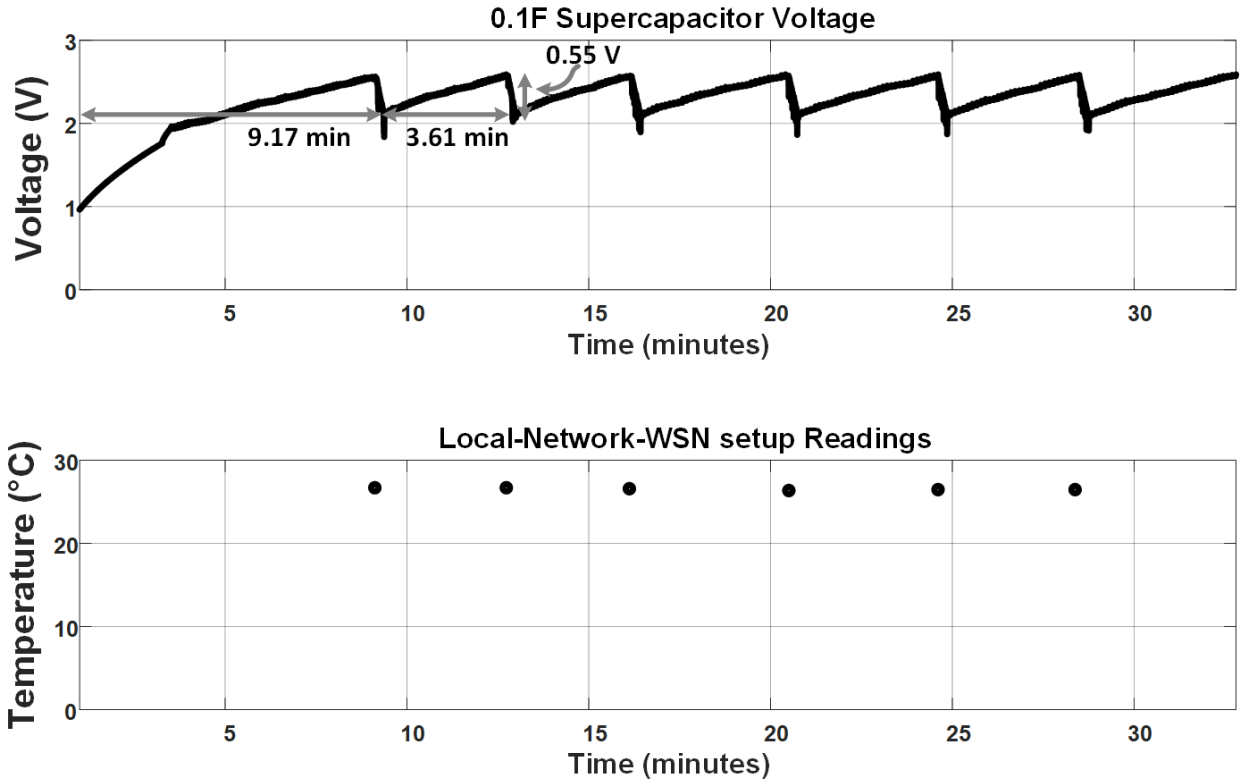

Figure 4.14: Local-network bluetooth sensor supercapacitor voltage waveform and (top) temperature measurements (bottom).

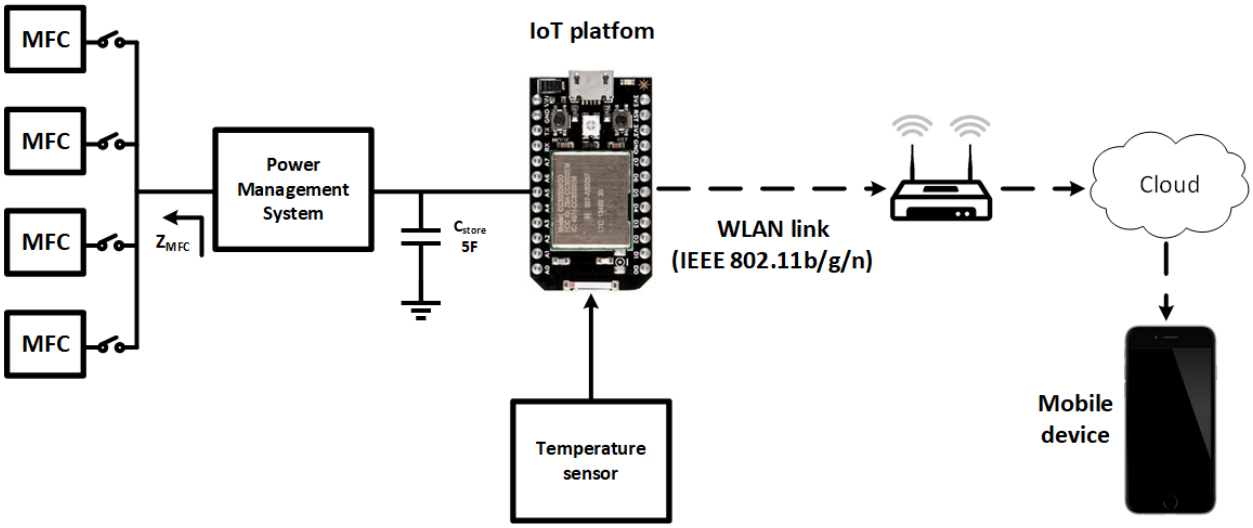

Figure 4.15: Internet of things sensor node hardware setup [100].

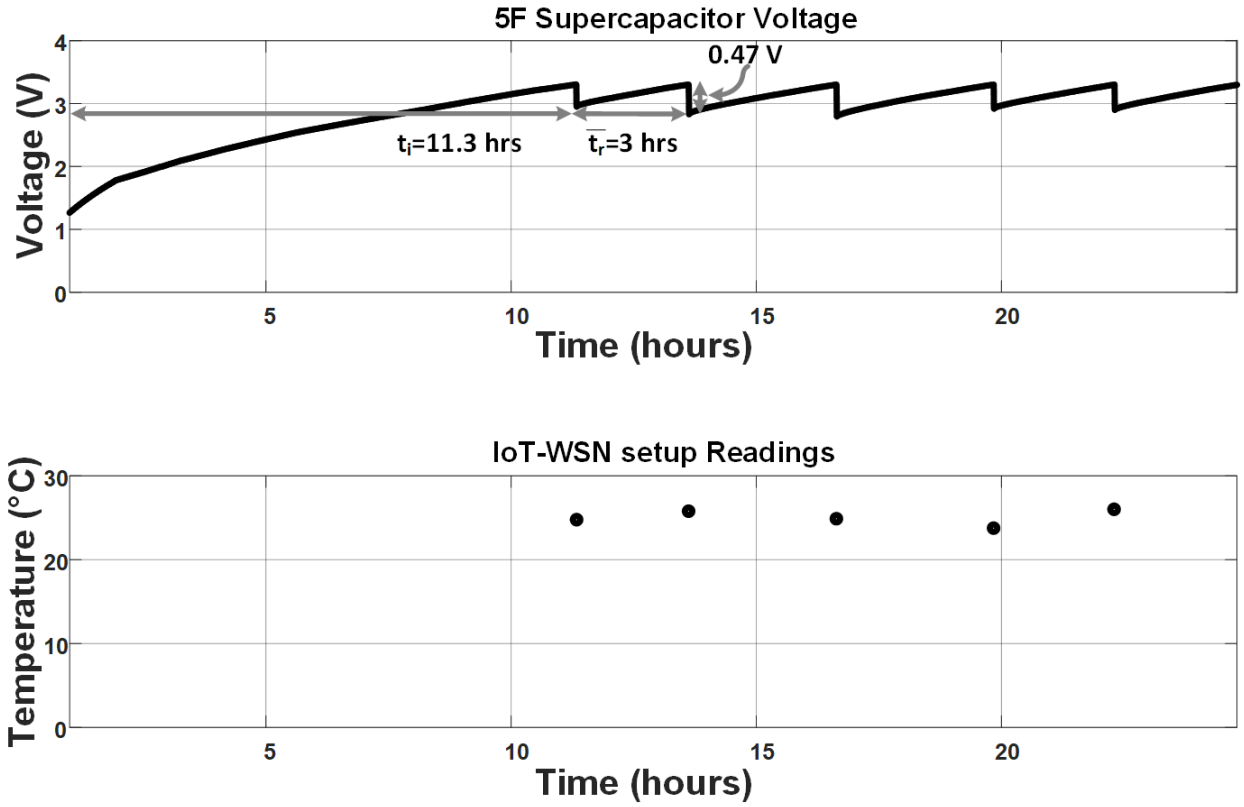

Figure 4.16: Internet of things sensor supercapacitor voltage waveform and (top) temperature measurements (bottom) [100].

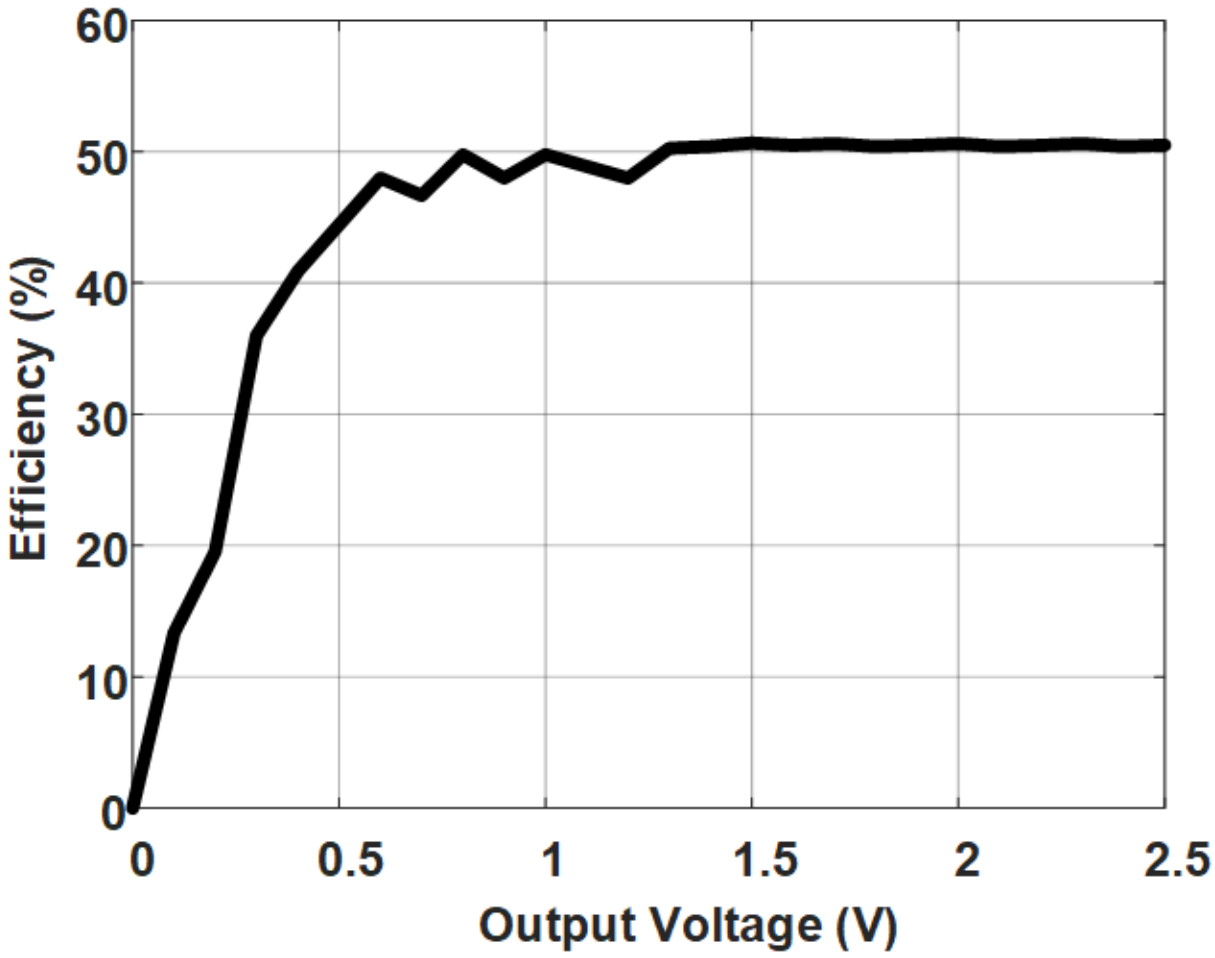

Figure 4.17: Measured Efficiency versus Output Voltage [100].

Specification	[115]	[90]	[92]	[91]	[96]	[116]	This Work
Input voltage	300 mV	300 mV	300–720 mV	300–600 mV	1.4 V (DC-DC converter input)	300 mV	330 mV
Output voltage	1 V	1.8 V	2.5 V	2.5 V	4.25 V	3.3 V	3.3 V
Inductor	$326.7\mu H$	$2\mu H$	$1.5mH$	$1.5mH$	Transformer $31.8mH$ (primary winding)	-	$22\mu H$
Output capacitor	$8\mu F$	$47\mu F$	$0.1F$ (supercapacitor)	$0.1F$	$68mF$	Multiple	$5F$
Maximum power extraction	-	-	Adaptable Maximum Power Extraction	Yes	MPPT	-	MPPT
Efficiency	74%	-	58%	30%	-	35.02%	50.7%
Implementation approach	Discrete Components	Discrete Components	Custom integrated circuit	Custom integrated circuit	Discrete Components	Discrete Components	Discrete Components
Multiple MFC power extraction	No	No	No	No	Yes	Multi anode	Yes (default support for 9 MFCs)
MFC health protection	-	-	-	-	No	No	Yes

Table 4.4: Comparison of MFC power management units [100].

4.5 Discussion

This chapter presents a methodology to charge a supercapacitor from multiple MFCs. The load circuit being powered was capable of sending data in a local network over the internet. All of this makes the MFCs a promising energy harvesting source for commercial applications in the IoT domain, which can potentially allow smart nodes to be self-powered and to be used in places not previously thought practical.

The proposed system can extract power from a single MFC in an MFC array at a time, which enables a custom MPPT for every single MFC, while at the same time allowing idle MFCs to recover and produce more charges, avoiding overly depleting the MFCs. The same feature also allows the system to continuously work in the presence of an MFC that does not provide significant charges, or even in the case of physical MFC detachment from the PMS. Such anti-MFC failure features significantly improve the reliability of the whole system.

The performance of the system not only proved to be several times more efficient than the old system's reliance on extracting power from a single MFC, but it also proved more efficient compared to works with custom-made ICs where PCB and external component losses are expected to be less.

This research also determined that MFC networks are capable of meeting the specifications of power hungry applications. An MFC system can also be scalable with minimum hardware modifications to provide higher amounts of power. The techniques used in this work are compatible with the design proposed in other works, and since the system was made using commercial off-the-shelf components, it can be easily replicable and modifiable.

4.6 Conclusions

This chapter presents a system design that can extract power from an array of MFCs using a time-interleave technique that not only enables a custom MPPT per MFC in the arrange but also allows a proper MFC charge-recovery time to avoid overly depleting the cells in the array, which can lead to an MFC failure or premature end-of-life. An optimal power harvesting process was

measured when enabling a maximum power point tracking in the DC-DC power conversion block across four different MFCs with an output characteristic power at MPPT ranging from 6400 νW to 435 νW with an observed 50.7% peak efficiency. The results of the proposed system show a robust performance of the proposed PMS after more than 24-h of MFC EH even in presence of weak or damaged MFCs.

The system was able to run autonomously to charge an output supercapacitor of 0.1 F to 2.5 V in 9.17 minutes to power a WSN. In the same way, the proposed PMS was able to charge an output supercapacitor of 5 F from 0 V to 3.3 V in 13.6 h and endure a 24-h power extraction with no signs of MFC over-depletion or failure. The system powered an internet-enabled smart node five times, and the information was correctly retrieved from a remote server using a smartphone device.

By successfully completing this MFC-powered IoT-sensor node demonstration, EH based on MFC technology has been verified as a promising area that has the capabilities to run power intense systems, such as internet-enabled technologies, which can potentially enable the arrival of a new generation of self-powered smart nodes.

Finally, future work in this area includes the development of efficient PMS startup circuits tailored to MFC technology, more efficient low-power data acquisition and processing techniques for remote sensing, in which the addition of new sensors and analytical models in the cloud can give accurate real-time and predictive information about the health state of the MFC.

5. RECONFIGURABLE SYSTEM FOR ELECTROMAGNETIC ENERGY HARVESTING WITH INHERENT ACTIVITY SENSING CAPABILITIES FOR WEARABLE TECHNOLOGY*

5.1 Introduction

Wearable technology is a dynamic and growing industry that is increasingly offering popular insights about the user's well-being [117], as is the case of health monitors [118]. Activity trackers, specifically, have two important characteristics: first, their limited set of features, makes them one of the most power efficient consumer electronics. Second, because these wearables are mainly intended to gauge user's activity, they are very likely to be at the core of high physical movement [119]. Figure 5.1 presents how these two characteristics make of activity-tracking devices a unique candidate for body-motion energy harvesting (EH), which can harness the mechanical energy and recycle it back to the wearable itself, to not only extend their battery life, but potentially to fully power it [120]. Especially if this family of devices is designed only for essential sensing, control and signal processing capabilities.

Research of EH sources to power efficient electronics [121] range from ambient light [122], radiofrequency [123], thermal [124, 76] and kinetic [125]. Human, animal, along with machine motion EH, are an attractive substitute for batteries in consumer electronics [126]. Piezoelectric generators, which produce energy from vibrations, have the potential to generate power for wearables; however, highly efficient piezoelectric technology often require the use of a cantilever setup to maximize its power production, which makes them not attractive for a highly-portable wearable application [127]. In contrast, a very cost-effective and highly scalable kinetic EH source can be found in electromagnetic (EM) transducers [128, 129]. Such transducers consist of a coil, made from magnetic wire, and a magnet assembled in a way to allow it to axially travel back and forth

*Reprinted with permission from "Reconfigurable System for Electromagnetic Energy Harvesting With Inherent Activity Sensing Capabilities for Wearable Technology," by A. Costilla Reyes, A. Abuellil, J. J. Estrada-López, S. Carreon-Bautista and E. Sánchez-Sinencio, 2019. IEEE Trans. On Circuits and Systems II: Express Briefs, vol. 66, no. 8, pp. 1302-1306, Aug. 2019,

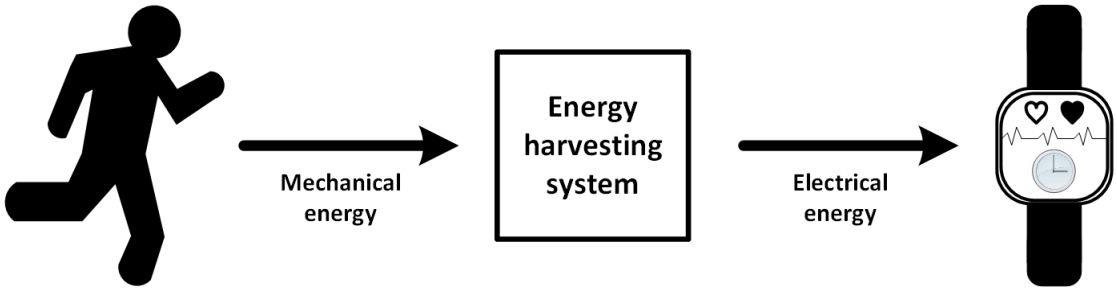

Figure 5.1: Concept of an EH-based system for wearables.

throughout the magnetic coil. The motion required to displace the magnet, can be found in the natural wrist motion of a person walking or running.

It is paramount to highlight that while previous EH systems based on an electromagnetic transducer for wearables have been reported, the intrinsic sensing capacity of the kinetic transducer to collect data from the user's activity is rarely exploited. In [130], an electromagnetic transducer interface design is presented by integrating a transducer topology based on an alternate winding and a differential rectifier to a boost converter. Here, while the active-resistance-matching technique allows an improved input matching efficiency, the proposed circuit does not have the capability to use the sensing data of the transducer to further improve its power efficiency. In [131], a rectifier based on a low-quiescent negative voltage converter (NVC) is presented. The AC/DC chopper employed was designed and simulated to use the self-inductance of the electromagnetic transducer. However, even though the properties of the EM transducer are inherently employed for the proposed circuit to operate, the system does not provide with a way to isolate the EM transducer and allow its use as a sensor to provide further system sensing functionalities.

In the same way, other works have explored novel solutions of harvesting low input voltages power sources. In [132], for example, an adaptive rectifier is proposed that can switch between two independent passive and active rectification blocks depending on the available power. However, this implementation was done using discrete components which incur in considerable power losses and has an important overall system size, that can make this application impractical for portable and low-power EH wearable systems. On the other hand, [61] and [133] integrate on-chip a similar

approach to reach significant improvements in efficiency by using independent passive and active rectification blocks. In both works, the redundant rectification CMOS circuits for rectification represents a considerable impact in the total area expenditure of the rectification block and a fixed passive power path for current leakage.

This chapter presents a system designed to harness energy from body motion while providing sensing capabilities which consist of an end-to-end EH system with inherit activity sensing tailored for wearable devices. The proposed work, shown in Fig. 5.2, involves the development of a compact EM transducer, a front-end circuit designed for rectification and sensing purposes, a power conversion block based on the Texas Instrument's BQ25505 DC-DC converter, and an efficient control block. The rectification stage proposed here, reconfigures from passive to active mode to improve its efficiency by rectifying lower input voltages from the source. A key characteristic of the proposed rectification stage is its ability to completely isolate the EM transducer to the power conversion stage to exclusively use it as a sensor and provide sensing information with proper logic levels to allow a subsequent digital-based data analysis. This digitalized sensor-data, makes this EH and sensing system a good substitute to supplementary sensors to gauge activity, such as an accelerometer or a gyroscope, traditionally needed to determine a user's number of steps or activity intensity.

This chapter is organized as follows: subsection 2 describes the design of the proposed system, subsection 3 elaborates on the system operation and subsection 4 presents the experimental results of this work. Conclusions are presented in subsection 5.

5.2 System design

In this subsection all end-to-end design specifications of an electromagnetic energy harvesting for wearable technology are specified and described. The proposed EH-based wearable system considers three main system blocks: EM transducer, reconfigurable rectifier and activity detection and power conversion stage. Figure 5.2 shows the top-level implementation of the EH-powered wearable application presented in this chapter.

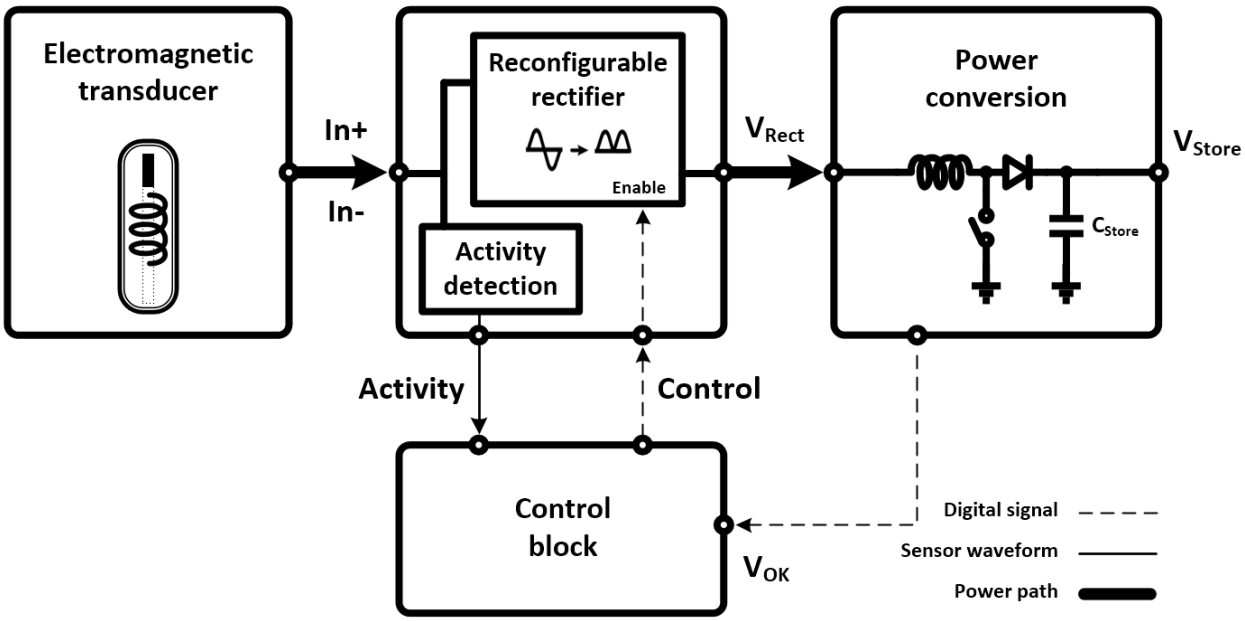

Figure 5.2: Top-level system implementation of EH-based system for wearables [30].

5.2.1 Electromagnetic transducer

The electromagnetic transducer, designed to be worn in the wrist to capture the mechanical energy from movement while walking or running. The design of the transducer followed the analysis presented in [128] and [129], considering the peak power delivered and the final dimensions as the main specifications for the construction of the transducer presented here.

A plastic casing was modeled and 3D printed using acrylonitrile butadiene styrene (ABS) filament. Its main purpose is to accommodate the different elements of the custom transducer shown in Fig. 5.3. The relative-axial movement of the main neodymium (NdFeB) magnet, of a diameter of 4.76 mm and 9.53 mm of length produces the magnetic flux linkage that can be harvested by the system when interacting with a 36 AWG magnetic wire. A plastic inner tube placed along the full axial movement of the magnet through the coil, and two lateral magnets placed at the ends of the 3D printed housing are intended to reduce mechanical friction losses. Due to the low operation frequency of the system ($5Hz$) this transducer was modeled according to the final transducer's specifications listed in Table 5.1.

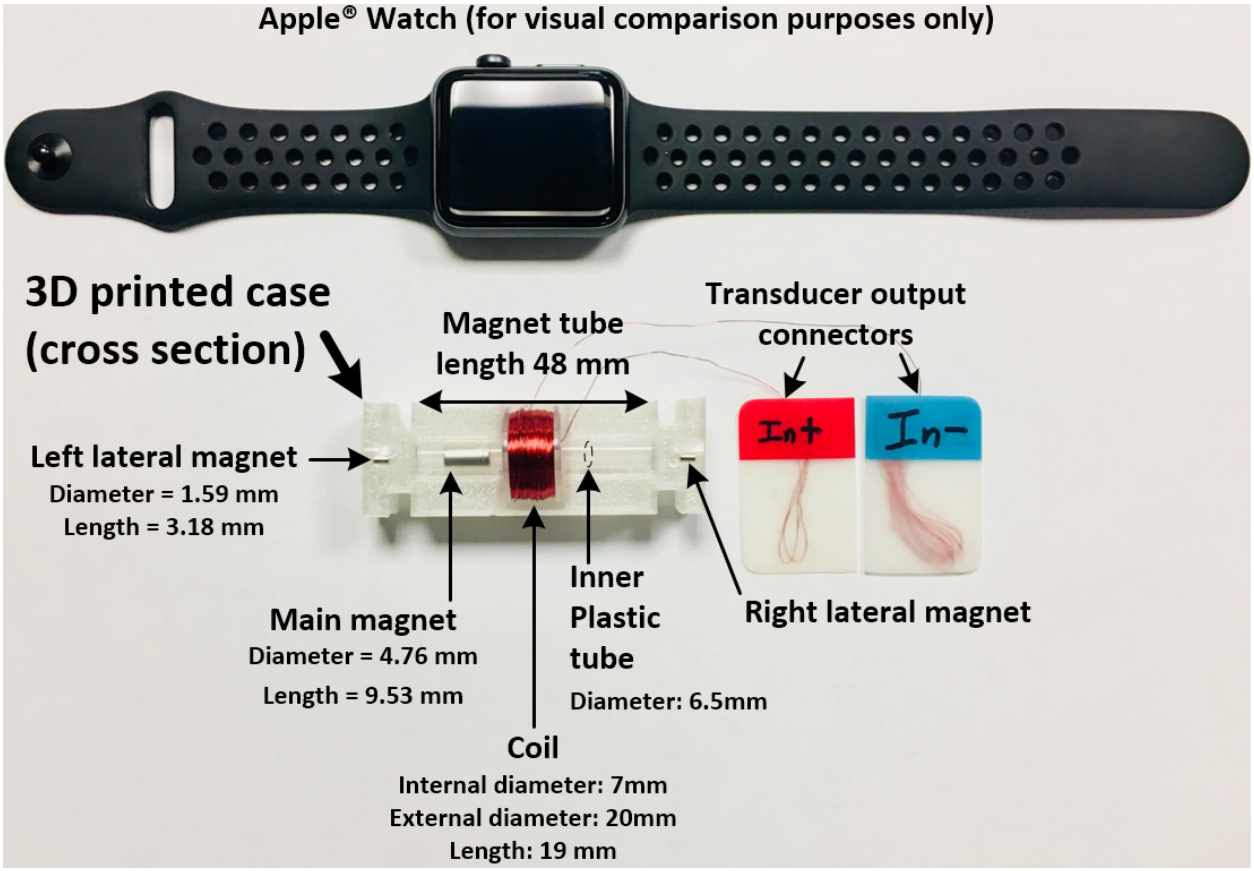

Figure 5.3: Electromagnetic transducer structure [30].

Specification	Value
DC resistance	61.68 Ω
Inductance	18.7 mH
Peak output voltage	2.5 V
Output power	7m W @ 100 Ω
Magnetic material	Neodymium
Magnetic wire	36 AWG

Table 5.1: Transducer specifications [30].

An acceleration sensor is commonly integrated into wearable devices to perform activities such as step counting. This information is often presented in the form of performance analytics that correlate the steps and its intensity to the amount of energy spent by a user during exercising, for example. The system presented here proposes the use of the EM transducer to gather basic infor-

mation similar to that provided by acceleration-based sensors. In Fig. 5.4, the output waveform of the EM transducer (top) is compared to the information provided by a Bosch BMA280 acceleration sensor (bottom). Both waveforms were retrieved when the user moved his hands with both sensors moving together. As it is observed, the EM transducer can be used to gather basic information similar to that provided by an accelerometer.

It is important to notice that the symmetry of the waveforms in the EM transducer are due to the interaction of the polarity of the main magnet to the coil. That is, the positive polarity of the magnet going forward through the coil has the same output waveform polarity as the negative polarity of the magnet going backward through the same coil, resulting in a symmetric waveform for peaks I, II and III. In contrast, the output waveform of the accelerometer presents a symmetry for peaks I and II of Fig. 5.4 (bottom), representing the forward movement of the user's hand at a top force close to 4g, whereas a backward movement of the hand presented in peak II, is a mirror representation of the waveform presented in peaks I and III.

Albeit simple, the information contained in the EM transducer waveform successfully showed the hand movements of the user as compared to an acceleration sensor x-axis output. The simplicity of the information in the presented kinetic transducer output waveform can be employed to easily determine number of hand movements and its speed for example. All of this from an element that not only no consumes power, but provides energy to the wearable system. To exploit this property found in the kinetic EM transducer, a front-end circuit is proposed and presented in the following subsections.

5.2.2 Reconfigurable rectifier

A reconfigurable rectifier is required to convert the AC voltage from the EM transducer to DC. To achieve this, a rectifier topology that reconfigures depending on the available power in the system is presented here. The proposed circuit, illustrated in Fig. **??**, reuses transistors $M_1 - M_4$, in the main power path, for the passive and active rectification configurations.

The passive rectification mode illustrated in Fig. **??**, is employed when the storage capacitor voltage V_{Store} is less than $1.8V$, no enough energy is stored in the system to power the control

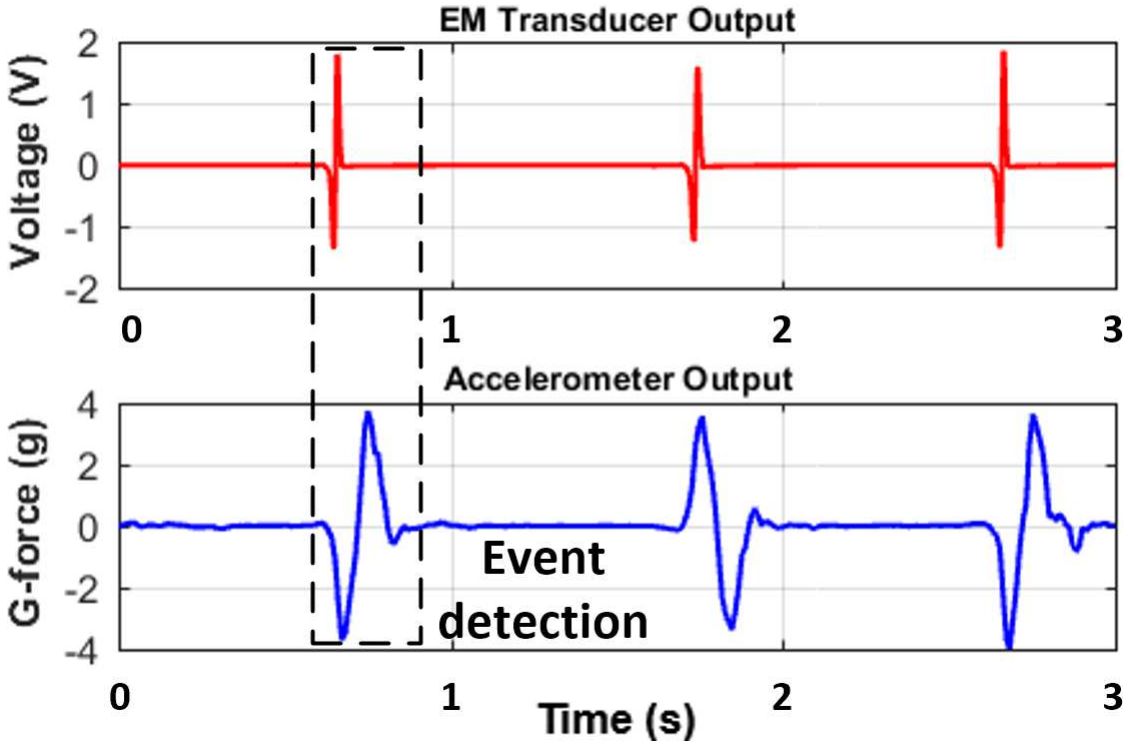

Figure 5.4: Electromagnetic transducer waveform output (top) and accelerometer y-axis waveform output (bottom) comparison [30].

circuit for an active rectification stage to operate. Passive rectification is achieved during startup when transmission gates $TG_1 - TG_4$ have a zero voltage on gate, operating as a short circuit, resulting in a standard negative voltage converter (NVC) topology, where the difference in voltage of the EM transducer connected at In+ and In- can enable either M_1 and M_4 or M_2 and M_3 for positive and negative AC input voltage swings, respectively. This NVC circuit presents a rectified signal at V_{Rect} and GND.

When the voltage at the storage capacitor reaches a minimum of 1.8 V, that is $V_{Store} > 1.8V$, then the active configuration of the rectifier is enabled as presented in Figure 5.6. Signals V_{OK} and $\overline{V_{OK}}$, provided by the DC-DC converter in the power conversion block, open transmission gates $TG_1 - TG_4$, reconfiguring from an NVC to the active rectification topology where $M_1 - M_4$ are controlled by signals $C_1 - C_4$ through $M_5 - M_8$, instead. This active configuration can rectify low input voltage swings commonly found in low-pace movements, such as walking. This is achieved

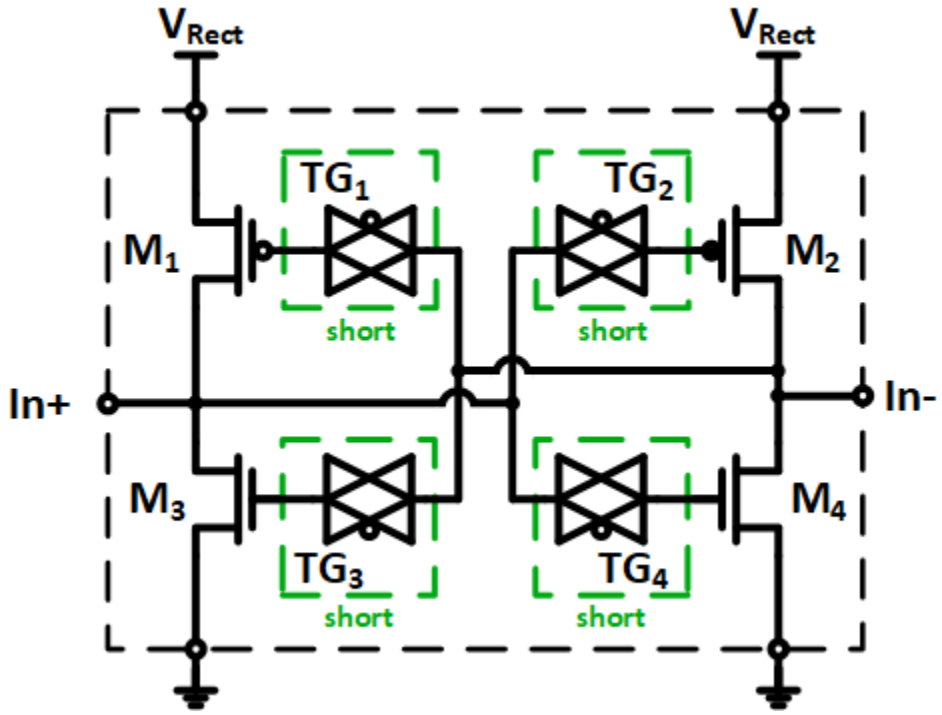

Figure 5.5: Reconfigurable rectifier in passive configuration [30].

with two TLV3691 nano-power comparators, referred to as U_1 and U_2 in Fig. 5.7, which enables branches M_1 and M_4 or M_2 and M_3 by comparing the polarity of the EM transducer and V_{Rect}.

An important feature of the active rectification topology is that transistors $M_1 - M_4$ can be turned off to fully isolate the transducer from the power path of the EH system and to enable the system's sensing capabilities. Since sensing is not permanently performed but intermittently performed due to power efficiency restrictions, the EH operations are not affected in a significant way; however, if the application does not require sensing, then EH mode can be enabled permanently.

Table 5.2 shows the reconfigurable rectifier's transistor sizes which design avoided a minimum length for transistor $M_1 - M_4$ to reduce its voltage threshold, while maximum conductive resistance and current specifications were limited to transducer's resistance and power available mentioned in Table 5.1.

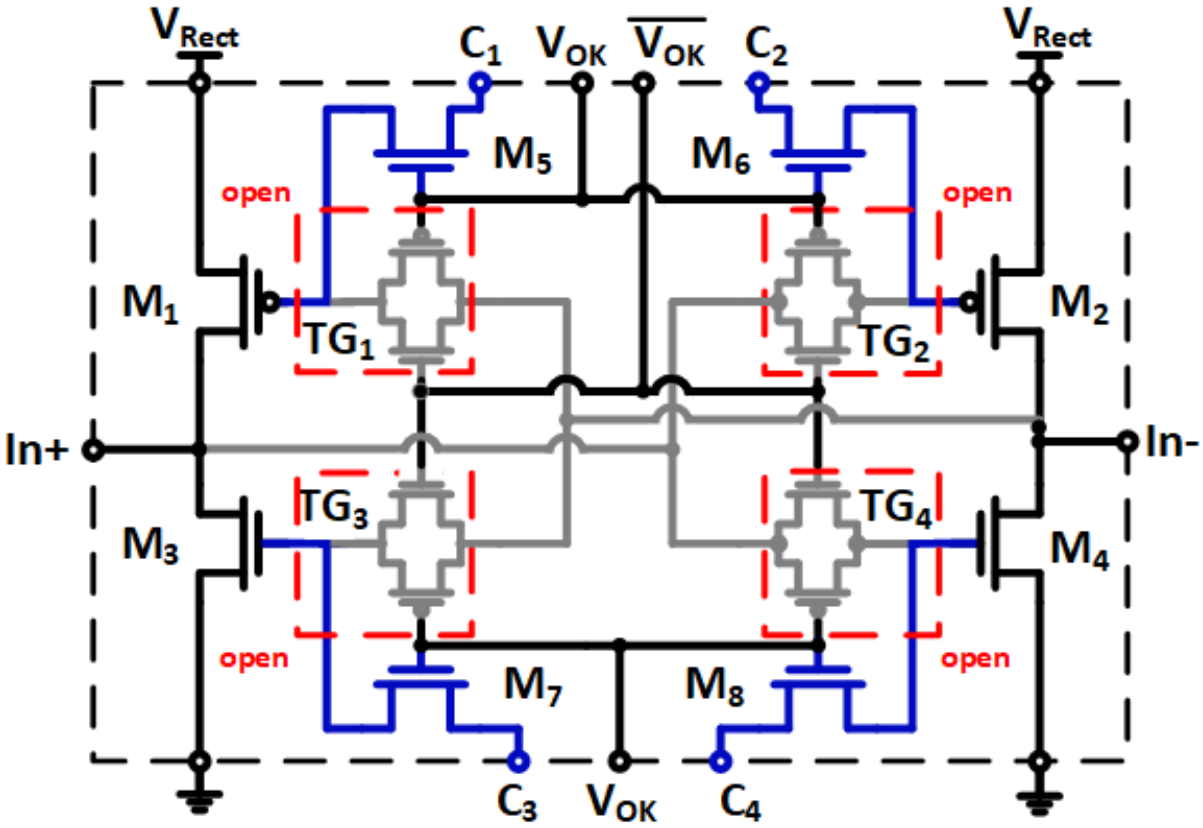

Figure 5.6: Reconfigurable rectifier in active configuration (detailed schematic view) [30].

Transistor	Size (μm)
$M_1 - M_4$	900 / 0.4
$M_5 - M_8$	0.5 / 5
$TG_1 - TG_4$	2 / 5 (PMOS & NMOS)

Table 5.2: Reconfigurable rectifier transistor sizes [30].

5.3 Activity detection

The activity detection sub-block is shown in Figure 5.8. The EM transducer is connected to this block through inputs In+ and In-. Transistors $M_9 - M_{10}$ allows the higher input voltage of the AC signal at the input to be copied at the gate of the transistor M_{11} to provide a rectified sensing signal at the activity node. Lastly, the leak current, represented by R_A, defines the output voltage

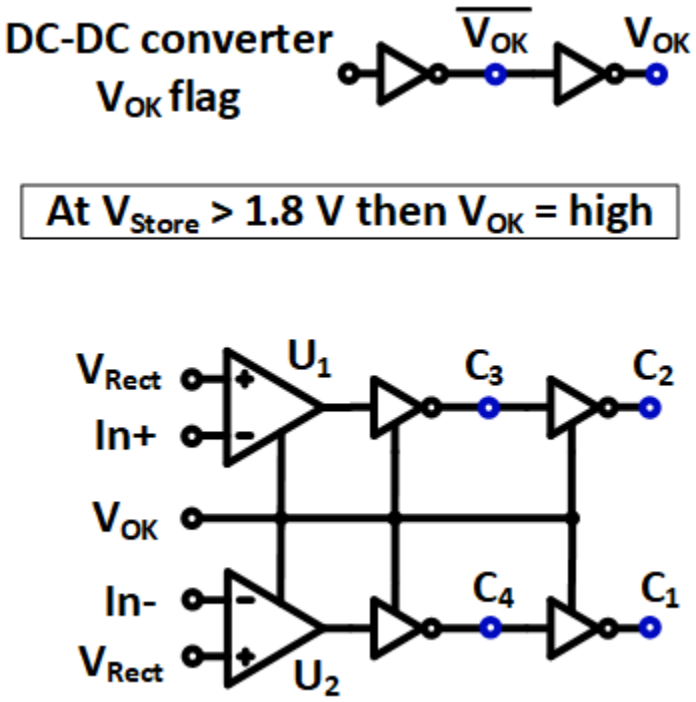

Figure 5.7: Control circuit sub-block for active configuration of reconfigurable rectifier [30].

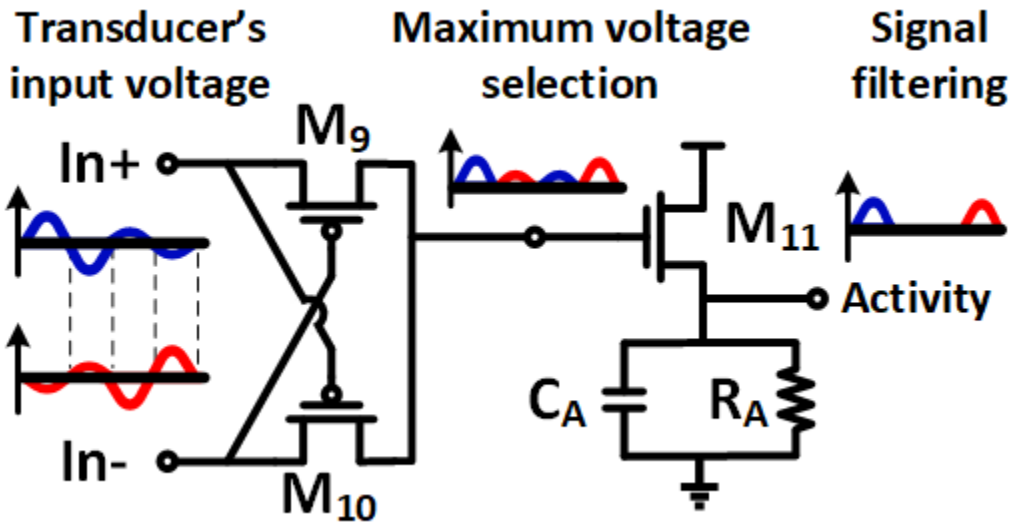

Figure 5.8: Activity detection transistor level circuit [30].

at no input condition while C_A filters the sensed signal.

The activity detection circuit is connected to the EM transducer in parallel with the input of the reconfigurable rectifier to provide a sensing signal to the system while providing energy to the system. However, the sensed signal is expected to be distorted if the transducer is used for both EH and sensing purposes. To accommodate these dual functions, the system must add the flexibility of choice - to work in either the EH-mode or sensing-mode.

The reconfigurable rectifier block in its active can remove the EM transducer from the power path by opening $M_1 - M_4$. By fully isolating the transducer through the rectification stage, it can be used exclusively for sensing operations. Notably, the ability to isolate the EM transducer was designed to provide a cleaner sensing signal and full-rail voltage swings. Table 5.3 presents the transistor sizes used for the implementation of the activity detector topology in this section.

Transistor	Size (μm)
M_9, M_{10}	0.5 / 4
$M_1 1$	100 / 0.56

Table 5.3: Activity detector topology transistor sizes [30].

5.3.1 Power conversion block

A Texas Instruments BQ25505 DC-DC converter for low power applications is used to boosts the V_{Rect} to a programmed 3.3 V. This component provides a voltage-okay flag $V_{OK} = high$, when $V_{Store} > 1.8V$, which triggers the active mode of the EH-based wearable system presented here.

5.4 System operation

The EH-based wearable system operation diagram is presented in Fig. 5.9. At the top of the diagram is the input signal from the kinetic transducer, which can be continuous or intermittent depending on the movement provided by the user; thus, signals $M_1 - M_4$ represent the state of the transistors of the rectifier, and V_{OK} determines the passive or active EH-mode. At the same time the activity detector output in the time diagram represents the output node of the activity detection

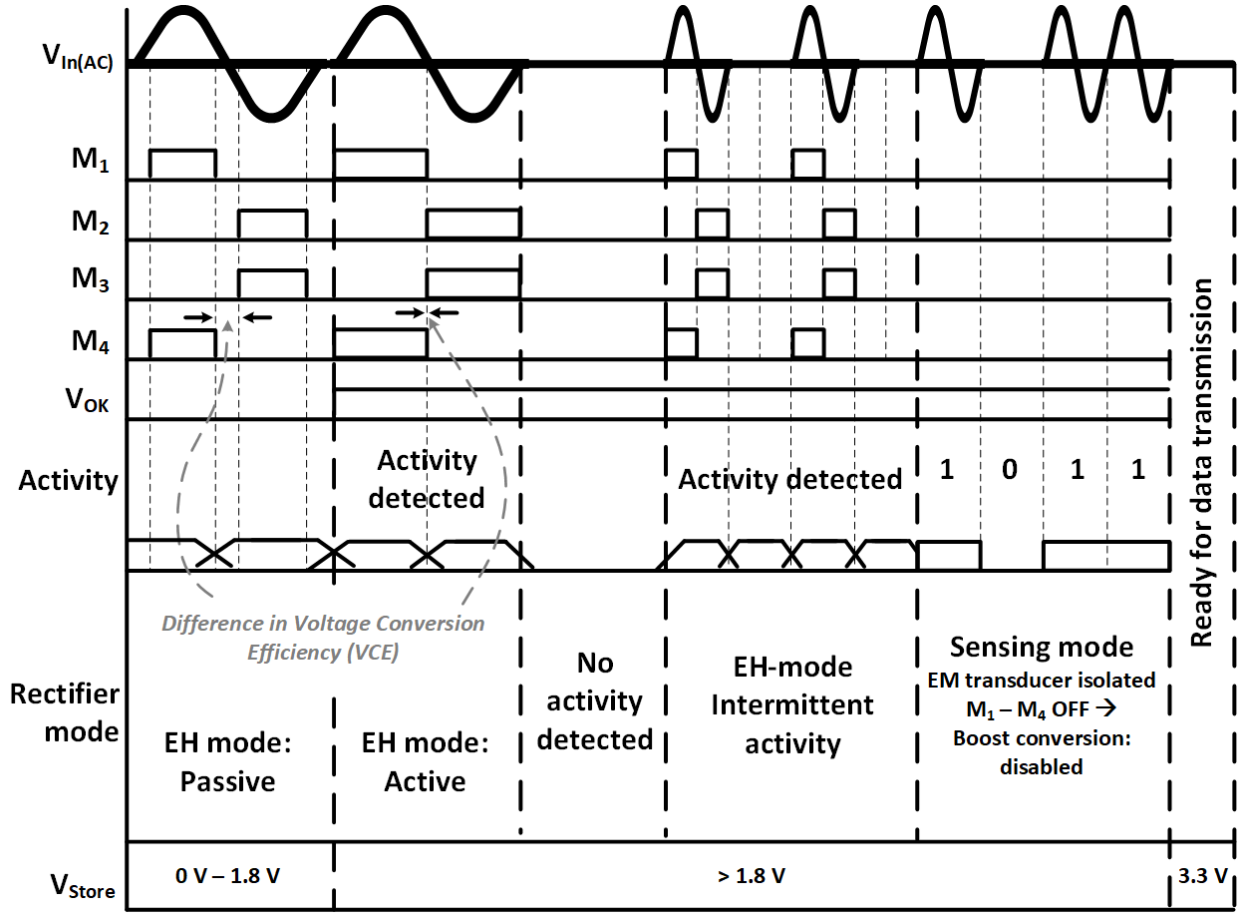

Figure 5.9: Energy harvesting system operation time diagram [30].

block. The rectifier mode along with the V_{Store} voltage levels are presented at the bottom of the diagram.

Initially, the reconfigurable rectifier starts in its passive mode, where the NVC-like configuration allows a passive AC to DC rectification. The rectified signal is fed to the DC-DC boost converter of the power conversion block.

When the voltage at the output storage capacitor reaches a minimum of 1.8 V, the boost converter sets up the V_{OK} flag that enables the active mode of the reconfigurable rectifier. If activity is sensed from the transducer, then the operation of the comparators for active rectification is enabled, whereas when no activity is detected, the input of the transducer to the DC-DC converter is disconnected to avoid any possible back-leakage. Any further activity by the user enables the

system to restart in the EH-mode. An active rectification allows a lower In+ and In- rectification, as compared to its passive rectification counterpart, associated with low-pace activity, such as walking.

The system also integrates the capability to enter a sensing-mode by turning off transistors $M_1 - M_4$ to isolate the EM transducer from the power conversion stage. The cleaner signal at the output of the activity detector node can reach full logic levels that can be represented as digital values that correlates to the activity from the user. Such digital information can potentially be used to know the number of steps or to determine walking speed if the time between pulses is measured and processed.

The resulting data obtained from the sensing mode can also be stored and transmitted to a larger system for a more comprehensive data analytics using the Bluetooth wireless module already integrated in a commercial wearable device.

Finally, if the output voltage drops below 1.8 V then the system configures as a passive rectifier and the process repeats.

5.5 Measurement results

The energy harvesting front-end was fabricated in a 130 nm TSMC CMOS technology with an active area of 0.0254 mm^2. The IC micrograph is shown in Figure 5.10, the printed circuit board of the EH system for wearables is shown in Figure 5.11 and the measurement setup is shown in Figure 5.12.

Figure 5.13 presents the passive operation of the circuit. At startup, a brief low pace movement section illustrates the drop in kinetic energy harvested during this period. At 1.8 V the active rectification is enabled. In this transition, a drop in the V_{Rect} amplitude can be appreciated, due to a change to a lower input impedance presented by the front-end circuit because the control circuit allows an improved charge conduction of the rectification transistors $M_1 - M_4$ in the power path, which in turn translates to a higher efficiency. The operation reaches its nominal output voltage at 3.3 V, and the test activity ends.

The activity detection measurement at the transition of the EH to the sensing mode is presented

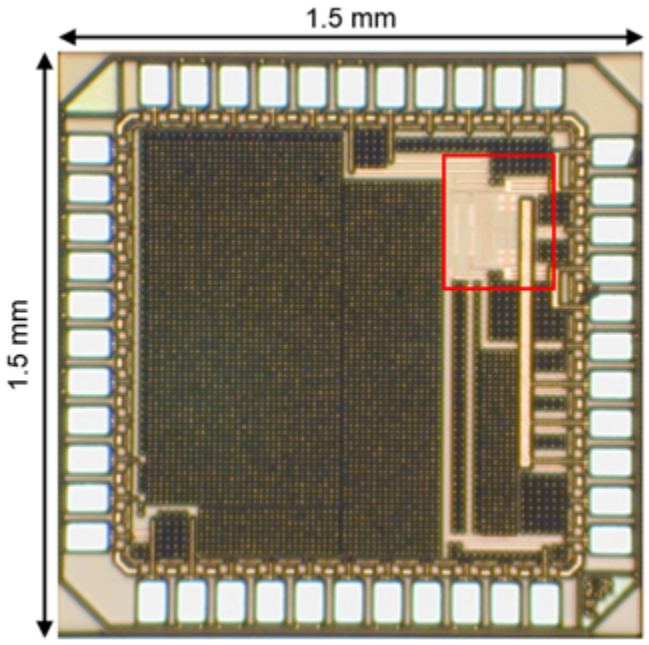

Figure 5.10: IC micrograph of the proposed power management system [30].

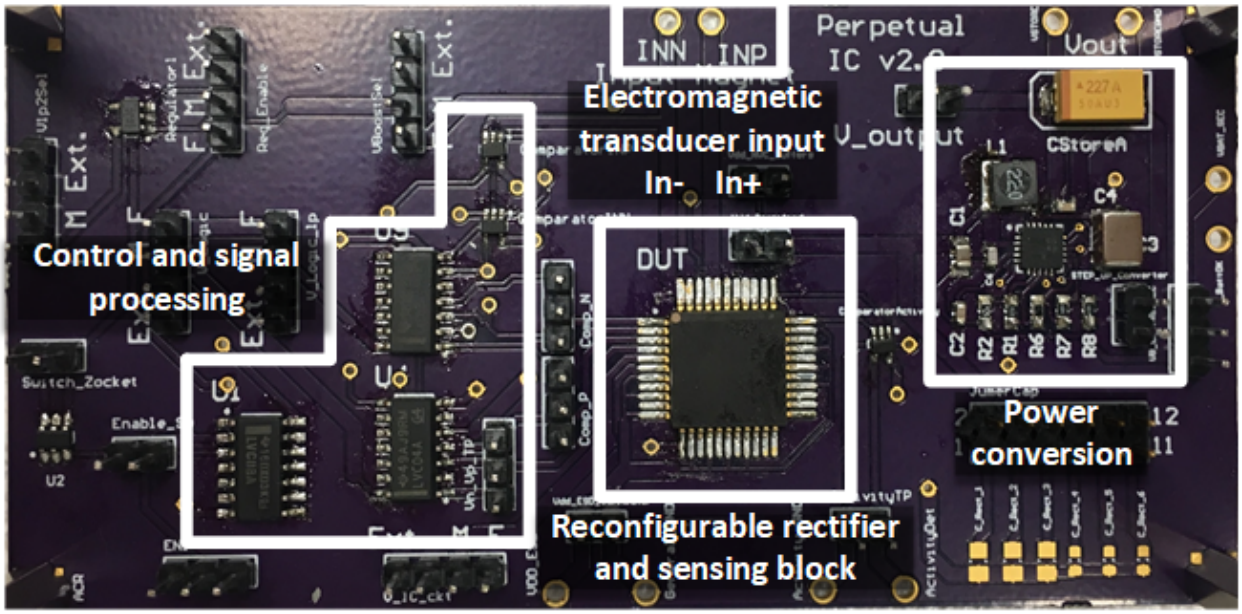

Figure 5.11: EH and sensing system printed circuit board of the proposed power management system [30].

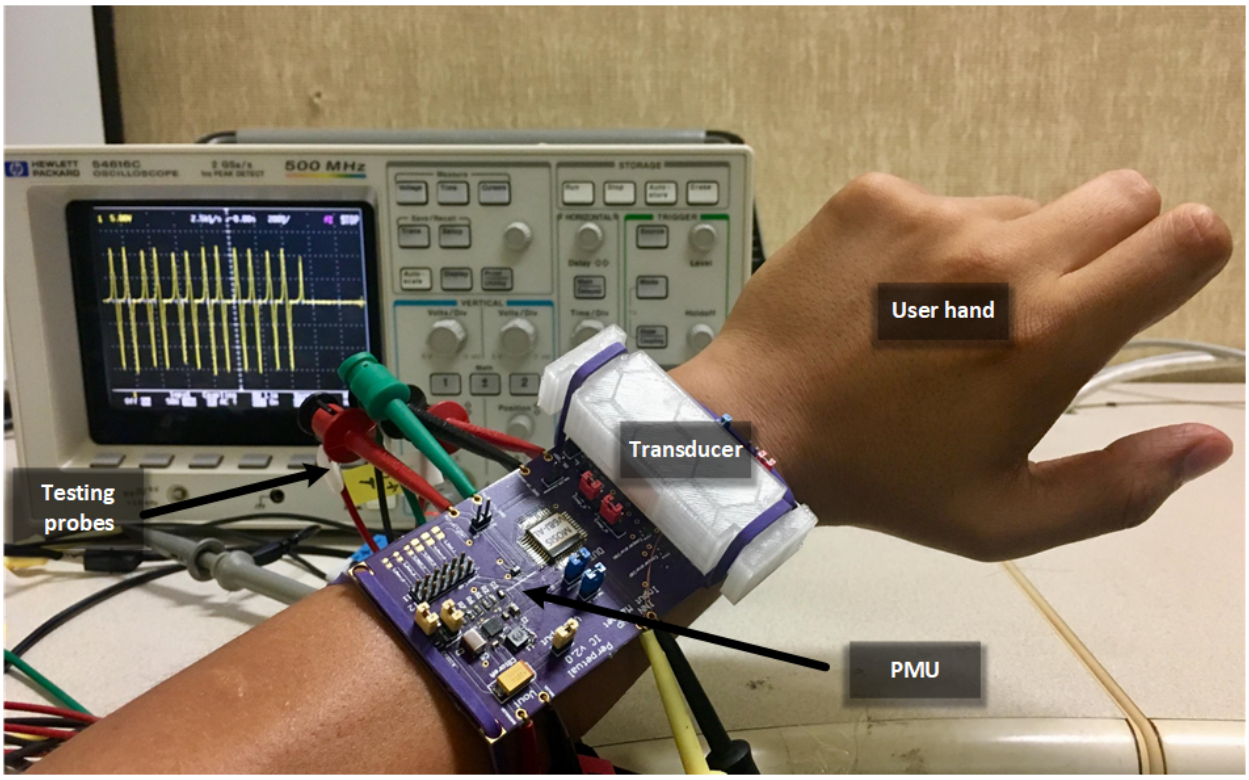

Figure 5.12: Picture of the measurement setup mounted on the user [30].

in Fig. 5.14. As expected, the isolation of the kinetic transducer to be used solely for sensing can provide digital logic compatible voltage signal levels, this feature not only prevents the signal to be further degraded due to the loading impedance in EH harvesting mode but also provides data of digital levels that can be used to analyze user activity without the need of a power hungry analog to digital converter but a faster and more efficient digital circuit. Applications of this feature include step-count estimation, and the implementation of gestures, which are particular hand movements to control a music player, for example.

Voltage conversion efficiency (VCE) was tested using (5.1). Measurements showed over 90% efficiency starting at 90 mV for active rectification, whereas a passive rectification configuration shows a VCE over 90% at around 390 mV. As shown in Fig. 5.15, the VCE remains relatively constant for higher input voltages at 99%.

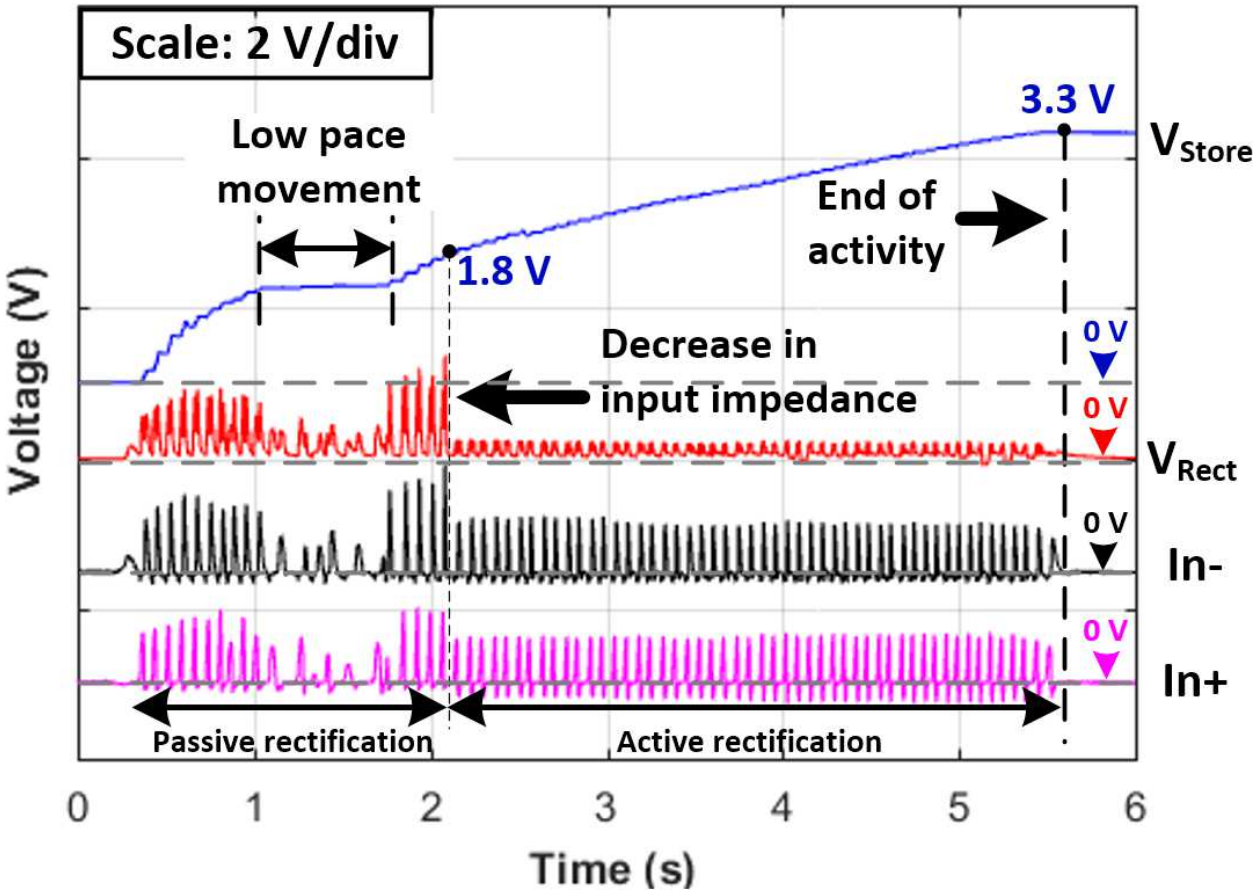

Figure 5.13: System operation waveforms: V_{Store} (top) V_{Rect} (bottom) [30].

$$VCE = \frac{\mathrm{V}_{Rect}}{\mathrm{V}_{Input_{(Peak)}}} \tag{5.1}$$

The power conversion efficiency (PCE), defined in (5.2), was measured using the setup shown in Fig. 5.16, where V_{Source} is a 1Hz sine waveform voltage source in series with a test resistance within conditions shown in Table 5.1, and it showed a peak efficiency of 92.4% at 1 V, 32.4 μA load. The power efficiency, presented in Fig. 5.17, decreases at low R_L because of a reduced input voltage derives in a lower VCE, as previously presents, which directly and negatively affects the PCE. At a higher R_L, the current consumed by the active rectification comparators becomes more significant compared to the power delivered to the load; consequently, the efficiency is deteriorated.

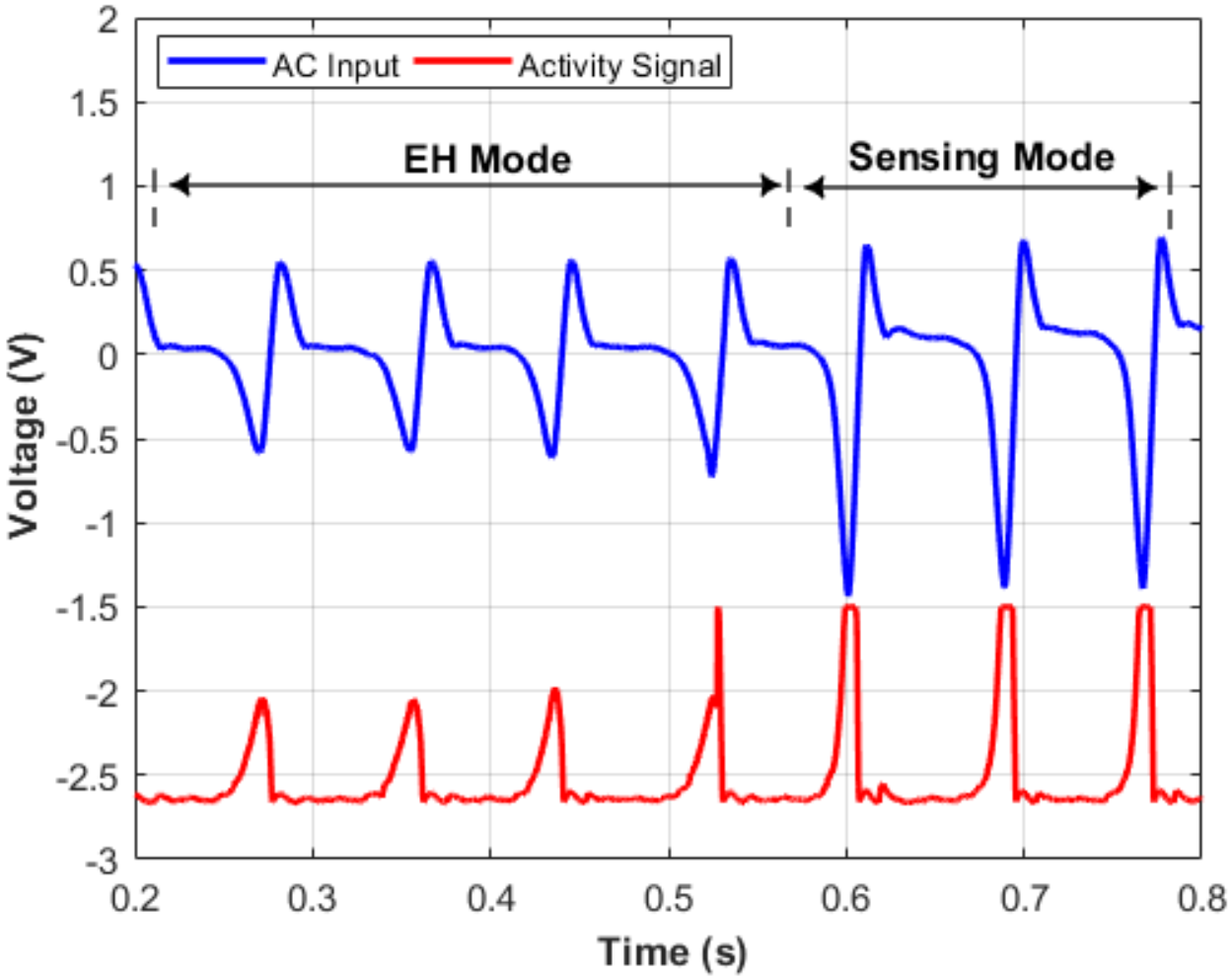

Figure 5.14: EH and sensing modes of operation output waveforms for AC input (top) and activity signal (bottom) [30].

$$PCE = \frac{1/T \int_0^T v_{out_n} i_{out_n}}{1/T \int_0^T v_{in_n} i_{in_n}} \tag{5.2}$$

As a proof of concept, the power management system presented here was used to recharge a Fitbit®Charge HR commercial wearable. Measurements showed that after 30 minutes of a Sprint Interval Training routine the system was capable of recharging 6.90% of the wearable device using an 80 mAh Li-ion battery or 4.02 hours of extra battery life.

Table 5.4 compares the performance of the EH system presented here to other state-of-the-art works [130, 131, 133], in terms of energy harvesting transductor used, process, peak power PCE

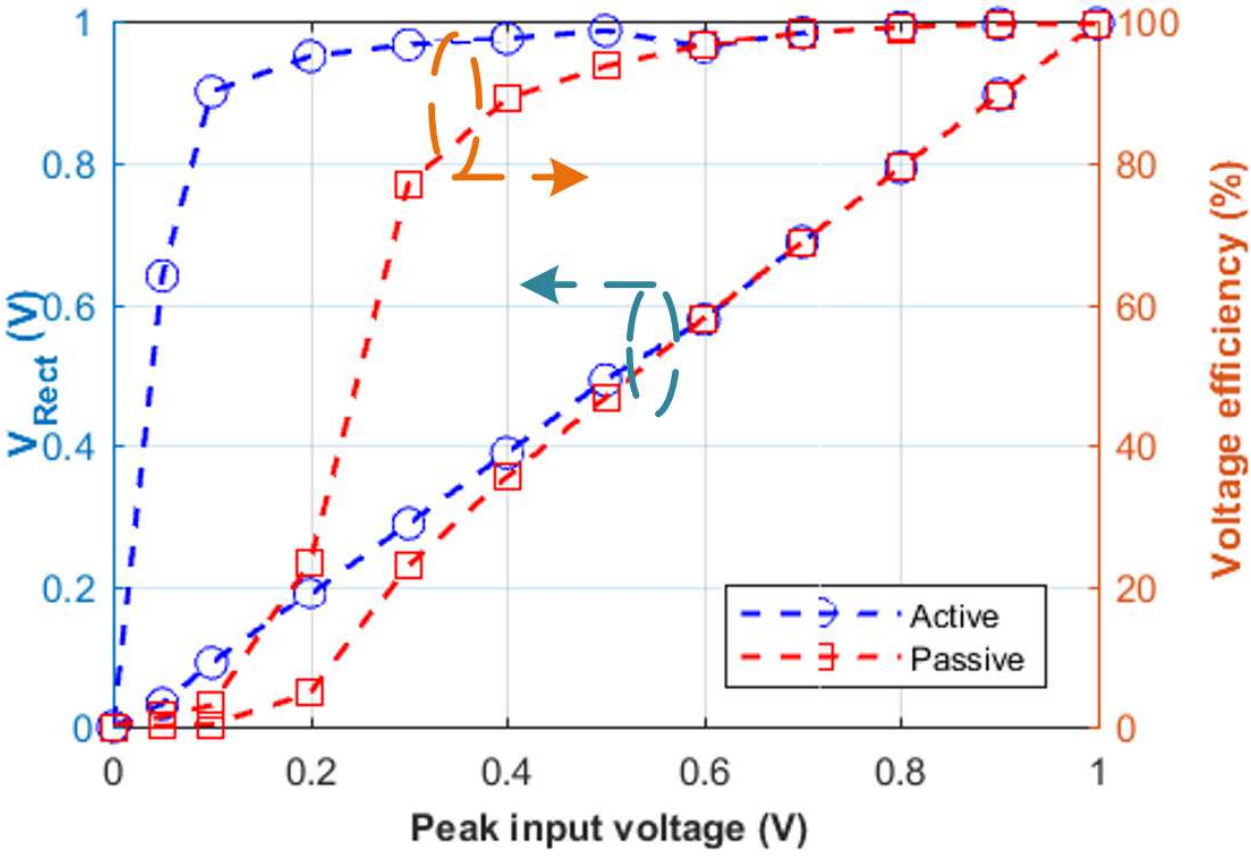

Figure 5.15: Measured voltage conversion efficiency output voltage (V) and voltage efficiency (%) [30].

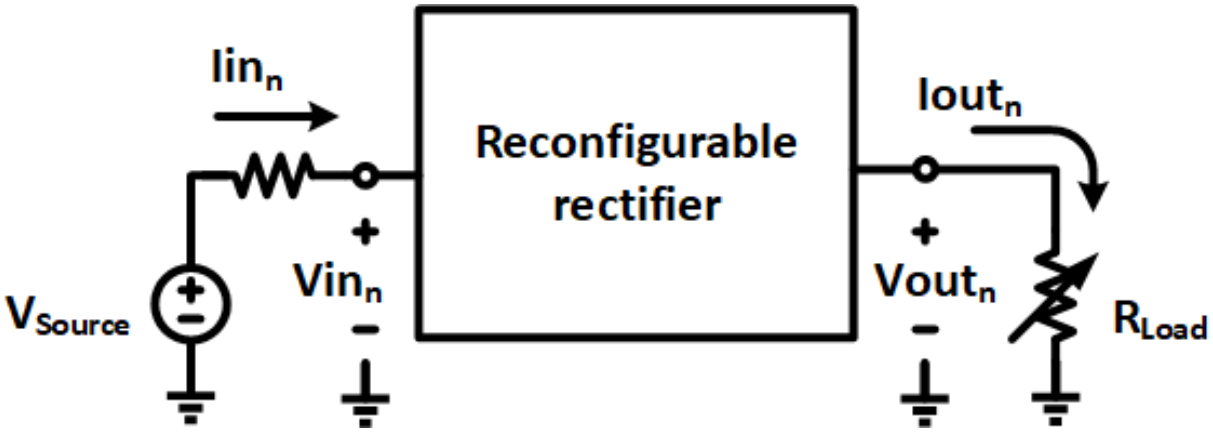

Figure 5.16: Set up circuit to measure power conversion efficiency [30].

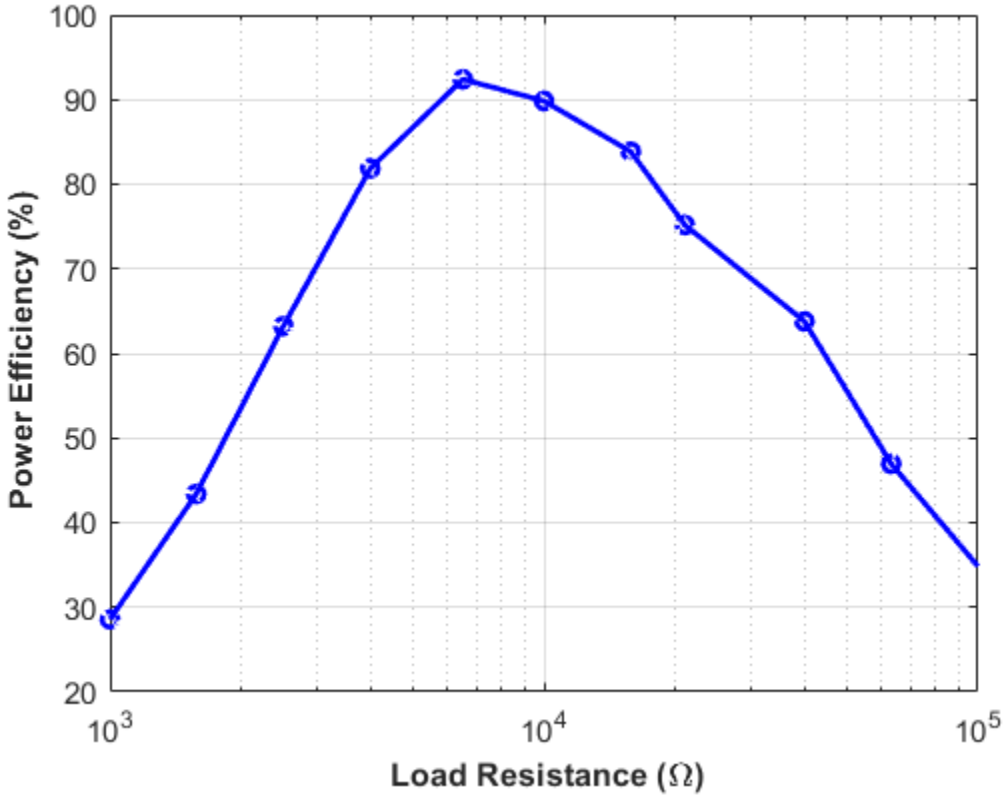

Figure 5.17: Measured power conversion efficiency [30].

and sensing capabilities, showing relevant results in efficiency and features tailored for wearable electronics based on EH.

5.6 Conclusion

In this chapter, a reconfigurable energy harvesting power management system with inherent activity sensing capabilities was designed for wearable applications and implemented in a 130 nm CMOS process. A custom-made EM transducer was employed to power the system, the AC to DC conversion is handled by a reconfigurable rectifier operates in a passive mode configuration during startup and a more power efficient active configuration for $V_{Store} > 1.8V$ with a peak 92.4% power conversion efficiency.

This work introduces an activity detection circuit that enables the use of the inherent sensing capabilities of the transducer used in EM-based EH. The combination of both, a reconfigurable

Reference	[130]	[131]	[133]	THIS WORK
Transducer	EM	EM	EM	EM
Process	180 nm	130 nm	180 nm	130 nm
Rectifier PCE_{Peak} (%)	97*	89*	86	92.4
Regulation Level (V)	-	-	3.0	3.3
Inherent sensing	No	No	No	Yes

Table 5.4: Comparison table with prior art. *Simulated [30].

rectifier and an activity detection circuit, and the EM transducer allows the system to gather similar information than that of an accelerometer, traditionally needed to determine the user's number of steps or activity intensity, but at a lower power consumption and cost.

6. SUMMARY AND CONCLUSIONS

This dissertation presented novel architectures of EH tailored for agricultural applications. The first chapter of this dissertation presented the research motivation and potential impact of the work presented here. It also introduced fundamental concepts on EH architectures, from transducers to power management and energy storage requirements in embedded systems based on intermittent power sources. Additionally, a detailed description of power conditioning circuits was discussed. Specifically, rectification stages were discussed to provide different design trade offs along with common metrics used to measure their performance; also dc-dc step-up converters were also described and power extraction techniques concerning multiple sources of energy.

The second part of this dissertation proposed and described two IoT solutions for agriculture. The first work introduced a Microbial fuel cell (MFC) a technology that is a novel energy harvesting source that can transform organic substrates in wastewater into electricity through a bioelectrochemical process. It showed that its limited output power available per liter is in the range of a few miliwatts, which results in very limited power. One way to reach a usable power output is to connect several MFCs in series or parallel; nevertheless, the high output characteristic resistance of MFCs and differences in output voltage from multiple MFCs, dramatically worsens the power efficiency of such an array. In this paper, a power management system (PMS) is proposed to allow maximum power harvesting from multiple MFCs while providing a regulated output voltage. To enable a more efficient and reliable power-harvesting process from multiple MFCs, a power ranking and MFC-failure protection algorithm was implemented in a PIC24F16KA102 microcontroller. Moreover, we propose as the power extraction sub-block of the system an ultra-low-power BQ25505 step-up DC-DC converter which integrates maximum power point tracking (MPPT) capabilities. The maximum efficiency measured of the PMS was $\approx 50.7\%$. The energy harvesting technique presented in this work was tested to power two temperature-sensing wireless applications: a local range data transmitting sensor and a power-hungry internet-enabled smart node.

The second work presents a power management system for wearable technology based on a

custom made electromagnetic (EM) transducer and a front-end circuit for energy harvesting (EH) and activity sensing. Due to the AC-output nature of the EM transducer, this work proposes a reconfigurable rectifier that can switch from passive operation to a more power-efficient active topology depending on the available power in the system. The passive mode operates as a negative voltage converter during start-up, while the active configuration is enabled and driven by a control block after the available voltage at an output storage capacitor surpasses 1.8 V. This work also introduces an activity detection circuit that enables the use of the inherent sensing capabilities of the EM transducer. The combination of both, a reconfigurable rectifier and an activity detection circuit, allows the system to gather information similar to that of an accelerometer regarding the activity of the user, but at net-zero power consumption and lower cost. The EH front-end described in this work was implemented in a 130 nm CMOS process with an area of 0.0254 mm^2. Measurements show that the circuit has a peak power conversion efficiency of 92.04%, while the power management system can extend the battery's charge of a Fitbit ®Charge HR by four hours for every 30 effective minutes of a sprint interval training routine.

All the solutions proposed here presented prototypes designed, fabricated and tested, its results were also reported as means to verify its operation and allow further research groups to utilize the results presented. Appendix A provides source code and schematics to help other scientist and engineers replicate the results for MFC technology presented here. Appendix B provides further information on how the EH solution for kinetic energy can also be applied to human-oriented applications.

REFERENCES

[1] F. F. Nchuchuwe and K. D. Adejuwon, "The challenges of agriculture and rural development in africa: The case of nigeria," *International Journal of Academic Research in Progressive Education and Development*, vol. 1, no. 3, pp. 45–61, 2012.

[2] S. Verma, R. Gala, S. Madhavan, S. Burkule, S. Chauhan, and C. Prakash, "An internet of things (iot) architecture for smart agriculture," in *2018 Fourth International Conference on Computing Communication Control and Automation (ICCUBEA)*, pp. 1–4, IEEE, 2018.

[3] J. Sherly and D. Somasundareswari, "Internet of things based smart transportation systems," *International Research Journal of Engineering and Technology*, vol. 2, no. 7, pp. 1207–1210, 2015.

[4] P. Pruet, C. S. Ang, D. Farzin, and N. Chaiwut, "Exploring the internet of "educational things"(ioet) in rural underprivileged areas," in *2015 12th International Conference on Electrical Engineering/Electronics, Computer, Telecommunications and Information Technology (ECTI-CON)*, pp. 1–5, IEEE, 2015.

[5] P. A. Laplante and N. Laplante, "The internet of things in healthcare: Potential applications and challenges," *IT Professional*, vol. 18, no. 3, pp. 2–4, 2016.

[6] A. Al-Fuqaha, M. Guizani, M. Mohammadi, M. Aledhari, and M. Ayyash, "Internet of things: A survey on enabling technologies, protocols, and applications," *IEEE Communications Surveys & Tutorials*, vol. 17, no. 4, pp. 2347–2376, 2015.

[7] R. A. Kjellby, T. E. Johnsrud, S. E. Loetveit, L. R. Cenkeramaddi, M. Hamid, and B. Beferull-Lozano, "Self-powered iot device for indoor applications," in *2018 31st International Conference on VLSI Design and 2018 17th International Conference on Embedded Systems (VLSID)*, pp. 455–456, IEEE, 2018.

[8] S. Jiang, "Internet of things (iot): Technologies and applications," in *2015 Fifteenth International Conference on Advances in ICT for Emerging Regions (ICTer)*, pp. 3–3, IEEE, 2015.

[9] S. Blackmore, "Precision farming: an introduction," *Outlook on Agriculture*, vol. 23, no. 4, pp. 275–280, 1994.

[10] J. A. Taylor, *Weather and agriculture*. Pergamon, 1967.

[11] S. Christensen, H. T. Søgaard, P. Kudsk, M. Nørremark, I. Lund, E. S. Nadimi, and R. Jørgensen, "Site-specific weed control technologies," *Weed Research*, vol. 49, no. 3, pp. 233–241, 2009.

[12] V. Marchal, R. Dellink, D. Van Vuuren, C. Clapp, J. Chateau, B. Magné, and J. Van Vliet, "Oecd environmental outlook to 2050," *Organization for Economic Co-operation and Development*, vol. 8, pp. 397–413, 2011.

[13] OECD, "Water and agriculture," *Environmental Performance of Agriculture in OECD Countries Since 1990*, March 2019. Available: https://www.oecd.org/agriculture/topics/water-and-agriculture/.

[14] OECD, "Water quality and agriculture: Meeting the policy challenge," *OECD Publishing*, p. 156, 2012.

[15] J. J. Estrada-López, A. Abuellil, A. Costilla-Reyes, and E. Sánchez-Sinencio, "Technology enabling circuits and systems for the internet-of-things: An overview," in *2018 IEEE International Symposium on Circuits and Systems (ISCAS)*, pp. 1–5, IEEE, 2018.

[16] B. Pozo, J. I. Garate, J. Á. Araujo, and S. Ferreiro, "Energy harvesting technologies and equivalent electronic structural models," *Electronics*, vol. 8, no. 5, p. 486, 2019.

[17] M. Prauzek, J. Konecny, M. Borova, K. Janosova, J. Hlavica, and P. Musilek, "Energy harvesting sources, storage devices and system topologies for environmental wireless sensor networks: A review," *Sensors*, vol. 18, no. 8, p. 2446, 2018.

[18] N. Q. Nguyen and K. V. Pochiraju, "Behavior of thermoelectric generators exposed to transient heat sources," *Applied Thermal Engineering*, vol. 51, no. 1-2, pp. 1–9, 2013.

[19] D. A. Howey, A. Bansal, and A. S. Holmes, "Design and performance of a centimetre-scale shrouded wind turbine for energy harvesting," *Smart Materials and Structures*, vol. 20, no. 8, p. 085021, 2011.

[20] S. Priya, H.-C. Song, Y. Zhou, R. Varghese, A. Chopra, S.-G. Kim, I. Kanno, L. Wu, D. S. Ha, J. Ryu, *et al.*, "A review on piezoelectric energy harvesting: materials, methods, and circuits," *Energy Harvesting and Systems*, vol. 4, no. 1, pp. 3–39, 2019.

[21] R. D'hulst and J. Driesen, "Power processing circuits for vibration-based energy harvesters," in *2008 IEEE Power Electronics Specialists Conference*, pp. 2556–2562, IEEE, 2008.

[22] S. P. Beeby, R. Torah, M. Tudor, P. Glynne-Jones, T. O'donnell, C. Saha, and S. Roy, "A micro electromagnetic generator for vibration energy harvesting," *Journal of Micromechanics and Microengineering*, vol. 17, no. 7, p. 1257, 2007.

[23] Y. Shu and I. Lien, "Analysis of power output for piezoelectric energy harvesting systems," *Smart Materials and Structures*, vol. 15, no. 6, p. 1499, 2006.

[24] S. Kerzenmacher, J. Ducrée, R. Zengerle, and F. Von Stetten, "Energy harvesting by implantable abiotically catalyzed glucose fuel cells," *Journal of Power Sources*, vol. 182, no. 1, pp. 1–17, 2008.

[25] Z. He, S. D. Minteer, and L. T. Angenent, "Electricity generation from artificial wastewater using an upflow microbial fuel cell," *Environmental Science & Technology*, vol. 39, no. 14, pp. 5262–5267, 2005.

[26] J. Siebert, J. Collier, and R. Amirtharajah, "Self-timed circuits for energy harvesting ac power supplies," in *ISLPED '05. Proceedings of the 2005 International Symposium on Low Power Electronics and Design, 2005.*, pp. 315–318, IEEE, Aug 2005.

[27] J. Wenck, R. Amirtharajah, J. Collier, and J. Siebert, "Ac power supply circuits for energy harvesting," in *2007 IEEE Symposium on VLSI Circuits*, pp. 92–93, IEEE, June 2007.

[28] G. D. Szarka, B. H. Stark, and S. G. Burrow, "Review of power conditioning for kinetic energy harvesting systems," *IEEE Transactions on Power Electronics*, vol. 27, pp. 803–815, Feb 2012.

[29] A. Rajasekaran, A. Hande, and D. Bhatia, "Buck-boost converter based power conditioning circuit for low excitation vibrational energy harvesting," in *Third Annual Austin Conference on Integrated Circuits and Systems, Austin, TX*, 2008.

[30] A. Costilla Reyes, A. Abuellil, J. J. Estrada-López, S. Carreon-Bautista, and E. Sánchez-Sinencio, "Reconfigurable system for electromagnetic energy harvesting with inherent activity sensing capabilities for wearable technology," *IEEE Transactions on Circuits and Systems II: Express Briefs*, vol. 66, no. 8, pp. 1302–1306, 2019.

[31] D. P. Arnold, "Review of microscale magnetic power generation," *IEEE Transactions on Magnetics*, vol. 43, no. 11, pp. 3940–3951, 2007.

[32] Y. Kushino and H. Koizumi, "Piezoelectric energy harvesting circuit using full-wave voltage doubler rectifier and switched inductor," in *2014 IEEE Energy Conversion Congress and Exposition (ECCE)*, pp. 2310–2315, IEEE, 2014.

[33] E. Lefeuvre, A. Badel, A. Benayad, L. Lebrun, C. Richard, and D. Guyomar, "A comparison between several approaches of piezoelectric energy harvesting," in *Journal de Physique IV (Proceedings)*, vol. 128, pp. 177–186, EDP sciences, 2005.

[34] W. Liu, Z. Feng, J. He, and R. Liu, "Maximum mechanical energy harvesting strategy for a piezoelement," *Smart Materials and Structures*, vol. 16, no. 6, p. 2130, 2007.

[35] U. Karthaus and M. Fischer, "Fully integrated passive uhf rfid transponder ic with 16.7$-\mu$w minimum rf input power," *IEEE Journal of Solid-State Circuits*, vol. 38, no. 10, pp. 1602–1608, 2003.

[36] P. Rakers, L. Connell, T. Collins, and D. Russell, "Secure contactless smartcard asic with dpa protection," *IEEE Journal of Solid-State Circuits*, vol. 36, no. 3, pp. 559–565, 2001.

[37] Y.-H. Lam, W.-H. Ki, and C.-Y. Tsui, "Integrated low-loss cmos active rectifier for wirelessly powered devices," *IEEE Transactions on Circuits and Systems II: Express Briefs*, vol. 53, no. 12, pp. 1378–1382, 2006.

[38] S. S. Hashemi, M. Sawan, and Y. Savaria, "A high-efficiency low-voltage cmos rectifier for harvesting energy in implantable devices," *IEEE Transactions on Biomedical Circuits and Systems*, vol. 6, no. 4, pp. 326–335, 2012.

[39] S. Hashemi, M. Sawan, and Y. Savaria, "A novel low-drop cmos active rectifier for rf-powered devices: Experimental results," *Microelectronics Journal*, vol. 40, no. 11, pp. 1547–1554, 2009.

[40] T. T. Le, J. Han, A. von Jouanne, K. Mayaram, and T. S. Fiez, "Piezoelectric micro-power generation interface circuits," *IEEE journal of Solid-State Circuits*, vol. 41, no. 6, pp. 1411–1420, 2006.

[41] A. Facen and A. Boni, "Power supply generation in cmos passive uhf rfid tags," in *2006 Ph. D. Research in Microelectronics and Electronics*, pp. 33–36, IEEE, 2006.

[42] J. Colomer-Farrarons, P. Miribel-Catala, A. Saiz-Vela, M. Puig-Vidal, and J. Samitier, "Power-conditioning circuitry for a self-powered system based on micro pzt generators in a 0.13-μm low-voltage low-power technology," *IEEE Transactions on Industrial Electronics*, vol. 55, no. 9, pp. 3249–3257, 2008.

[43] Z. Zhu, B. Jamali, and P. H. Cole, "Brief comparison of different rectifier structures for rfid transponders," in *Auto-ID labs workshop, St Gallen, Switzerland*, 2004.

[44] T. Lehmann and Y. Moghe, "On-chip active power rectifiers for biomedical applications," in *2005 IEEE International Symposium on Circuits and Systems*, pp. 732–735, IEEE, 2005.

[45] C. . Chen, K. . Chen, and S. . Liu, "Efficiency-enhanced cmos rectifier for wireless telemetry," *Electronics Letters*, vol. 43, no. 18, pp. 976–978, 2007.

[46] C. Peters, O. Kessling, F. Henrici, M. Ortmanns, and Y. Manoli, "Cmos integrated highly efficient full wave rectifier," in *2007 IEEE International Symposium on Circuits and Systems*, pp. 2415–2418, IEEE, 2007.

[47] S. Guo and H. Lee, "An efficiency-enhanced integrated cmos rectifier with comparator-controlled switches for transcutaneous powered implants," in *2007 IEEE Custom Integrated Circuits Conference*, pp. 385–388, IEEE, 2007.

[48] G. Bawa and M. Ghovanloo, "Analysis, design, and implementation of a high-efficiency full-wave rectifier in standard cmos technology," *Analog Integrated Circuits and Signal Processing*, vol. 60, no. 1-2, pp. 71–81, 2009.

[49] H.-M. Lee and M. Ghovanloo, "An integrated power-efficient active rectifier with offset-controlled high speed comparators for inductively powered applications," *IEEE Transactions on Circuits and Systems I: Regular Papers*, vol. 58, no. 8, pp. 1749–1760, 2011.

[50] H. Kobayashi and T. Nabeshima, *Handbook of Power Management Circuits*. Pan Stanford, 2016.

[51] G. Yang, B. H. Stark, S. J. Hollis, and S. G. Burrow, "Challenges for energy harvesting systems under intermittent excitation," *IEEE Journal on Emerging and Selected Topics in Circuits and Systems*, vol. 4, no. 3, pp. 364–374, 2014.

[52] K. Lundager, B. Zeinali, M. Tohidi, J. K. Madsen, and F. Moradi, "Low power design for future wearable and implantable devices," *Journal of Low Power Electronics and Applications*, vol. 6, no. 4, p. 20, 2016.

[53] A. A. A. Rahman, W. A. W. Jamil, and A. A. Umar, "Configurable impedance matching to maximise power extraction for enabling self-powered system based-on photovoltaic cells," *Electronic Materials Letters*, vol. 12, no. 4, pp. 545–550, 2016.

[54] F. Deng, X. Yue, X. Fan, S. Guan, Y. Xu, and J. Chen, "Multisource energy harvesting system for a wireless sensor network node in the field environment," *IEEE Internet of Things Journal*, vol. 6, no. 1, pp. 918–927, 2018.

[55] N. Sridhar, G. Anitha, and M. Sumathi, "Analysis of energy harvesting from multiple sources for wireless sensor networks with focus on impedance matching," in *2017 International Conference on Circuit, Power and Computing Technologies (ICCPCT)*, pp. 1–5, IEEE, 2017.

[56] G. Chowdary, A. Singh, and S. Chatterjee, "An 18 na, 87% efficient solar, vibration and rf energy-harvesting power management system with a single shared inductor," *IEEE Journal of Solid-State Circuits*, vol. 51, no. 10, pp. 2501–2513, 2016.

[57] H. Lhermet, C. Condemine, M. Plissonnier, R. Salot, P. Audebert, and M. Rosset, "Efficient power management circuit: From thermal energy harvesting to above-ic microbattery energy storage," *IEEE Journal of Solid-State Circuits*, vol. 43, no. 1, pp. 246–255, 2008.

[58] D. Carli, D. Brunelli, L. Benini, and M. Ruggeri, "An effective multi-source energy harvester for low power applications," in *2011 Design, Automation & Test in Europe*, pp. 1–6, IEEE, 2011.

[59] Y. K. Tan and S. K. Panda, "Energy harvesting from hybrid indoor ambient light and thermal energy sources for enhanced performance of wireless sensor nodes," *IEEE Transactions on Industrial Electronics*, vol. 58, no. 9, pp. 4424–4435, 2010.

[60] S. Bandyopadhyay and A. P. Chandrakasan, "Platform architecture for solar, thermal, and vibration energy combining with mppt and single inductor," *IEEE Journal of Solid-State Circuits*, vol. 47, no. 9, pp. 2199–2215, 2012.

[61] M. Dini, A. Romani, M. Filippi, V. Bottarel, G. Ricotti, and M. Tartagni, "A nanocurrent power management ic for multiple heterogeneous energy harvesting sources," *IEEE Transactions on Power Electronics*, vol. 30, no. 10, pp. 5665–5680, 2015.

[62] M. A. Abouzied, H. Osman, V. Vaidya, K. Ravichandran, and E. Sanchez-Sinencio, "An integrated concurrent multiple-input self-startup energy harvesting capacitive-based dc adder combiner," *IEEE Transactions on Industrial Electronics*, vol. 65, no. 8, pp. 6281–6290, 2017.

[63] J. J. Estrada-López, A. Abuellil, A. Costilla-Reyes, M. Abouzied, S. Yoon, and E. Sánchez-Sinencio, "A fully integrated maximum power tracking combiner for energy harvesting iot applications," *IEEE Transactions on Industrial Electronics*, vol. 67, no. 4, pp. 2744–2754, 2020.

[64] A. Abuellil, J. J. Estrada-López, A. Bommireddipalli, A. Costilla-Reyes, Z. Zeng, and E. Sánchez-Sinencio, "Multiple-input harvesting power management unit with enhanced boosting scheme for iot applications," *IEEE Transactions on Industrial Electronics*, vol. 67, no. 5, pp. 3662–3672, 2020.

[65] C. Y. Chong and S. P. Kumar, "Sensor networks: Evolution, opportunities, and challenges," *Proceedings of the IEEE*, vol. 91, no. 8, pp. 1247–1256, 2003.

[66] V. Güngör and G. Hancke, *Industrial Wireless Sensor Networks: Applications, Protocols, and Standards*. Industrial Electronics, Taylor & Francis, 2013.

[67] A. Tiwari, F. L. Lewis, and S. S. Ge, "Wireless sensor network for machine condition based maintenance," *2004 8th International Conference on Control, Automation, Robotics and Vision, Vols 1-3*, pp. 461–467, 2004.

[68] R. A. Swartz, J. P. Lynch, S. Zerbst, B. Sweetman, and R. Rolfes, "Structural monitoring of wind turbines using wireless sensor networks," *Smart Structures and Systems*, vol. 6, no. 3, pp. 183–196, 2010.

[69] C. Konstantopoulos, E. Koutroulis, N. Mitianoudis, and A. Bletsas, "Converting a plant to a battery and wireless sensor with scatter radio and ultra-low cost," *IEEE Transactions on Instrumentation and Measurement*, vol. 65, no. 2, pp. 388–398, 2016.

[70] W. Y. Toh, Y. K. Tan, W. S. Koh, and L. Siek, "Autonomous wearable sensor nodes with flexible energy harvesting," *IEEE Sensors Journal*, vol. 14, no. 7, pp. 2299–2306, 2014.

[71] Y. Wang, J. P. Lynch, and K. H. Law, "Design of a low-power wireless structural monitoring system for collaborative computational algorithms," *Health Monitoring and Smart*

Nondestructive Evaluation of Structural and Biological Systems IV, vol. 5768, pp. 106–117, 2005.

[72] L. Atzori, A. Iera, and G. Morabito, "The internet of things: A survey," *Computer Networks*, vol. 54, no. 15, pp. 2787–2805, 2010.

[73] W. K. Seah, Y. Tan, and A. T. Chan, *Research in energy harvesting wireless sensor networks and the challenges ahead*, pp. 73–93. Springer, 2012.

[74] Z. G. Wan, Y. K. Tan, and C. Yuen, "Review on energy harvesting and energy management for sustainable wireless sensor networks," in *Communication Technology (ICCT), 2011 IEEE 13th International Conference on*, pp. 362–367.

[75] V. Raghunathan, A. Kansal, J. Hsu, J. Friedman, and M. Srivastava, "Design considerations for solar energy harvesting wireless embedded systems," *2005 Fourth International Symposium on Information Processing in Sensor Networks*, pp. 457–462, 2005.

[76] J. Zarate-Roldan, S. Carreon-Bautista, A. Costilla-Reyes, and E. Sánchez-Sinencio, "A power management unit with 40 dB switching-noise-suppression for a thermal harvesting array," *IEEE Transactions on Circuits and Systems I: Regular Papers*, vol. 62, no. 8, pp. 1918–1928, 2015.

[77] B. H. Calhoun, D. C. Daly, N. Verma, D. F. Finchelstein, D. D. Wentzloff, A. Wang, S. H. Cho, and A. P. Chandrakasan, "Design considerations for ultra-low energy wireless microsensor nodes," *IEEE Transactions on Computers*, vol. 54, no. 6, pp. 727–740, 2005.

[78] R. J. M. Vullers, R. v. Schaijk, H. J. Visser, J. Penders, and C. V. Hoof, "Energy harvesting for autonomous wireless sensor networks," *IEEE Solid-State Circuits Magazine*, vol. 2, no. 2, pp. 29–38, 2010.

[79] R. Moghe, Y. Yang, F. Lambert, and D. Divan, "A scoping study of electric and magnetic field energy harvesting for wireless sensor networks in power system applications," *2009 IEEE Energy Conversion Congress and Exposition, Vols 1-6*, pp. 3423–3430, 2009.

[80] H. M. Wang, J. D. Park, and Z. Y. Ren, "Active energy harvesting from microbial fuel cells at the maximum power point without using resistors," *Environmental Science & Technology*, vol. 46, no. 9, pp. 5247–5252, 2012.

[81] B. E. Logan, B. Hamelers, R. A. Rozendal, U. Schrorder, J. Keller, S. Freguia, P. Aelterman, W. Verstraete, and K. Rabaey, "Microbial fuel cells: Methodology and technology," *Environmental Science & Technology*, vol. 40, no. 17, pp. 5181–5192, 2006.

[82] D. R. Lovley, "The microbe electric: conversion of organic matter to electricity," *Current Opinion in Biotechnology*, vol. 19, no. 6, pp. 564–571, 2008.

[83] B. E. Logan, "Exoelectrogenic bacteria that power microbial fuel cells," *Nature Reviews Microbiology*, vol. 7, no. 5, pp. 375–381, 2009.

[84] D. Pant, G. Van Bogaert, L. Diels, and K. Vanbroekhoven, "A review of the substrates used in microbial fuel cells (mfcs) for sustainable energy production," *Bioresource Technology*, vol. 101, no. 6, pp. 1533–1543, 2010.

[85] F. Ivars-Barcelo, A. Zuliani, M. Fallah, M. Mashkour, M. Rahimnejad, and R. Luque, "Novel applications of microbial fuel cells in sensors and biosensors," *Applied Sciences-Basel*, vol. 8, no. 7, 2018.

[86] C. Donovan, A. Dewan, D. Heo, and H. Beyenal, "Batteryless, wireless sensor powered by a sediment microbial fuel cell," *Environmental Science & Technology*, vol. 42, no. 22, pp. 8591–8596, 2008.

[87] L. M. Tender, S. A. Gray, E. Groveman, D. A. Lowy, P. Kauffman, J. Melhado, R. C. Tyce, D. Flynn, R. Petrecca, and J. Dobarro, "The first demonstration of a microbial fuel cell as a viable power supply: Powering a meteorological buoy," *Journal of Power Sources*, vol. 179, no. 2, pp. 571–575, 2008.

[88] D. R. Bond, D. E. Holmes, L. M. Tender, and D. R. Lovley, "Electrode-reducing microorganisms that harvest energy from marine sediments," *Science*, vol. 295, no. 5554, pp. 483–485, 2002.

[89] J. D. Park and Z. Ren, "Hysteresis-controller-based energy harvesting scheme for microbial fuel cells with parallel operation capability," *IEEE Transactions on Energy Conversion*, vol. 27, no. 3, pp. 715–724, 2012.

[90] A. Meehan, H. Gao, and Z. Lewandowski, "Energy harvesting with microbial fuel cell and power management system," *IEEE Transactions on Power Electronics*, pp. 176–181, 2011.

[91] C. Erbay, S. Carreon-Bautista, E. Sanchez-Sinencio, and A. Han, "High performance monolithic power management system with dynamic maximum power point tracking for microbial fuel cells," *Environmental Science & Technology*, vol. 48, no. 23, pp. 13992–13999, 2014.

[92] S. Carreon-Bautista, C. Erbay, A. Han, and E. Sanchez-Sinencio, "Power management system with integrated maximum power extraction algorithm for microbial fuel cells," *IEEE Transactions on Energy Conversion*, vol. 30, no. 1, pp. 262–272, 2015.

[93] S. Carreon-Bautista, C. Erbay, A. Han, and E. Sanchez-Sinencio, "An inductorless dc-dc converter for an energy aware power management unit aimed at microbial fuel cell arrays," *IEEE Journal of Emerging and Selected Topics in Power Electronics*, vol. 3, no. 4, pp. 1109–1121, 2015.

[94] A. Zanella, N. Bui, A. Castellani, L. Vangelista, and M. Zorzi, "Internet of things for smart cities," *IEEE Internet of Things Journal*, vol. 1, no. 1, pp. 22–32, 2014.

[95] I. Lee, G. Kim, S. Bang, A. Wolfe, R. Bell, S. Jeong, Y. Kim, J. Kagan, M. Arias-Thode, B. Chadwick, D. Sylvester, D. Blaauw, and Y. Lee, "System-on-mud: Ultra-low power oceanic sensing platform powered by small-scale benthic microbial fuel cells," *IEEE Transactions on Circuits and Systems I-Regular Papers*, vol. 62, no. 4, pp. 1126–1135, 2015.

[96] F. Khaled, O. Ondel, and B. Allard, "Optimal energy harvesting from serially connected microbial fuel cells," *IEEE Transactions on Industrial Electronics*, vol. 62, no. 6, pp. 3508–3515, 2015.

[97] A. Shantaram, H. Beyenal, R. Raajan, A. Veluchamy, and Z. Lewandowski, "Wireless sensors powered by microbial fuel cells," *Environmental Science & Technology*, vol. 39, no. 13, pp. 5037–5042, 2005.

[98] E. Dallago, A. L. Barnabei, A. Liberale, G. Torelli, and G. Venchi, "A 300-mv low-power management system for energy harvesting applications," *IEEE Transactions on Power Electronics*, vol. 31, no. 3, pp. 2273–2281, 2016.

[99] Y. Plekhanova, S. Tarasov, V. Kolesov, I. Kuznetsova, M. Signore, F. Quaranta, and A. Reshetilov, "Effects of polymer matrices and carbon nanotubes on the generation of electric energy in a microbial fuel cell," *Membranes (Basel)*, vol. 8, no. 4, 2018.

[100] A. Costilla-Reyes, C. Erbay, S. Carreon-Bautista, A. Han, and E. Sánchez-Sinencio, "A time-interleave-based power management system with maximum power extraction and health protection algorithm for multiple microbial fuel cells for internet of things smart nodes," *Applied Sciences*, vol. 8, p. 2404, Nov 2018.

[101] G. Yang, C. Erbay, S.-i. Yi, P. de Figueiredo, R. Sadr, A. Han, and C. Yu, "Bifunctional nano-sponges serving as non-precious metal catalysts and self-standing cathodes for high performance fuel cell applications," *Nano Energy*, vol. 22, pp. 607–614, 2016.

[102] C. Erbay, X. Pu, W. Choi, M.-J. Choi, Y. Ryu, H. Hou, F. Lin, P. de Figueiredo, C. Yu, and A. Han, "Control of geometrical properties of carbon nanotube electrodes towards high-performance microbial fuel cells," *Journal of Power Sources*, vol. 280, pp. 347–354, 2015.

[103] C. Erbay, G. Yang, P. de Figueiredo, R. Sadr, C. Yu, and A. Han, "Three-dimensional porous carbon nanotube sponges for high-performance anodes of microbial fuel cells," *Journal of Power Sources*, vol. 298, pp. 177–183, 2015.

[104] J. You, J. Greenman, and I. Ieropoulos, "Novel analytical microbial fuel cell design for rapid in situ optimisation of dilution rate and substrate supply rate, by flow, volume control and anode placement," *Energies*, vol. 11, no. 9, 2018.

[105] H. Lin, S. Wu, and J. Zhu, “Modeling power generation and energy efficiencies in air-cathode microbial fuel cells based on freter equations,” *Applied Sciences*, vol. 8, no. 10, p. 1983, 2018.

[106] X. Zhang, H. Ren, S. Pyo, J. I. Lee, J. Kim, and J. Chae, “A high-efficiency dc-dc boost converter for a miniaturized microbial fuel cell,” *IEEE Transactions on Power Electronics*, vol. 30, no. 4, pp. 2041–2049, 2015.

[107] Z. Y. Ren, T. E. Ward, and J. M. Regan, “Electricity production from cellulose in a microbial fuel cell using a defined binary culture,” *Environmental Science & Technology*, vol. 41, no. 13, pp. 4781–4786, 2007.

[108] P. Aelterman, K. Rabaey, H. T. Pham, N. Boon, and W. Verstraete, “Continuous electricity generation at high voltages and currents using stacked microbial fuel cells,” *Environmental Science & Technology*, vol. 40, no. 10, pp. 3388–3394, 2006.

[109] A. Dewan, H. Beyenal, and Z. Lewandowski, “Scaling up microbial fuel cells,” *Environmental Science & Technology*, vol. 42, no. 20, pp. 7643–7648, 2008.

[110] Microchip Technology, "20/28-pin general purpose, 16-bit flash microcontrollers with nanowatt xlp technology," PIC24F16KA102 datasheet, October 2011. Available: www.microchip.com.

[111] Texas Instruments, "Ultra low-power boost charger with battery management and autonomous power multiplexer for primary battery in energy harvester applications," BQ25505 datasheet, August 2013. Available: www.ti.com.

[112] Y. Zhang, F. Zhang, Y. Shakhsheer, J. D. Silver, A. Klinefelter, M. Nagaraju, J. Boley, J. Pandey, A. Shrivastava, and E. J. Carlson, “A batteryless 19μ w mics/ism-band energy harvesting body sensor node soc for exg applications,” *IEEE Journal of Solid-State Circuits*, vol. 48, no. 1, pp. 199–213, 2013.

[113] Y. K. Ramadass and A. P. Chandrakasan, “A battery-less thermoelectric energy harvesting interface circuit with 35 mv startup voltage,” *IEEE Journal of Solid-State Circuits*, vol. 46, no. 1, pp. 333–341, 2011.

[114] Particle, "Internet of things hardware development kit," Photon datasheet, November 2017. Available: www.particle.io.

[115] N. Degrenne, F. Buret, F. Morel, S.-E. Adami, D. Labrousse, B. Allard, and A. Zaoui, “Self-starting dc: Dc boost converter for low-power and low-voltage microbial electric generators,” in *Energy Conversion Congress and Exposition (ECCE), 2011 IEEE*, pp. 889–896, IEEE.

[116] R. Umaz, C. Garrett, F. Qian, B. Li, and L. Wang, “A power management system for multi-anode benthic microbial fuel cells,” *IEEE Transactions on Power Electronics*, vol. 32, no. 5, pp. 3562–3570, 2017.

[117] H. Baali, H. Djelouat, A. Amira, and F. Bensaali, “Empowering Technology Enabled Care Using IoT and Smart Devices: A Review,” *IEEE Sensors Journal*, 2017.

[118] A. Dionisi, D. Marioli, E. Sardini, and M. Serpelloni, “Autonomous wearable system for vital signs measurement with energy-harvesting module,” *IEEE Transactions on Instrumentation and Measurement*, vol. 65, no. 6, pp. 1423–1434, 2016.

[119] G. V. Merrett, H. Huang, and N. M. White, “Modeling the effect of orientation on human-powered inertial energy harvesters,” *IEEE Sensors Journal*, vol. 15, no. 1, pp. 434–441, 2015.

[120] V. Leonov, “Energy harvesting for self-powered wearable devices,” in *Wearable Monitoring Systems*, pp. 27–49, Springer, 2011.

[121] J. A. Paradiso and T. Starner, “Energy scavenging for mobile and wireless electronics,” *IEEE Pervasive Computing*, vol. 4, no. 1, pp. 18–27, 2005.

[122] X. Liu and E. Sánchez-Sinencio, "An 86% efficiency 12 μW self-sustaining PV energy harvesting system with hysteresis regulation and time-domain MPPT for IOT smart nodes," *IEEE Journal of Solid-State Circuits*, vol. 50, no. 6, pp. 1424–1437, 2015.

[123] X. Lu, P. Wang, D. Niyato, D. I. Kim, and Z. Han, "Wireless networks with RF energy harvesting: A contemporary survey," *IEEE Communications Surveys & Tutorials*, vol. 17, no. 2, pp. 757–789, 2015.

[124] S. Yoon, S. Carreon-Bautista, and E. Sánchez-Sinencio, "An Area Efficient Thermal Energy Harvester With Reconfigurable Capacitor Charge Pump for IoT Applications," *IEEE Transactions on Circuits and Systems II: Express Briefs*, 2018.

[125] A. Khaligh, P. Zeng, and C. Zheng, "Kinetic energy harvesting using piezoelectric and electromagnetic technologies—state of the art," *IEEE Transactions on Industrial Electronics*, vol. 57, no. 3, pp. 850–860, 2010.

[126] P. D. Mitcheson, E. M. Yeatman, G. K. Rao, A. S. Holmes, and T. C. Green, "Energy harvesting from human and machine motion for wireless electronic devices," *Proceedings of the IEEE*, vol. 96, no. 9, pp. 1457–1486, 2008.

[127] S. Roundy, E. S. Leland, J. Baker, E. Carleton, E. Reilly, E. Lai, B. Otis, J. M. Rabaey, P. K. Wright, and V. Sundararajan, "Improving power output for vibration-based energy scavengers," *IEEE Pervasive Computing*, vol. 4, no. 1, pp. 28–36, 2005.

[128] E. Dallago, M. Marchesi, and G. Venchi, "Analytical model of a vibrating electromagnetic harvester considering nonlinear effects," *IEEE Transactions on Power Electronics*, vol. 25, no. 8, pp. 1989–1997, 2010.

[129] G. D. Szarka, B. H. Stark, and S. G. Burrow, "Review of power conditioning for kinetic energy harvesting systems," *IEEE Transactions on Power Electronics*, vol. 27, no. 2, pp. 803–815, 2012.

[130] S.-W. Wang, Y.-W. Ke, P.-C. Huang, and P.-H. Hsieh, "Electromagnetic Energy Harvester Interface Design for Wearable Applications," *IEEE Transactions on Circuits and Systems II: Express Briefs*, vol. 65, no. 5, pp. 667–671, 2018.

[131] R. Bolt, M. Magno, T. Burger, A. Romani, and L. Benini, "Kinetic AC/DC Converter for Electromagnetic Energy Harvesting in Autonomous Wearable Devices," *IEEE Transactions on Circuits and Systems II: Express Briefs*, vol. 64, no. 12, pp. 1422–1426, 2017.

[132] D. Porcarelli, D. Spenza, D. Brunelli, A. Cammarano, C. Petrioli, and L. Benini, "Adaptive rectifier driven by power intake predictors for wind energy harvesting sensor networks," *IEEE Journal in Emerging and Selected Topics in Power Electronics*, vol. 3, no. 2, pp. 471–482, 2015.

[133] H. Uluşan, Ö. Zorlu, A. Muhtaroğlu, and H. Külah, "Highly Integrated 3 V Supply Electronics for Electromagnetic Energy Harvesters With Minimum 0.4 V_{peak} Input," *IEEE Transactions on Industrial Electronics*, vol. 64, no. 7, pp. 5460–5467, 2017.

APPENDIX A

MICROBIAL FUEL CELL SUPPLEMENTARY MATERIAL

A.1 Source code

The main program of the source code for the multi-MFC -cell power ranking algorithm is provided here,

```
void MFC_PowerExtraction (void);
void MFC_PowerRank(void);

unsigned int ADCResult[9]={0, 0, 0, 0, 0, 0, 0, 0, 0};
unsigned int ADCResultCopy[9]={0, 0, 0, 0, 0, 0, 0, 0, 0};
unsigned int i, j, k, ch, MFCcount, MFCth;

//channel selection in port
              //MFC:   1    2    3    4    5    6    7    8    9
unsigned char MFCChannel[9]={0x0C, 0x05, 0x03, 0x02, 0x01, 0x00, 0x0A,
   0x0B, 0x0C};

//Switch selection for for:
               //MFC:   1     2     3     4     5     6     7     8
                     9
unsigned short MFC_LATA [9]={0x0008, 0x0010, 0x0000, 0x0000, 0x0000,
   0x0080, 0x0040, 0x0000, 0x0000};
unsigned short MFC_LATB [9]={0x0000, 0x0000, 0x0040, 0x0100, 0x0200,
   0x0000, 0x0000, 0x0400, 0x0800};

unsigned char counter;
```

```
/*
                    Main application
 */

//LUT ranking
 int cmpfunc (const void * a, const void * b)
{
  return ( *(int*)b - *(int*)a );
}

int main(void)
{
   // initialize the device
   SYSTEM_Initialize();

   NBoost_SetLow();
   LATA = 0x0000;              //Port A initialized to avoid voltage
      reversal
   LATB = 0x0000;              //Port B initialized to avoid voltage
      reversal
   Cap_Discharge_SetLow();     //Set defaults as no power measurement
      to be performed
   while (1)
   {
      MFC_PowerRank();      //Power Ranking algorithm

      MFC_PowerExtraction(); //Power Extraction subroutine
   }
```

```
   return -1;
}
void MFC_PowerExtraction (void){
      /*Stage 2: Power Extraction using LUT*/
      /* Power Extraction routine*/
      for (i=0 ; i<9 ; i++){              //MFC_Channel selector
         pointer
         for (j=0 ; j<9 ; j++){
            if (ADCResultCopy[i] == ADCResult[j]){ //Extraction starts
               from the strongest MFC *ADCResultCopy has the Ranked
               values in LUT
               MFCth = ADCResultCopy[i] >> 1; //50% MFC health point
               ch = 1;
               while(ch){
                     NBoost_SetHigh();           //Boost converter
                        disabled
                     __delay32(90000);           //EH optimization
                        delay
                     //Test MFC's health

                     NBoost_SetLow();           //Boost converter
                        disabled
                     LATB = 0x0000;             //Clear LATCHB to
                        avoid voltage reversal.
                     LATA = MFC_LATA[j];        //Set Corresponding
                        Channel.
                     LATB = MFC_LATB[j];

                     ADC1_Start();
```

```
                    while(!ADC1_IsConversionComplete());
                        //ADC1_IsConversionComplete() 1==Yes then go
                        out
                    ADC_result = (unsigned int)
                        ADC1_ConversionResultGet();

                    if (ADC_MFC_result<MFCth){ //MFC's health check
                        up point
                        //Exit Energy Harvesting if MFC health doesn't
                            meet minimum criteria
                        ch=0;
                        LATA = 0x0000;
                        LATB = 0x0000;
                        NBoost_SetLow();
                        j=9;
                    }
                }
            }
        }
    }
}
void MFC_PowerRank(void){

    /*Stage 1: MFC Ranking code Starts*/
    //Initialization
    NBoost_SetLow();          //Boost converter disabled
    Cap_Discharge_SetHigh();  //Capacitor initial voltage = 0V
    LATA = 0x0000;            //Port A initialized to avoid voltage
        reversal
```

```
LATB = 0x0000;              //Port B initialized to avoid voltage
   reversal
for (ch=0 ; ch<9 ; ch++)
{
   LATB = 0x0000;              //Port B initialized to avoid
      voltage reversal
   LATA = MFC_LATA[ch];        //Cap Charge Selection instruction
      when boost converter is disabled
   LATB = MFC_LATB[ch];        //Cap Charge Selection instruction
      when boost converter is disabled
   Cap_Discharge_SetLow();    //Capacitor Charging for Power
      Measurement enabled
   //Capacitor voltage is read below
   /*Stage 2: Measurement starts here*/
   ADC1_ChannelSelect(MFCChannel[ch]); //Dynamic Channel
      Selection (Cap Charge))
   ADCResult[ch] = 0;
   ADC1_Start();
   ADC1_Stop();
   //Routine to discharge Cap
   LATA = 0x0000;              //Port A initialized. Cap
      Discharge is in this I/O port range
   LATB = 0x0000;              //Port B initialized.
   Cap_Discharge_SetHigh();    //Capacitor reset
   while(!ADC1_IsConversionComplete());
      //ADC1_IsConversionComplete() 1==Yes then continue
   ADCResult[ch] = (unsigned int) ADC1_ConversionResultGet();
   ADCResultCopy[ch] = ADCResult[ch]; //Store ADC result in LUT
   /*Measurement ends here*/
```

```
        }
        /*Stage 3: Rank LUT*/
        AD1CON1bits.ADON=0; //Turn the ADC off (Power efficiency feature)
        Cap_Discharge_SetLow(); //MFCs power be extracted
        qsort(ADCResultCopy, 10, sizeof(int), cmpfunc); //ADC result
           sorted
        /*MFC Ranking code Ends*/
}
```

A.2 Circuit Schematics

A circuit schematics of Supplementary material for chapter on A Time-Interleave-Based Power Management System with Maximum Power Extraction and Health Protection Algorithm for Multiple Microbial Fuel Cells for Internet of Things Smart Nodes is provided in this appendix.

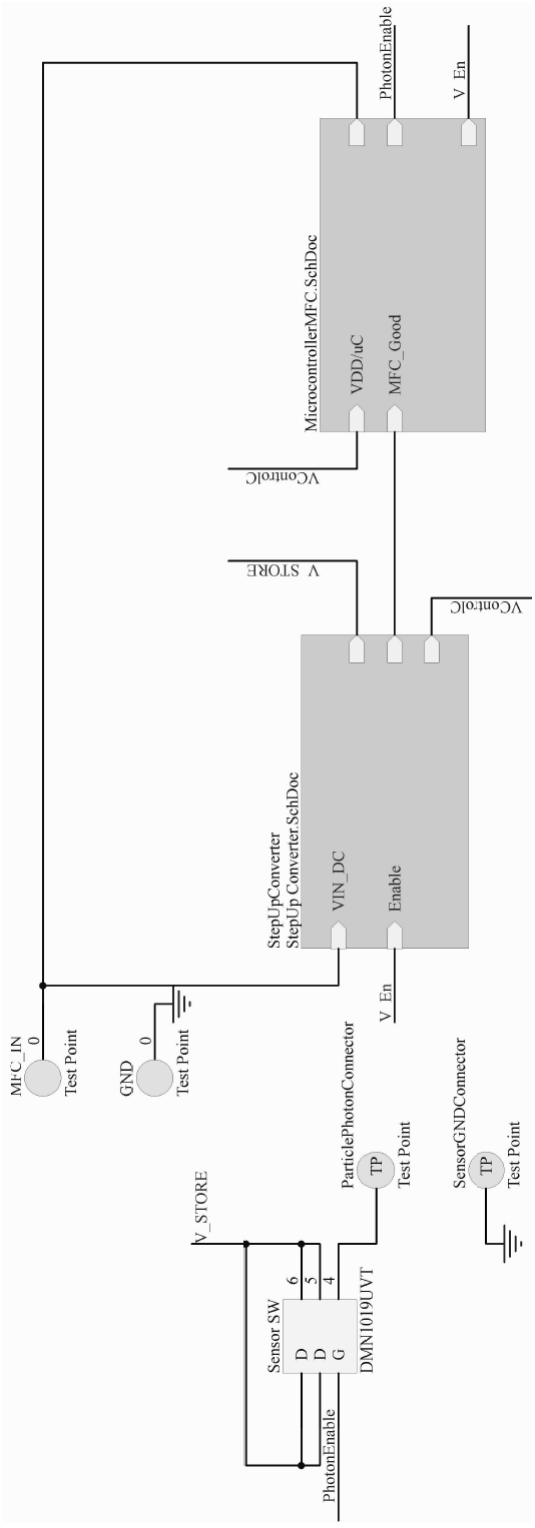

Figure A.1: Power management system circuit for multiple MFCs

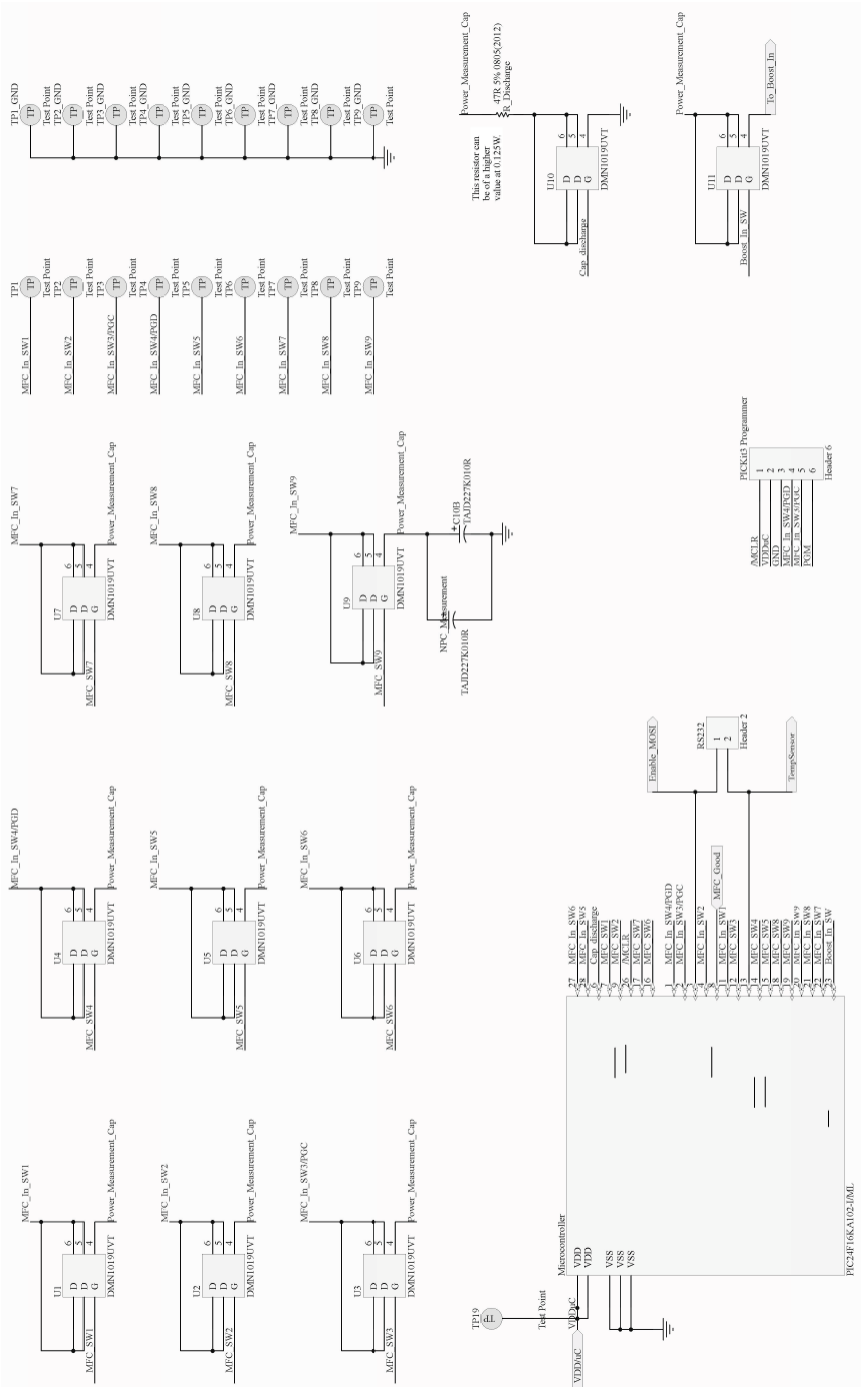

Figure A.2: Microcontroller MFC block schematic

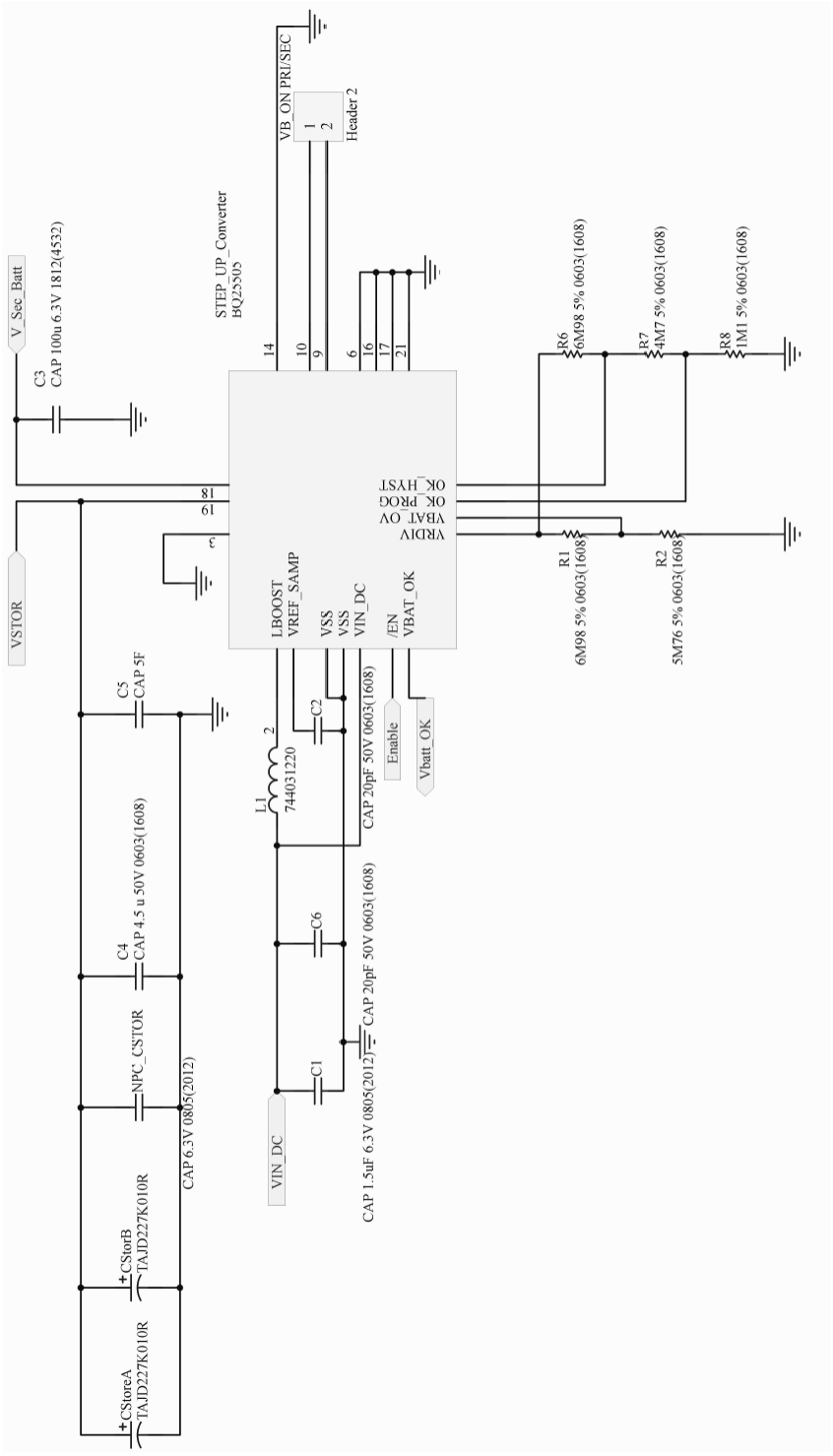

Figure A.3: Step-Up Converter block schematic

APPENDIX B

RECONFIGURABLE RECTIFIER TEST CASES

The proposed reconfigurable rectifier is capable of signal gestures, steps and running information which in turn can be presented to the user as a means for them to correlate activity to energy being produced.

In this section two test cases are presented that can be used for activity detection and categorization and a simple security application denominated "gesture-based binary passcode"

B.1 Activity detection

In test case number one, it is possible to differentiate running from walking in the power each activity generates.

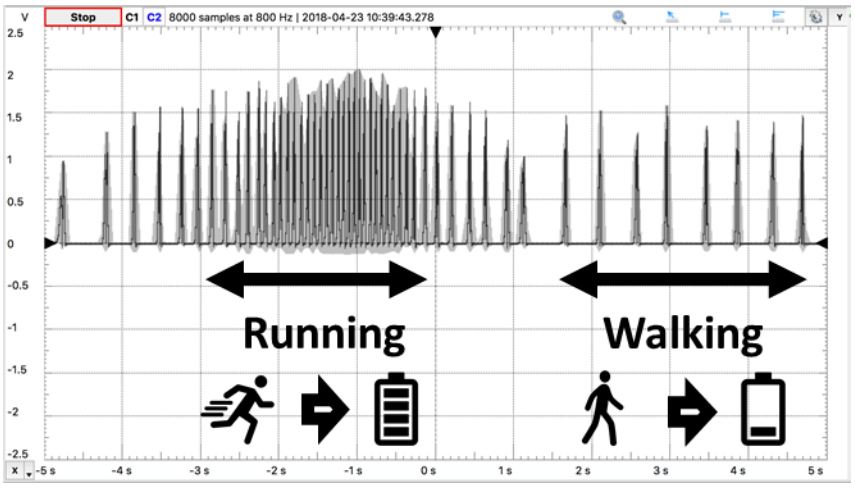

Figure B.1: PMU test case for running to walk activity.

B.2 Binary passcode

Test case number two, proposes the use the custom reconfigurable rectifier and activity detector to signal gestures which can be used to elicit actions such as unlock screen, pause/resume workout

and music controls, to name a few, such commands are determined by hand movements and the time between their digital output.

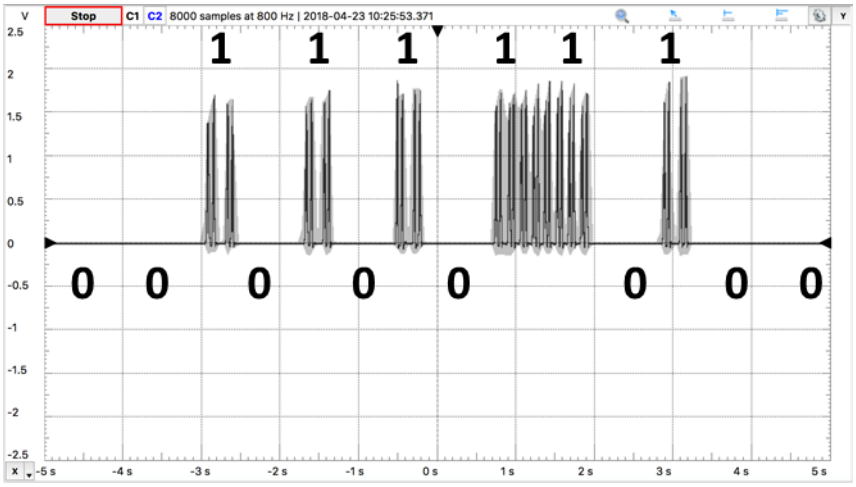

Figure B.2: PMU test case for binary passcode detection features.

APPENDIX C

ACADEMIC CONTRIBUTIONS

C.1 Journals

- **A. Costilla-Reyes**, Amr Abuellil, Johan J. Estrada-López, Salvador Carreon-Bautista and E. Sánchez-Sinencio, "Reconfigurable Front-End for Electromagnetic Energy Harvesting Rectification and Activity Sensing for Wearable Technology," *IEEE Transactions on Circuits and Systems II: Express Briefs*, 2018.

- **A. Costilla-Reyes**, Celal Erbay, Salvador Carreon-Bautista, Arum Han, and Edgar Sánchez-Sinencio. "A Time-Interleave-Based Power Management System with Maximum Power Extraction and Health Protection Algorithm for Multiple Microbial Fuel Cells for Internet of Things Smart Nodes." *Applied Sciences* 8, no. 12 (2018): 2404.

- A. Abuellil, J. J. Estrada López, A. Vighnesh, **A. Costilla-Reyes**, Z. Zeng and E. Sánchez-Sinencio, "Multiple-Input Harvesting PMU with Enhanced Boosting Scheme for IoT Applications," *IEEE Transactions in Industrial Electronics*, 2019.

- J. J. Estrada Lopez, A. Abuellil, **A. Costilla-Reyes**, M. Abouzied, S. Yoon and E. Sanchez-Sinencio, "A Fully Integrated Maximum Power Tracking Combiner for Energy Harvesting IoT Applications," *IEEE Transactions on Industrial Electronics*, 2019.

- J. Zarate-Roldan, S. Carreon-Bautista, **A. Costilla-Reyes** and E. Sánchez-Sinencio, "A Power Management Unit With 40 dB Switching-Noise-Suppression for a Thermal Harvesting Array," *IEEE Transactions on Circuits and Systems I: Regular Papers*, vol. 62, no. 8, pp. 1918-1928, Aug. 2015.

C.2 Conferences

- J. J. Estrada-López, A. Abuellil, **A. Costilla-Reyes** and E. Sánchez-Sinencio, "Technology Enabling Circuits and Systems for the Intemet-of-Things: An Overview," 2018 *IEEE International Symposium on Circuits and Systems (ISCAS)*, Florence, Italy, 2018, pp. 1-5.

- J. Zarate-Roldan, S. Carreon-Bautista, **A. Costilla-Reyes** and E. Sanchez-Sinencio, "An ultra-low power power management unit with -40dB switching-noise-suppression for a 3x3 thermoelectric generator array with 57% maximum end-to-end efficiency," *Proceedings of the IEEE 2014 Custom Integrated Circuits Conference*, San Jose, CA, 2014, pp. 1-4.

C.3 Poster/Oral presentations

- **A. Costilla-Reyes** and E. Sánchez-Sinencio PhD, "Showcase pitch of BitGrange and Blackstone Launchpad at Texas A&M University a campus-based program designed to assist and mentor students about entrepreneurship opportunities at Texas A&M University," *South By Southwest®Edu (SXSW®edu)*, Austin, USA, 2018.

- **A. Costilla-Reyes** and E. Sánchez-Sinencio PhD, "Educative platform for indoors vegetable production based on the Internet of Things," *Second International Forum of Mexican Talent INNOVATION MATCH MX*, Mexico City, Mexico, June 2017.

- **A. Costilla-Reyes**, G. Fan and E. Sánchez-Sinencio PhD, "BitGrange: development of a smart hydroponics device to grow vegetables indoors," Texas A&M University *College of Engineering's National Labs Day*, College Station, USA, 2017.

- **A. Costilla-Reyes**, J. J. Estrada-López, E. Sanchez-Sinencio PhD. "Energy Harvesting Applications for Building Automation". *The 52nd Annual Technical Meeting, The Society of Engineering Science*, College Station, TX, 2015.